ISSN 0077-880X

THE UNIVERSITY OF
NEW SOUTH WALES

STUDIES FROM
SCHOOL OF CIVIL AND ENVIRONMENTAL ENGINEERING

BEHAVIOUR OF CFRP-STRENGTHENED DETERIORATED RC BEAMS SUBJECTED TO FATIGUE

BY

M K Y LOO, S J FOSTER and S T SMITH

UNICIV REPORT No. R-455 JUNE 2009
THE UNIVERSITY OF NEW SOUTH WALES
SYDNEY 2052 AUSTRALIA
http://www.civeng.unsw.edu.au

ISBN: 85841 422 8

The University of New South Wales

SCHOOL OF CIVIL AND ENVIRONMENTAL ENGINEERING

BIBLIOGRAPHIC DATA SHEET **ISSN ????**

1. UNICIV Report No. R-455	2. ISBN: 85841 422 8	3. DATE: June 2009

4. Title and Subtitle:

Behaviour of CFRP-Strengthened Deteriorated RC Beams Subjected to Fatigue

---

5. Author(s):

Mindy K Y Loo, Stephen J Foster and Scott T Smith

---

6. Keywords:

CFRP, Reinforced Concrete, Beams, Deteriorated, Fatigue, Repair

---

7. Abstract:

Deterioration due to corrosion is a significant issue in marine structures and bridges. These structures are often subjected to oscillating loads that cause fatigue, significantly reducing the life of the structure. External repair using CFRPs (carbon fibre reinforced polymers) is one of the more recent approaches that have shown promise compared to traditional methods, mainly due to their outstanding mechanical properties. This report reviews the literature on reinforced concrete (RC) beams, and FRP strengthened RC beams, in fatigue and presents the results of an experimental study on the performance of corroded reinforced concrete beams repaired with CFRP and tested in fatigue. The beams were first subjected to an accelerated corrosion procedure under sustained loading. Once the target corrosion level was achieved, a repair procedure was carried out that involved removal of the deteriorated concrete, followed by mortar repair and the externally bonded CFRP plate. As expected, in the corroded specimens the tensile reinforcing bars had become more susceptible to fatigue failure than for the bars in the non-corroded control beams. The CFRP strengthening delayed the fatigue life of corroded specimen by reducing the stress level of the tensile reinforcement. The dominant failure was by fracture of one or more of the tensile reinforcing bars, followed by debonding of the CFRP plate. On fatigue failure of the reinforcing steel, the load transferred to the CFRP plate as observed by a marked increase in strain in the CFRP. After the load transfer, however, the beams were capable of withstanding just a few thousand additional cycles before debonding. While the CFRP delayed the fatigue failure it did not restore the cyclic resistance of the beams to that of the control specimens. A size effect was also observed with smaller scaled specimens capable of withstanding more fatigue cycles with CFRP strengthening. Thus, specimen size is an issue needing consideration in the transfer of knowledge developed from scale model testing to that of full scale structures.

---

8. Number of pages: 150

ACKNOWLEDGEMENTS

The tests were conducted at the University of New South Wales Heavy Structures Laboratory at the School of Civil and Environmental Engineering. Particular thanks go to the laboratory staff members who provided invaluable assistance during the conducting of the experiments Mr William Terry, Mr. Ron Moncay, Mr John Gilbert, Mr Tony Macken and Mr Paul Gwynne.

This study was funded via Australian Research Council (ARC) Discovery Grant DP0453096. The support of the ARC is acknowledged with thanks.

ABSTRACT

Deterioration due to corrosion is a significant issue in marine structures and bridges. These structures are often subjected to oscillating loads that cause fatigue, significantly reducing the life of the structure. External repair using CFRPs (carbon fibre reinforced polymers) is one of the more recent approaches that have shown promise compared to traditional methods, mainly due to their outstanding mechanical properties. This report reviews the literature on reinforced concrete (RC) beams, and FRP strengthened RC beams, in fatigue and presents the results of an experimental study on the performance of corroded reinforced concrete beams repaired with CFRP and tested in fatigue. The beams were first subjected to an accelerated corrosion procedure under sustained loading. Once the target corrosion level was achieved, a repair procedure was carried out that involved removal of the deteriorated concrete, followed by mortar repair and the externally bonded CFRP plate. As expected, in the corroded specimens the tensile reinforcing bars had become more susceptible to fatigue failure than for the bars in the non-corroded control beams. The CFRP strengthening delayed the fatigue life of corroded specimen by reducing the stress level of the tensile reinforcement. The dominant failure was by fracture of one or more of the tensile reinforcing bars, followed by debonding of the CFRP plate. On fatigue failure of the reinforcing steel, the load transferred to the CFRP plate as observed by a marked increase in strain in the CFRP. After the load transfer, however, the beams were capable of withstanding just a few thousand additional cycles before debonding. While the CFRP delayed the fatigue failure it did not restore the cyclic resistance of the beams to that of the control specimens. A size effect was also observed with smaller scaled specimens capable of withstanding more fatigue cycles with CFRP strengthening. Thus, specimen size is an issue needing consideration in the transfer of knowledge developed from scale model testing to that of full scale structures.

TABLE OF CONTENTS

1 INTRODUCTION

Due to the significant level of investment that developed countries have placed in their public and private infrastructure, and the aging of this infrastructure, rehabilitation and strengthening of existing reinforced concrete structures has become a research focus. With the advent of carbon fibre reinforced polymers (CFRP) new strengthening approaches have come to the fore using external bonding technologies. These approaches have shown significant advantages compared to traditional methods, mainly due to the outstanding mechanical properties of the composite materials, their light weight and the simple application to structural members. However, these and other investigations have revealed new, often brittle, failure modes due to mechanisms such as debonding at the interface between the FRPs and the parent structure and fracture of reinforcing steel in fatigue.

Deterioration due to corrosion is a significant issue in marine structures and bridges. These structures are often subjected to oscillating loads that cause fatigue, significantly reducing the life of the structure. External repair using CFRP is one of the more recent approaches that have shown promise compared to traditional methods, mainly due to their outstanding mechanical properties. This report presents the results of an experimental study on the performance of corroded reinforced concrete (RC) beams repaired with CFRP and tested in fatigue. Four series of RC beams were cast and tested of three different sizes to investigate any size related effects in the response. In each series, three beams were cast, one control specimen and two specimens subjected to accelerated corrosion processes to achieve a target 15% mass loss of the tensile steel reinforcement. For the two corrosion damaged specimens in each series, the specimens were then repaired using a standard repair technique by brushing back the corroded reinforcing steel and replacing the damaged concrete with a high performance epoxy based repair mortar. One of the two repaired specimens in each series was then strengthened using carbon fibre reinforced polymer plates bonded to the soffit of the specimens.

The objectives of the experimental program are to investigate the potential of the CFRP flexural repair technique in restoring/improving the fatigue life of conventionally repaired corroded RC beams and to study the effect of specimen size on the test results.

2 REVIEW OF LITERATURE

2.1 Introduction

Interest in fatigue in concrete structures arises because structures such as bridges, offshore structures and pavements are subjected to cyclic loading. According to Zhang et al. (2001), concrete overlays for highway bridge decks are expected to resist millions of cycles of repeated axle loads from passing traffic during their service lives. Barnes and Garden (1999) cite the figure of 7 x 10^8 cycles during the course of a 120 year lifespan of a bridge. There are two important reasons for consideration of fatigue in design, namely: cyclic load may cause structural fatigue failure and the effects of repeated loading on the characteristics of materials strength, stiffness, toughness and durability under service loading.

Täjlsten (2002) suggested that the problems related to fatigue have become more important in the last few years in the construction industry as

(i) design and analysis methods have been improved and refined. Previously rough calculation methods and overly conservative safety factor have somewhat accounted for the risk of fatigue. In today's refined methods, the safety for fatigue must be evaluated separately.

(ii) the quality of material is improving and higher strengths are being attained. However, higher failure strength often means that the material becomes more brittle and the fatigue strength in relation becomes lower.

(iii) new types of structures are being built where fatigue loads occur to a greater extent than what has previously been common.

The following briefly detail the fatigue behaviour of components in a typical reinforced concrete structure.

2.1.1 Fatigue behaviour of plain concrete

The fatigue properties of concrete are a function of the accumulation of irreversible energy deformation, which manifests itself as inelastic strains in the form of cracks and creep. The fatigue strength of a typical concrete member corresponding to a life of ten million cycles is about 55 percent of the initial static strength of the member (ACI Committee 215, 1974). According to ACI Committee 215 (1974), factors that govern this behaviour include the range of load, rate and frequency of loading, loading eccentricity, history, material properties and environmental conditions.

In general, three phases can be found in a fatigue process; crack initiation, propogation and failure. Crack initiation is where microcracks initiate at discontinuities and stress concentrations and are formed during the hardening process of concrete. Crack propagation is where a crack grows a small amount with each load change andeventually leads to failure.

2.1.2 Fatigue behaviour of steel reinforcement

Cyclic load on steel reinforcement causes microcracking that, in-turn initiates a stress concentration on the bar surface. The crack then propagates as the stress continues to cycle. At a critical crack length, the propagation can become unstable leading to sudden fracture.

Helgason and Hanson (1974) reported the lowest stress range known to have caused a fatigue failure in their tests on bars in a concrete beam, which was at 145 MPa. ACI Committee 215 (1974) recommended that the maximum allowable stress range ($\Delta\sigma$) for reinforcing steel subjected to fatigue be 161 MPa.

2.1.3 Fatigue behaviour of corroded reinforcement

Tilly (1988) compiled fatigue data on 6 mm diameter 250 grade plain bars that, after 20 years of service in a bridge deck, had experienced pitting corrosion. The loss of fatigue strength was reportedly more than could be accounted for by loss of bar cross section. Reduction factors of 1.35 and 1.7 for fatigue stress range were proposed for bars experiencing up to 25 percent and more than 25 percent of section loss, respectively.
Apostolopoulos and Papadopoulos (2007) tested the cyclic behaviour of corroded S400 grade reinforcing steel with yield strength of 400 MPa. Bars of diameter 10 mm were subjected to salt spray tests between durations of 10 to 90 days to induce corrosion before being tested cyclically to failure. Mass loss was reported to be between 1.6 percent to 8.5 percent. Corroded bars were subjected to sinusoidal load equivalent to ±1 percent strain. It was reported that a mass loss of about 2 percent caused a 22 percent reduction in number of cycles to failure while a 3 percent mass loss corresponded to a 47 percent reduction in number of cycles to failure.

2.2 Fatigue behaviour of conventional RC beams

A significant body of works exist on the fatigue behaviour of reinforced concrete beams with state-of-the-art reports by ACI Committee 215 (1982), CEB-FIP (1988) and Mallett (1991). It is not the intention of this review to go into great depth on this aspect, rather the reader is referred to the listed references. A brief review is undertaken where it relates more directly on the investigation in this study.

Susceptibility of a reinforced concrete beam to fatigue will vary throughout the member as fatigue is dependent upon the stress level of its components at each section, which are the reinforcing steel and concrete. Depending on the design of a reinforced concrete beam, the governing failure can vary. An under reinforced member has its flexural fatigue performance dominated by the main longitudinal steel, but a heavily reinforced one can fail in flexure or in shear. Barnes and Mays (1999) noted that as fatigue loading of a beam progresses, and the subsequent cracks propagate, there is a redistribution of stress. Hence, fatigue failure is not always the same mechanism as if the member is loaded under static conditions. ACI Committee 215 (1974) recommended that in straight, deformed, reinforcement in beams the maximum stress range, ($\Delta\sigma$) be limited to

$$\Delta\sigma = 161 - 0.33\sigma_{min} \geq 138 \text{ MPa} \tag{2.1}$$

where σ_{min} is the minimum stress in MPa.

Acccording to CEB-FIP (1988), if the quality of steel and concrete is uniform, the fatigue performance for both can be determined quite precisely by testing the individual materials and with the same performance observed for fatigue testing with the composite material. However, in the loaded reinforced concrete element, the stresses are complicated and are, thus, calculated using simplified models. The model stresses are not the real ones and the real stresses determine the fatigue performance of the element. Therefore, the fatigue life tests exhibit a large amount of scatter.

2.3 Fatigue behaviour of FRP-strengthened RC beams

Wang and Zhang (1993) investigated the performances of 30 reinforced concrete beams reinforced with GFRP. Twenty-four specimens were tested under static loads and with six tested in fatigue. For the static test, three methods of strengthening were adopted as given in Table 2.1. In the fatigue test, five strengthened and one unstrengthened specimens were reinforced with 5 mm thick GFRP plates using soffit strengthening (Method A in Table 2.1, shown in Figure 2.1). The loading frequency was at 60 Hz, which was very high for any structural member in service.

In regards to fatigue tests, Wang & Zhang (1993) observed that under the same load range, the fatigue life of the strengthened beams were three times longer than that of the unstrengthened beam. The fatigue strength increased from 15 to 30 percent and the mid-span deflection reduced by 40 percent.

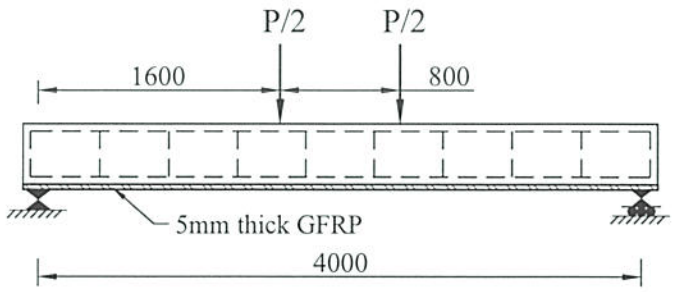

Figure 2.1 – Test specimen of Wang and Zhang (1993).

Table 2.1 - Method of strengthening investigated by Wang and Zhang (1993).

Method	Method of strengthening
A	Soffit strengthening
B	U-shaped sheet strengthening
C	U-shaped sheet strengthening with bolts as anchorage

In experiments by Meier (1995), 70 flexural reinforced concrete beams with spans between 2.0 m and 7.0 m were tested. No details are given in the paper of the actual cyclic testing and no information is provided regarding the applied load levels, loading frequency, fatigue strengths or fatigue lives. However, the research work showed the validity of the strain compatibility method in the analysis of various cross sections, which implies that calculation of flexure in reinforced concrete elements externally strengthened with CFRP can be performed in a similar way to that for conventional reinforced concrete elements. The Meier tests indicated that occurrence of shear cracks may lead to peeling of the FRP laminate. The fracture of internal steel reinforcement was the governing failure during fatigue tests.

Meier also reported on works by Kaiser (1989) who investigated a 2.0 m span beam under fatigue loading. The beam was externally strengthened with a glass/carbon fibre hybrid composite. The fatigue loading was at a frequency of 4 Hz and the specimen was tested in four-point bending. Fatigue failure occurred in the internal steel reinforcement, with a secondary failure by damage of the composite in the form of fractures of individual rovings of the laminate. According to Meier, however, the test was executed with unrealistically high steel stresses and, hence, Meier undertook a fatigue test a 6 m long beam under more realistic conditions. The Meier specimen was a reinforced concrete T-beam strengthened with a CFRP plate (Figure 2.2). After 10 million cycles of loading at room temperature, the beam was

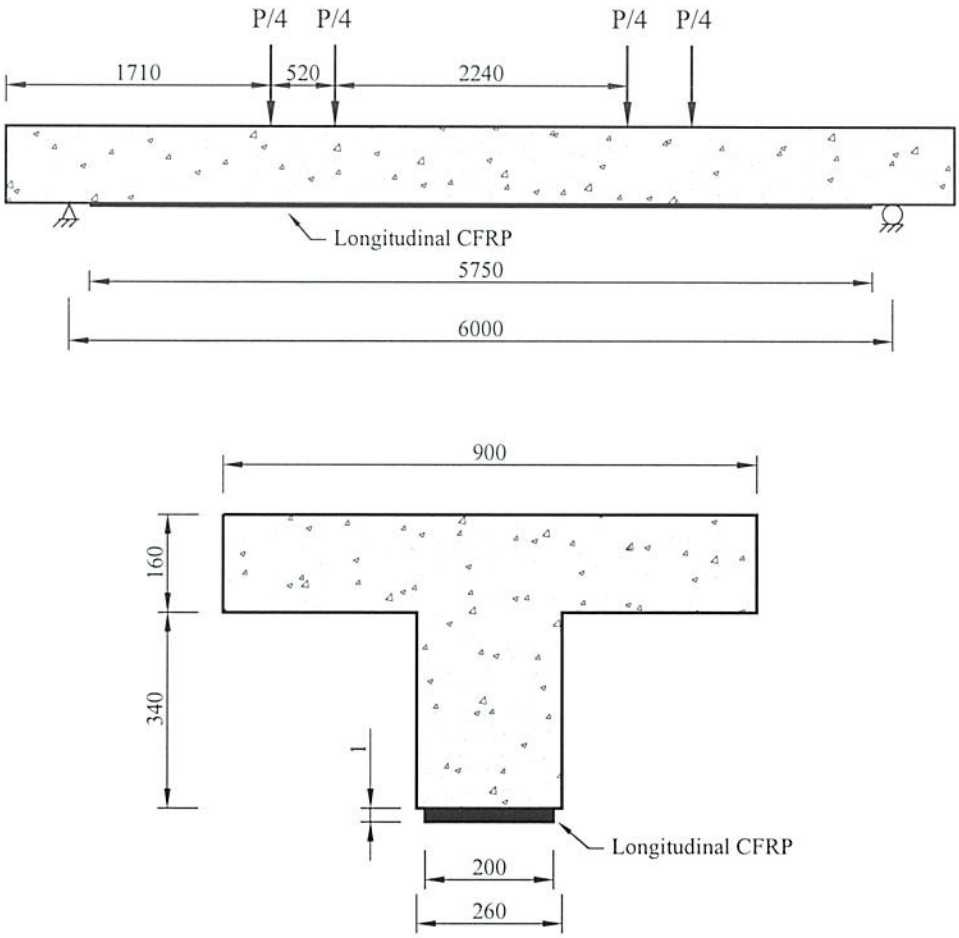

Figure 2.2 – Details of test specimen by Meier (1995).

loaded at an elevated temperature of 40 °C and a relative humidity of 95 percent. After 12 million cycles, the first steel reinforcement bar failed due to fatigue. After three of the reinforcement bars had failed the CFRP debonded from the concrete. The joint between CFRP laminate and the concrete did not present any severe straining due to the fatigue.

Meier (1995) conducted further tests on beams strengthened with prestressed CFRP laminates. The CFRP was attached to the soffit and prestressed to 50 percent of the laminate strength. The specimen strengthened with prestressed CFRP did not show any damage whatsoever, even after 30 million cycles. According to Meier (1995), when the prestressing force is too high failure of the beam due to release of the pretension will occur at the two ends because of the development of high shear stresses in the concrete layer immediately above the CFRP. Tests and calculations have shown that without special end anchorages, CFRP laminates can shear off from the end zones at just 5 percent of their ultimate failure strength.

Muszynski and Sierakowski (1996) tested twenty beams of 760 mm spans under third-point loading at 20 Hz for 2 million cycles. The maximum loads varied between 50 to 90 percent of the static capacity. The minimum load was at 10 percent of the static capacity (determined from tests on four control specimens). The number of cycles applied to the specimen was based on Brandshaug (1978) which indicated that if a specimen could withstand 2 million cycles without failure, it could last, for all practical purposes, forever. Prior to fatigue tests, four beams were tested for pulse velocity and longitudinal frequency to determine the pulse modulus of elasticity (PMOE) and the dynamic modulus of elasticity (DMOE). After 2 million cycles, beams which did not fail were retested non-destructively for both pulse velocity and longitudinal frequency and, then, destructively tested in third-point static flexure to determine the residual static flexural strength and toughness. The endurance limit, defined in Wu et al. (1989), is the taken as the maximum fatigue flexural stress at which the concrete can withstand 2 million cycles of fatigue loading, expressed as a percentage of the modulus of rupture of plain concrete.

Muszynski and Sierakowski (1996) observed that the static modulus of rupture (MOR) and the toughness of the strengthened beams were more than three and forty times, respectively, than that of the control beams. Unstrengthened specimens tested at 90, 80 and 60 percent of the maximum stress failed before 2 million cycles whereas those at 50 and 40 percent successfully endured 2 million cycles. Almost no change in MOR, PMOE and DMOE was observed after 2 million cycles. The strengthened specimens tested at 90 and 80 percent of the maximum stress, failed to meet the 2 million cycle criteria whereas those at 70, 60 and 50 percent successfully endured 2 million cycles. Again, almost no change in the MOR and toughness was observed after the conclusion of the cyclic loading. However the PMOE and, to a greater degree, the DMOE were reduced after 2 million cycles of fatigue loading. The endurance limit for the unstrengthened beams was a load of less than 50 percent of the static capacity while the limit for the CFRP strengthened beams was 256 percent of the control concrete beam's static flexural strength.

Barnes and Garden (1999) tested five beams of 1.0 m span that were plated with a pre-pregnated CFRP plate, and cyclically loaded at a frequency of 1 Hz. The minimum and maximum load applied were 2 percent and 90 percent of the yield stress of the steel reinforcement, respectively. For the control unstrengthened beams, the minimum and maximum load applied were 3 percent and 59 percent of the yield, respectively. All the specimens were loaded to an upper level of approximately half of their ultimate capacity representing 132 percent of the serviceability load in the strengthened beam cases. The failure of the unstrengthened specimen was by steel reinforcement fracture. For the strengthened specimens, the failure was also by fracture of the steel reinforcement but at a greater number

of cycles than that for the unstrengthened specimen. The conclusion derived from the experiment was that for beams having a shear span to beam depth ratio between 3.4 and 4.0, and loaded under cyclic loading, it is necessary to incorporate a bolted plate end anchorage system for the CFRP.

Following the experiment by Barnes and Garden (1999), Barnes and Mays (1999) further investigated the effectiveness of CFRP strengthening under cyclic loading on 2.30 m long (2.1 m span) rectangular steel-reinforced concrete beams. Five beams were tested under the ROBUST programme. Two were unstrengthened and used as control beams, three were strengthened at their soffit with CFRP plates with end anchorages provided. Steel plates were bolted to the CFRP plates and secured to the beam using mild steel bolts. Prior to the cyclic loading, the load was taken to the maximum load to be used in the subsequent fatigue cycles. The beams were then loaded in fatigue through four-point bending at a frequency of 1 Hz. The loading options were selected by Barnes and Mays (refer to Table 2.2), so that meaningful comparisons could be established between the results of strengthened and unstrengthened beams.

The observations from the tests showed that strengthened beams had a flexural stiffness 46 percent higher than that of the unstrengthened beams. The unstrengthened beams failed by internal steel reinforcement yielding, whereas the strengthened beams failed by fracture of the internal steel reinforcement. The strengthened beams exhibited greater fatigue life than the unstrengthened beams due to CFRP plate delaying the onset of cracking and reducing crack widths. With respect to loading options 1 and 2 (Table 2.2), the strengthened beams have considerably enhanced fatigue lives. For the case of loading option 3, the fatigue life of the strengthened beams was less than that of the unstrengthened beams. The suggestion by Barnes and Mays for anchorage at the ends of the CFRP plates was because of the belief that premature failure may occur due to debonding of the plate ends.

With regards to the conclusion of Barnes and May (1999) about end anchorage plates, testing by Hollaway and Leeming (1999) on static tests on 18 m long beams strengthened with the same CFRP showed that anchorages were unnecessary when the plates extended over the full tension zone. Furthermore, Hollaway and Leeming suggested that design of anchorage, in particular bolted anchorage systems in composite materials, is considerably more complex than with standard structural materials such as steel, since fibre reinforced materials can be significantly weakened by the introduction of holes as high stress concentrations can develop in regions of discontinuities. Hence, if the need for end anchorages can be avoided, the strengthening technique becomes more practical.

Table 2.2- Loading options chosen by Barnes and Mays (1999).

Load type	Loading option	Reason
1	Apply same loads to both strengthened and unstrengthened beams.	Simulate the case where the loading on strengthened structure does not increase after rehabilitation of the beams.
2	Apply loads so that same stress range in the internal steel reinforcement to both strengthened and unstrengthened beams.	Fatigue life of RC beam is dependent on stress range of internal steel reinforcement.
3	Apply same percentage of ultimate load capacity to both strengthened and unstrengthened beams.	Testing if the fatigue life of the unstrengthened beam is achieved in strengthened beam under increased load.

Shahawy and Beitelman (1999) studied static and fatigue performance of reinforced concrete beams strengthened with CFRP sheets. A total of sixteen 6 m long, 5.79 span, T-beams were tested with 10 beams tested under monotonic load and six under fatigue load. Three variables were studied in the static tests; the concrete compressive strength, the placement of CFRP reinforcement and the number of CFRP laminates. In both the static and cyclic load tests, the effects of two and three layers of CFRP laminate strengthening systems were investigated. Description of the test specimens tested under fatigue is shown in Table 2.3. Control specimen C-OL5-FB in the fatigue test was initially damaged in fatigue to approximately one-half of its fatigue life, and then rehabilitated with CFRP sheets (re-labelled as specimen C-2L5-FB). For all specimens in fatigue, CFRP laminates were applied at both the soffit and sides of the beam (U-shaped), and from face-to-face of supports (Figure 2.3). Loading was conducted at a frequency of 1 Hz at loads ranging from 25 to 50 percent of the ultimate capacity.

In the Shahawy and Beitelman fatigue tests, all specimens failed at cycles considerably below the expected value for the stress ranges to which the internal steel reinforcement were subjected. This was attributed to the stirrups being welded to the main steel reinforcement. The rehabilitated specimen performed extremely well under fatigue, exceeding the fatigue life of the control, even though it had been significantly pre-damaged before rehabilitation. The fatigue life of specimens strengthened with two and three layers of CFRP laminates were

Table 2.3 – Fatigue test program of Shahawy and Beitelman (1999).

Specimen	Number of cycles, *N*	Description
C-OL5-FA	295,000	Control specimen fatigued to failure.
C-OL5-FB	150,000	Cycled for 150,000 (About ½ fatigue life)
C-2L5-FB	2,000,000	Specimen C-OL5-FB (after 150,000), reinforced with 2 layers of U-shaped CFRP laminates.
F-2L5-A	1,800,000	2 layers of U-shaped CFRP laminates.
F-2L5-B	1,756,000	2 layers of U-shaped CFRP laminates
F-3L5-A	3,000,000	3 layers of U-shaped CFRP laminates.
F-3L5-B	3,215,000	3 layers of U-shaped CFRP laminates.

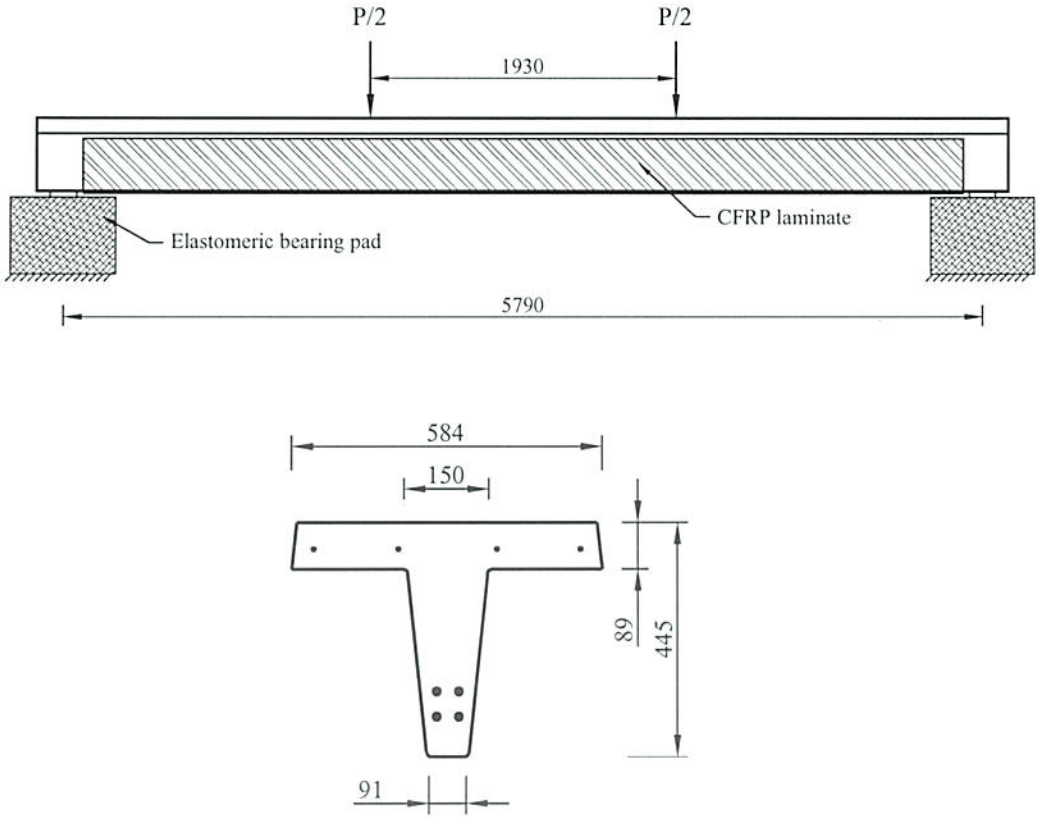

Figure 2.3 – Details of test specimens by Shahawy and Beitelman (1999).

better by seven and 10 times respectively, when compared to the control specimen although the ductility was reduced with an increasing number of plies.

Papakonstantinou et al. (2001) studied the effects of GFRP rehabilitation systems on fatigue performance of 17 rectangular reinforced concrete beams 1.32 m long (span 1.22 m). All beams were tested in four-point bending with eight beams strengthened at their soffit with GFRP. Three beams (two unstrengthened, one strengthened) were initially tested under monotonic loading to establish their ultimate load carrying capacity with the design of the beams such that they failed in flexure. The applied load levels were selected such that the internal steel reinforcement stresses were similar for both strengthened and unstrengthened specimens.

In the static tests of Papakonstantinou et al., the strengthened specimen was stiffer than the unstrengthened one before and after yielding of the internal steel reinforcement. The strengthened specimen had an increased capacity of approximately 50 percent of the unstrengthened specimen but a reduction in ultimate deflection of less than 10 percent. Both strengthened and unstrengthened specimens had the same primary failure mechanism, yielding of the internal steel reinforcement. The strengthened specimen also failed by delamination of the GFRP sheets from the beam soffit.

From the fatigue tests of Papakonstantinou et al., all specimens exhibited a similar primary mode of failure of fatigue of internal steel reinforcement. Debonding of the GFRP sheets was the secondary failure mechanism for the strengthened beams and always started between two close flexural cracks. All but one specimen exhibited debonding of the GFRP sheet, either with or without the concrete cover torn off the specimens (Figure 2.4a). One specimen, which was subjected to a maximum load equal to the yielding load, experienced a secondary failure mechanism due to propagation of a major shear crack from a load point to its nearest support, leading to debonding of GFRP sheet (Figure 2.4b). The final deflections of specimens subjected to fatigue loading were very close to that recorded during static tests. The fatigue life of the strengthened specimens for the same load range is about three times greater than that of the unstrengthened specimens. The strengthened and unstrengthened specimens subjected to the same stress in their internal steel reinforcement exhibited a similar number of cycles to failure.

Aidoo et al. (2004) conducted large-scale experiments on eight 6.1 m long reinforced concrete T-beams with a span of 5.64 m. The size of the beams represented a 62 percent scaling of an actual 40-year-old bridge girder over Cherokee Creek in South Carolina, USA.

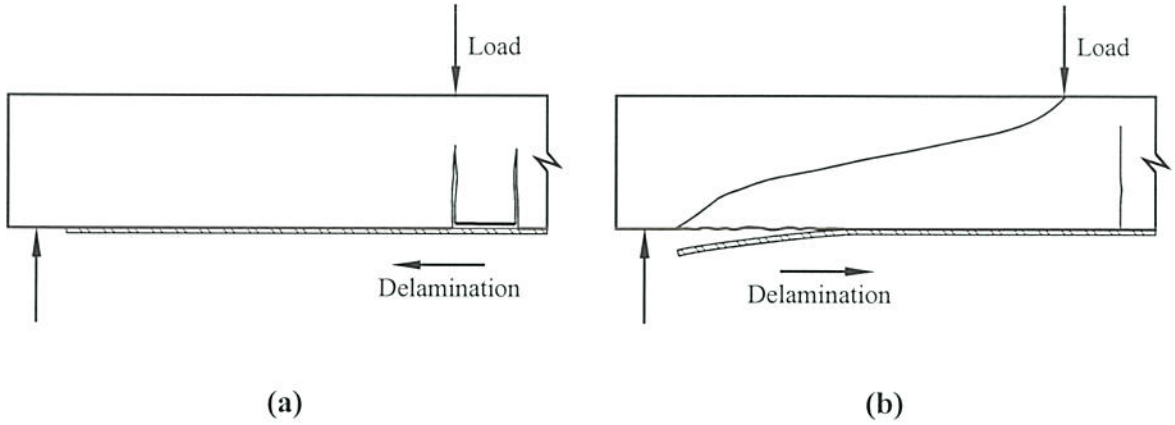

Figure 2.4 – Secondary failure modes by debonding of GFRP sheet initiating from (a) two close flexural cracks and (b) base of shear crack.

Two types of CFRP were used, a hand lay-up unidirectional fabric and a preformed strip. Four beams served as control beams and four beams were strengthened with CFRP at the web soffit. Seven specimens were loaded under fatigue by applying two levels of constant internal stress in the steel reinforcement (one high, one low) and one specimen was loaded monotonically. The cyclic loading was set at 1 Hz and the specimens were tested using three-point loading.

In the Aidoo et al. tests, shear cracks were observed near the midspan region of the beam, which widened as the test progressed. These cracks initiated the debonding of the CFRP near midspan with the debonding propagating towards the beam support as testing progressed. The beam failed by debonding with a sudden energy release coming from the fracture.

All seven fatigue tests of Aidoo et al. failed with little or no warning beyond a more rapid increase in deflection. Examination of the reinforcing steel fracture surfaces revealed that, in all cases, classic fatigue fracture of the reinforcing steel had occurred. Specimens loaded with high steel reinforcement stress levels failed earlier compared to those with low stress level, that is the fatigue life increased as the stress range in the reinforcing steel decreased.

The improvement observed in the fatigue life of the Aidoo et al. tests was limited by debonding of the CFRP from the concrete. Debonding generally occurred through the cement matrix and concrete cover rather than through the adhesive or the CFRP. This indicates that the bond strength of the system is controlled by the tensile capacity of the substrate cover concrete. Delamination of the strip retrofit was noted earlier than for the fabric retrofit in

tests. In conclusion, Aidoo et al. observed that the fatigue behaviour of the beams is governed by the fatigue behaviour of the primary steel reinforcement with the fatigue life of the concrete T-beams prolonged with the application of the CFRP reinforcement. That is, the improved fatigue performance results from the CFRP relieving the stress demand on the steel reinforcement.

In the tests of Aidoo et al., debonding of the laminate was initiated as a result of the relatively large spacing of stirrups in the midspan portion of the beam causing large shear cracks to develop. As the crack widths increased, relative movement of the concrete on each side of the crack caused the CFRP to pull away from the concrete on the support side of the crack. Once initiated, debonding progressed as the shear distortions of the beam increased with continued cycling.

Eight rectangular reinforced concrete beams were tested by Breña et al. (2002) in four point bending. Four beams spanned 2.69 m (Group A) and the other four spanned 3.00 m (Group B). The beams had different cross section dimensions but had the same shear span to beam depth ratio. Two different types of CFRPs with different strengthening methods were adopted, as detailed in Table 2.4 and shown in Figure 2.5. The fatigue load simulations were conducted at load amplitudes that generated stresses representative of service and overload conditions in a bridge. For the service load representation, the beams were subjected to maximum repeated loads that generate strains equivalent to 33 percent and 50 percent of the yield load of the beams. For the overload representation, strains of approximately 90 percent and 110 percent were generated.

Table 2.4 - Strengthened beam configurations by Breña et al. (2002).

Specimen Group	Type of CFRP	Method of Strengthening
A	Unidirectional sheets	2 CFRP sheets at the soffit, 4 U-shaped CFRP sheets at each shear span at 178 mm spacings.
B	Pultruded plate	Plate bonded longitudinally to side of the beam near the soffit, 4 U-shaped woven fabric payers at each shear span at 203 mm spacings.

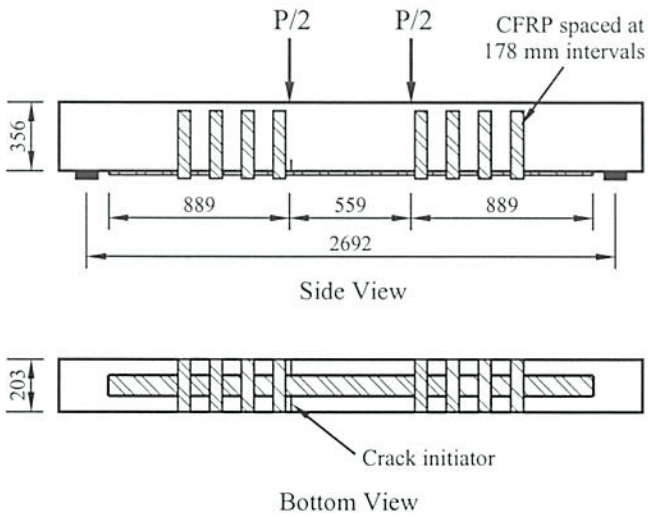

(a)

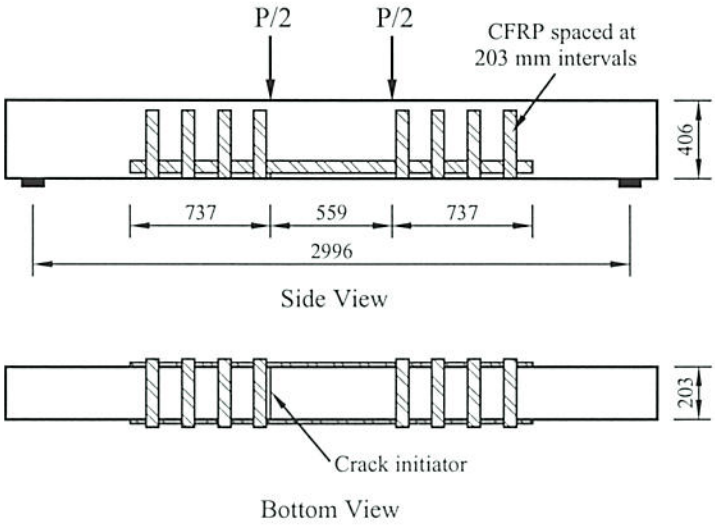

(b)

Figure 2.5 – Details of test specimens in (a) Group A and (b) Group B of Breña et al. (2002).

In the Breña et al. tests, application of fatigue load was achieved using a closed-loop system programmed to apply a load that varied sinusoidally at a maximum frequency of 2 Hz. Specimens that did not fail after one million cycles were then loaded statically to failure. For specimens representing beams subjected to service load conditions, new cracks stopped forming after approximately 100 cycles and, at the same time, existing cracks stabilised and did not propagate further. In cases of overload simulations, however, cracks grew and increased in width during load cycling. The measured midspan deflections increased with cycling and this increase was more pronounced for beams subjected to peak loads

approximately equal to the yield load. Seven of the specimens failed by CFRP debonding, whereas one specimen from Group A and subjected to an overload simulation, failed by fracture of steel reinforcement. Load-deflection plots of beams that were tested statistically to failure after one million cycles reduced to that of the undamaged beam static test.

Dong (2002) conducted a series of tests involving ten reinforced concrete beams of span 2.90 m and loaded under fatigue. The investigation was aimed at determining the significance and influence of loading range on the fatigue failure mode of CFRP-strengthened beams. CFRP fabric was bonded to the beam soffit after pre-loading the beam to give a few observed flexural cracks. The load ranges were between 10 and 35 percent, and 10 and 90 percent of the expected ultimate load capacity. The specimens were loaded under fatigue at the frequencies of 0.8 to 2 Hz. Results from the tests by Dong showed that all the beams failed in the form of steel reinforcement rupture, except for three beams. One, which was subjected to a much lower load range, did not fail after 2 million cycles. For the other two beams, which were loaded at a high range, one failed by FRP debonding, and the other through shear failure. The beam that did not fail after 2 million cycles was loaded monotonically to failure and concrete crushing along with FRP debonding at midspan occurred almost simultaneously.

In the Dong tests, debonding failure was by concrete cover separation at midspan and interface failure towards the plate ends. The beams that failed through steel reinforcement rupture experienced debonding at almost the same time. Debonding always started from the flexural cracks which were the closest to the location of steel fracture. In the beam that failed through debonding of the FRP, debonding occurred for only half of the FRP width, and initiated in the vicinity of a crack below one of the load points, and propagated towards the end. Further cycles then caused FRP-concrete interface debonding towards the plate end and concrete cover separation towards midspan. All this time, the steel reinforcement was still effective. The beam that failed in shear had major shear cracks. Debonding initiated at one of the cracks and propagated rapidly. The final deflections of the beams under fatigue are larger than the average maximum deflection of beams under static load, as shown in Figure2.6.

Lopez et al. (2003) studied the use of CFRP to strengthen four reinforced concrete beams subjected to low temperature conditions (-29°C). Two specimens were tested monotonically to failure and two tested under high amplitude cyclic load. The cyclic load was taken as 10 to 80 percent of the failure load obtained from the static test. Details of the test specimens are given in Figure 2.7. Test specimens A and C were loaded using displacement control at a rate of 0.13 mm/s. while specimens B and D were loaded cyclically at a frequency of 3 Hz. Both test specimens A and B failed by partial debonding of the CFRP plate. The epoxy adhesive

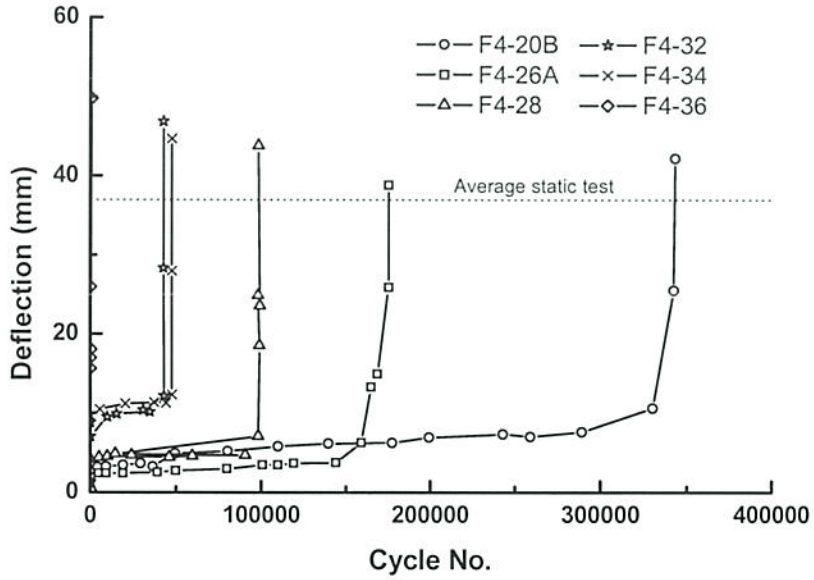

Figure 2.6 – Deflection versus cycle number of test specimens under fatigue by Dong (2002).

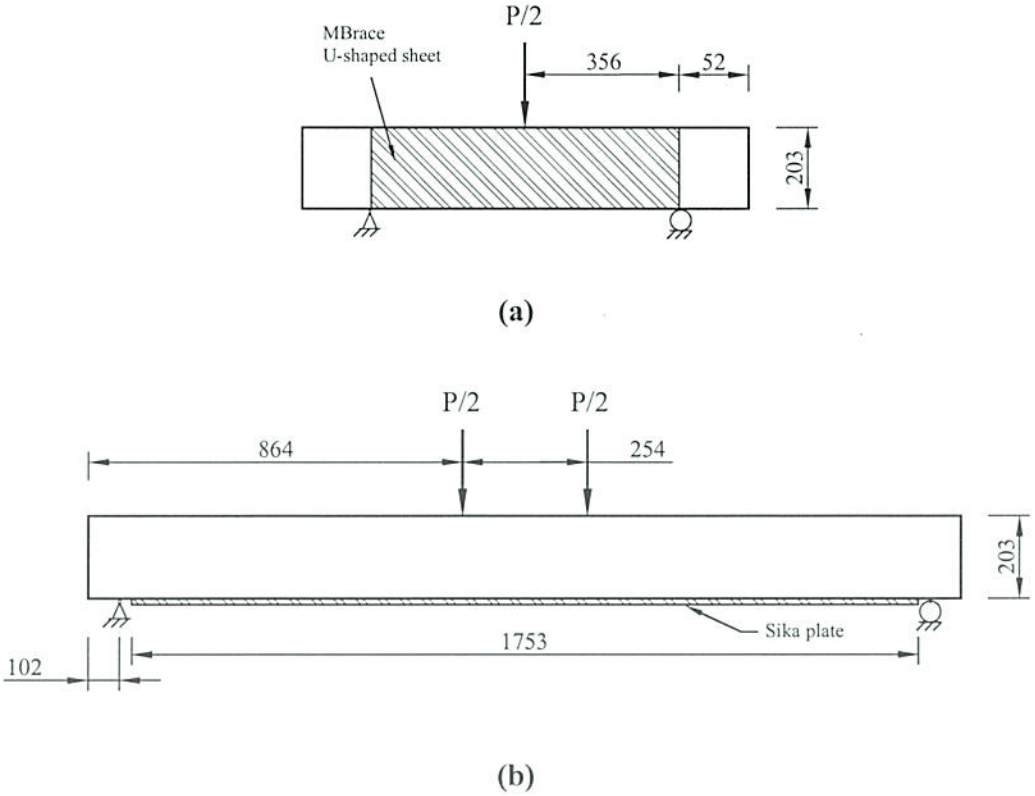

Figure 2.7 – Test specimens of Lopez et al. (2003): (a) Specimens A and B, and (b) Specimens C and D.

between the concrete and the CFRP tore out the concrete just above the interface. The debonding length was around 1.06 m, which was 60 percent of the bonded CFRP length. There was no evidence of the effects of fatigue cycles or low temperatures on the failure mode. Test specimen D failed by fatigue of three of the steel bars in the extreme layer of reinforcement and under the load point.

Wu et al. (2003) presented results of an experimental study on static and fatigue behaviour of pre-cracked reinforced concrete beams strengthened with CFRP sheets under three-point bending. The specimens were 700 mm long (600 mm span) and were initially crack-damaged by pre-loading until the sum of two crack widths was equal to 0.7 mm. Of the 11 test specimens, four beams, of which two were CFRP-strengthened, were subjected to static loading and seven specimens, of which four were CFRP-strengthened, were subjected to fatigue loading. The strengthened beams were reinforced with one layer of CFRP sheet at the soffit and U-shaped strips on the sides at the end of the beams. Two kinds of U-shaped strips were implemented for shear strengthening. One had a width of 75 mm, the other was wider such that one of the CFRP edges met with the initial cracks (Figure 2.8). Cyclic loading was applied at 4 Hz with different load ranges.

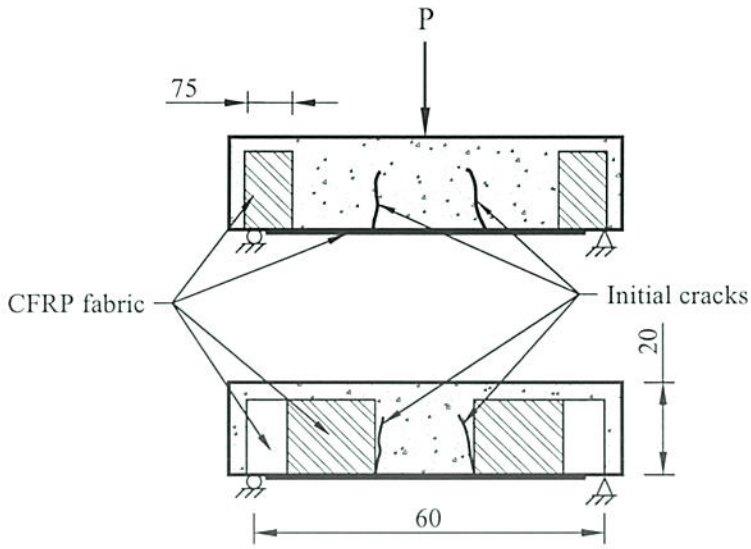

Figure 2.8 – Test specimens of Wu et al. (2002).

The fatigue failure of the Wu et al. control specimens happened suddenly due to fracture of the internal steel reinforcement. It was observed that the larger the stress range, the smaller the number of cycles to fatigue failure of the beams. One of the strengthened beams, which did not fail after 2 million cycles was loaded statically and was found to have a similar failure

load as that of strengthened beams only loaded statically. At the end of the fatigue test, delamination of concrete was observed at the middle of the beam, and debonding was observed at the end of CFRP sheet. For all strengthened specimens, it was observed that during the fatigue test, the CFRP sheets were still in good condition after the break of internal steel reinforcement, and they continued to take the fatigue loading.

The Wu et al. test results showed that the strengthened beam had a better fatigue life than the unstrengthened beams when both had the same stress range in the steel reinforcement. Their conclusion was that for beams with small shear span/beam depth ratio, besides strengthening at soffit, additional shear strengthening is usually necessary under static and fatigue loads. The CFRP sheet reduced the propagation of cracks because of the bridging effect. On the other hand, the stress redistribution with CFRP sheet and steel reduce the stress range in the internal steel reinforcement. The main reason of fatigue failure of reinforced concrete beams strengthened with CFRP is the fracture of internal steel reinforcement and the specimen may not fail completely after steel fracture.

Gheorghiu et al. (2004) investigated 13 rectangular reinforced concrete beams of length 1.22 m that were exposed to environmental fatigue and static loads. Twelve of the specimens were strengthened with CFRP, of which six were with Sika CarboDur unidirectional plate and remaining six with Mitsubishi REPLARK sheets. The method of strengthening for both CFRP types were different. The ones with Sika CarboDur plate were bonded to the beam soffit starting 400 mm from each end, leaving length of 260 mm unbonded in the central portion (Figure 2.9). This configuration was selected to avoid concrete crushing and to trigger failure by delamination of the CFRP near the centre. For the REPLARK type strengthened specimens, the plates were bonded fully to the beam soffit. In addition, U-shaped GFRP were bonded at each end to act as an anchorage. After strengthening, the beams were submitted to accelerated aging conditions by two methods. The first method was a series of wet-dry cycles for 13 weeks and the second was continual immersion in ordinary water and saltwater. The loading frequency used for the cyclic loading was 2 Hz, with load level oscillating between 15 and 35 percent of the calculated yield load.

Results from the tests by Gheorghiu showed that the exposure to saltwater or ordinary water was not found to be a significant parameter for this series of tests. From the first cycle of loading, large strains were measured in the CarboDur reinforcement, whereas it took a certain level of concrete cracking before the REPLARK reinforcement would be activated. For the range of applied cyclic loads tested, the extent of damage in the CFRP-reinforced beams was minimal. Local stiffness seemed to degrade more rapidly for the REPLARK reinforced specimens.

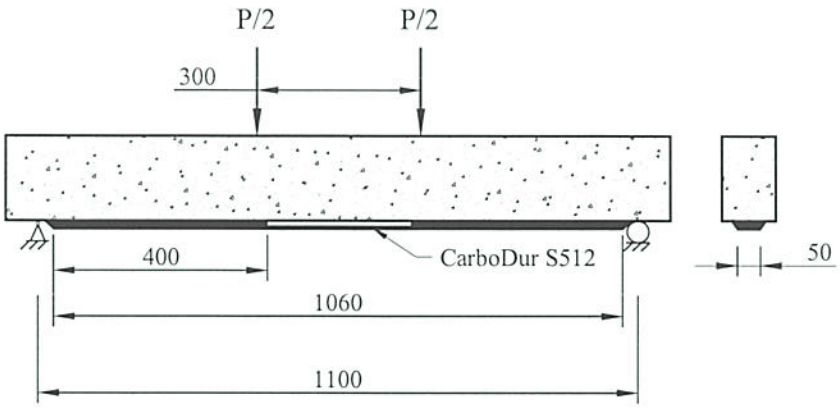

Figure 2.9 – Test specimen of Gheorghiu et al. (2004) strengthened with CarboDur plates.

Heffernan and Erki (2004) loaded twenty 3.0 m (2.85 m span) and six 5.0 m (4.80 m span) rectangular reinforced concrete beams monotonically and cyclically to failure. Two types of CFRP were investigated; a carbon fibre unidirectional pre-pregnated sheet, used for the 3.0 m beams, and REPLARK carbon fibre sheets, used for the 5.0 m beams. Prior to testing, representative samples of the concrete for the beam tests were shaped into cylinders and tested for their monotonic and cyclic characteristics. Similarly, representative samples of the steel reinforcement were tested. Coupon specimens of both CFRP types were tested for their tensile modulus of elasticity. However, a test for the ultimate capacity of the fibres was not performed due to its complexity and beam failure due to FRP fracture was not anticipated. Also, cyclic properties of the CFRP were not determined owing to the difficulty of gripping the ends of the coupons.

Heffernan and Erki applied three types of cyclic loading to give a target fatigue failure of the steel reinforcement at between 10^6 and 10^7 cycles. The loading plan was chosen so that it provided a certain percentage of stress range in the steel reinforcement, listed in. Table 2.5. The 3 m beams were strengthened with seven layers of CFRP sheets and loading was conducted at 3 Hz. In the 5.0 m beam tests, reinforcement configurations in terms of layers of CFRP sheets were investigated. The number of strengthening layers used was two, four and six. The beams were loaded at frequency of 1.5 Hz.

Heffernan and Erki observed from the cyclic loading of concrete cylinders in their ancillary tests that the concrete underwent softening with an increasing numbers of loading cycles. The centre span displacements for strengthened beams were lower than the unstrengthened ones. Displacements were constant until just prior to failure, when displacements increased rapidly. The failure mode of the strengthened and unstrengthened beams was the same, which was fatigue fracture of internal steel reinforcement.

Table 2.5 – Test specimen configuration of Heffernan and Erki (2004).

Specimen size (mm)	No. of specimens	Testing stress	
		Minimum stress / Yield stress	Minimum stress / Yield stress
150 x 300 x 3000	2 controls, 2 with FRP	0.2	0.8
	2 controls, 2 with FRP	0.2	0.7
	2 controls, 2 with FRP	0.2	0.6
300 x 574 x 5000	2 controls	0.2	0.7
	1 with FRP (2 layers)	0.2	0.7
	1 with FRP (4 layers)	0.2	0.7
	1 with FRP (6 layers)	0.2	0.7

Heffernan and Erki did not observe any damage to the CFRP for the strengthened beams during failure. Despite failure through steel reinforcement fracture, the strengthened beams were still able to continue supporting load cycles. After failure, the CFRP sheets failed through a combination of shearing, peeling or sudden rupture of the fibres. When tested at high, medium and low load ranges, the average increase in fatigue lives of the strengthened beam compared to the unstrengthened ones were 155, 182 and 537 percent, respectively. In the 5.0 m beams, the fatigue life of the strengthened beams with two layers of CFRP was 7.5 percent lower than the unstrengthened beams, whereas those strengthened with four and six layers were 85 and 200 percent longer than the unstrengthened beams. In conclusion, concrete softening due to cyclic loads leads to an increase in the steel reinforcement stress. By strengthening with CFRP, the increases in steel stress were not as large as that in the unstrengthened specimens. No significant degradation in the CFRP sheets or CFRP-concrete interface was observed due to cyclic loading.

2.4 Fatigue behaviour of corroded RC beams

Roper and Hetherington (1982) studied the fatigue performance of fifty 1.8 m long reinforced concrete beams in air, 3 percent salt solution and sea water. The types of reinforcement used were hot-rolled and cold-worked deformed bars that were similar in chemical compositions. Only results of the specimens with hot-rolled bars are presented here. The beams were tested at 6.7 Hz and the fatigue lives varied from 200,000 cycles to greater than 10 million cycles. Under the same stress range, fatigue lives were longest for beams tested in air, followed by those tested in seawater and lastly in salt solution. Pitting corrosion was observed in the reinforcement of the beams tested in the salt solution and in seawater. The exact mass loss, however, was not reported.

Radain (1989) investigated the cyclic behaviour of 900 mm long beams submerged in seawater. The load ranges were from 41 to 92 percent of the static failure load. All beams failed by fatigue fracture of the tensile reinforcing bars. Measurement taken of the electrical potential indicated a high probability of corrosion in the steel reinforcement, however, the mass loss was not reported.

Oyado et al. (2003) tested ten by 2.1 m long reinforced concrete beams that were subjected to accelerated corrosion. The parameters investigated were the level of corrosion damage (mass loss of reinforcement of 8, 15 and 20 percent), diameter of tensile steel reinforcement (13 mm and 16 mm) and the design number of load cycles to failure (0.2 million, 0.5 million and 2.0 millions). As expected, the fatigue lives decreased as the corrosion level increased.

2.5 Fatigue behaviour of mortar-repaired RC beams

Paterson and Dill (1987) reported an investigation by Laing on the fatigue behaviour of reinforced concrete beams repaired with either cementitious or epoxy-based material. Eight beams were cast with pockets extending 250 mm from the centre of the beams and having either 0 mm (shallow pocket) or 25 mm (deep pocket) clearance between the tensile reinforcement bars and the concrete (Figure 2.10) After curing, the beams were exposed to seawater for one month before repair to allow corrosion to take place in the exposed bars. After repair using cementitious material, beams with shallow pockets were observed to

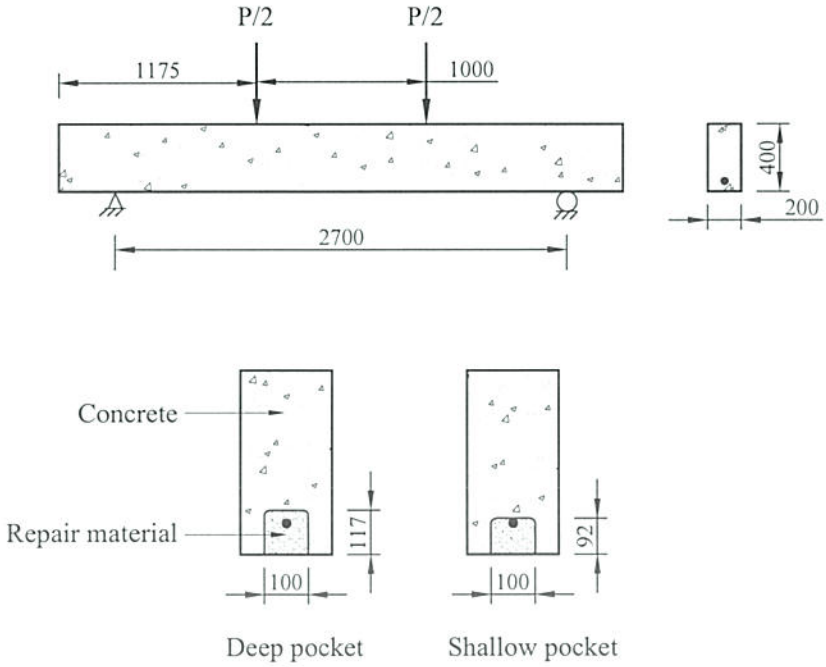

Figure 2.10 – Details of test specimens by Paterson and Dill (1987).

behave as a normal beam would under fatigue in seawater. Beams with deep pockets had results that were within the lower bound of the normal scatter of beams in seawater. Those with deep pockets and repaired with epoxy-based materials had significantly reduced fatigue lives, about half the lives of comparable normal beams, whereas beams with shallow pockets showed mixed results of failing at a life either below the lower bound life or within the upper bound life of normal beams. These limited tests shows that repair using cementitious repair material provides more positive protection against continued corrosion of the reinforcement and that better bond to the reinforcement is provided by allowing a clearance between the bar and the parent concrete prior to repair.

Emberson and Mays (1996) tested 12 by 2.54 m long (2.42 m span) reinforced concrete beams that were repaired with each of five types of mortar repair and one concrete repair in either the tension or compression zones over a length of 1.76 m. Endurances of the repaired beams ranged from 70 percent to 280 percent of the control beams. The relatively high strengths of the mortar systems caused a significant reduction in cracking and, consequently, a much lower deflection range under cyclic loading. Repairing of the beams gave a beneficial effect in terms of fatigue performance.

2.6 Fatigue behaviour of FRP-repaired corroded RC beams

To date, there are only two published research papers, conducted by the one research group, that have investigated the fatigue behaviour of FRP-repaired corroded reinforcement. Masoud et al. (2001) tested eight corroded reinforced concrete beams of length 2.0 m (span 1.8 m) strengthened with CFRP sheets, with five tested under fatigue. Two parameters were studied in this experiment; the types of CFRP sheets (Forca-Tow manufactured by Tonen Group and Sika-Wrap manufactured by Sika Canada) and the strengthening schemes (Scheme 1: shear only and Scheme 2: combined shear and flexure using CFRP, shown in Figure 2.11). The specimens were subjected to accelerated corrosion and the mass loss was predicted to be 9 percent. It was revealed that longitudinal cracks were observed after the accelerated corrosion process for both strengthened and unstrengthened specimens, but the crack width for the strengthened one was just 20 percent of the unstrengthened specimen. All five specimens failed by rupture of internal tensile steel reinforcement.

For the Masoud et al. tests, the corroded but unstrengthened specimen had just 12 percent of the fatigue life of the control specimen, which was neither strengthened nor corroded. The fatigue life of the CFRP strengthened and corroded specimens with only shear strengthening was 2.5 and 3.8 times the fatigue life of corroded but unstrengthened specimen for CFRP Forca-Tow type and Sika-Wrap type, respectively. The fatigue life of the corroded and strengthened specimen with combined shear and flexural strengthening scheme had an

increase of 138 percent compared to that of a similar corroded specimen but with shear strengthening only. Both the strengthening schemes used by Masoud et al. (2001) extensively increased the fatigue lives of the beams.

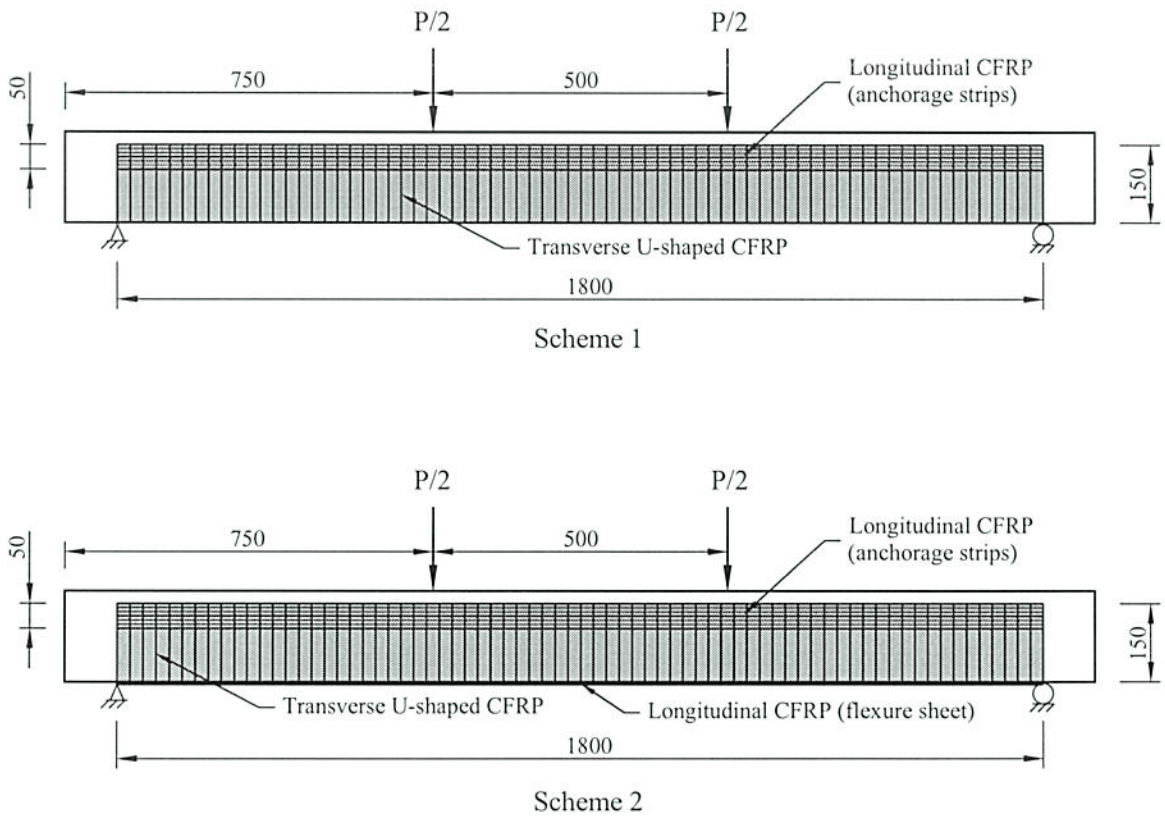

Figure 2.11 – Test specimens of Masoud et al. (2001).

Further studies on the behaviour of CFRP on strengthening corroded reinforced concrete beams were conducted by Masoud (2002). Twenty test specimens of length 3.2 m (3.0 m span) were used to investigate the strengthening effects of GFRP and CFRP on beams with different levels of corrosion in the steel reinforcement, shown in Figure 2.12. Half of the specimens were loaded statically and the other half cyclically. Short term and long term behaviours of FRP-strengthened concrete beams were investigated.

To investigate the short and long term behaviours, the Masoud specimens were first corroded to 5 percent mass loss and then repaired using either FRP repair for shear only or combined shear and flexure. For the long term tests, the specimens underwent further corrosion to either 10 or 15 percent mass loss before being tested to failure. Cyclic loading was applied to the specimens at a frequency of 1.7 Hz.

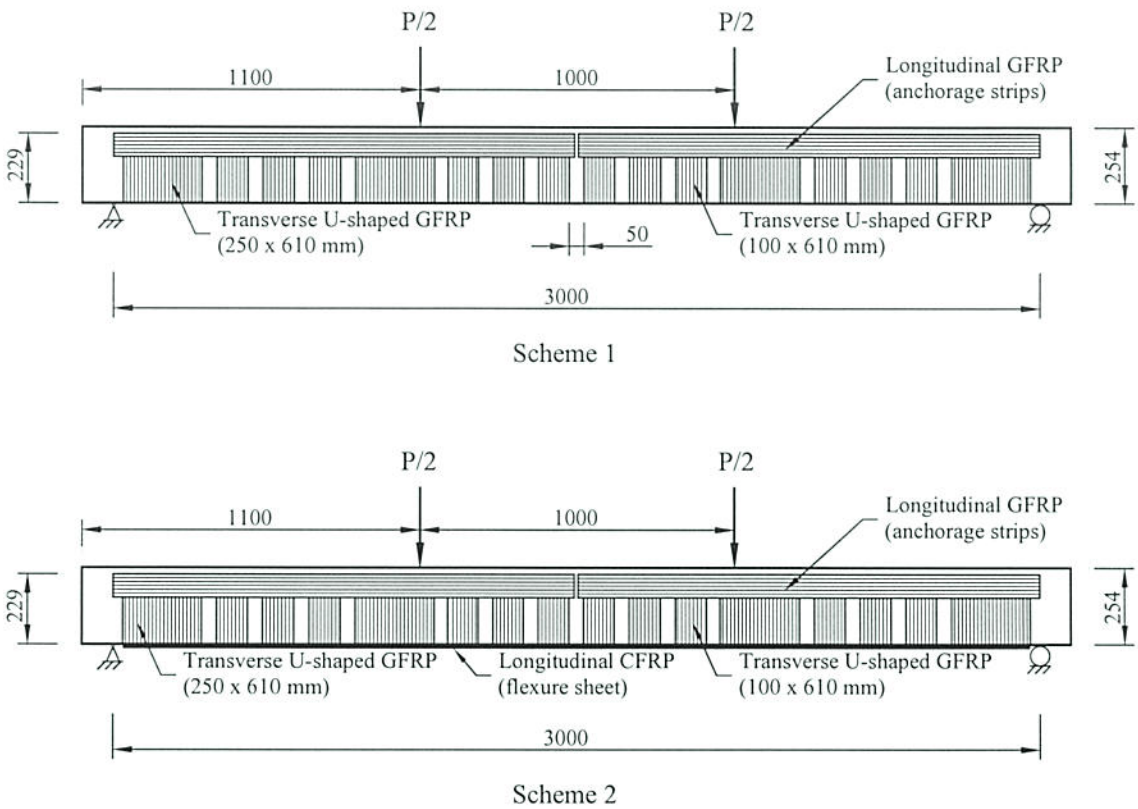

Figure 2.12 – Test specimens of Masoud (2002).

Masoud (2002) set the upper and lower load limits for the tests at 9 and 78 percent of the nominal static strength of the control beam, respectively. All of the specimens failed by fracture of one of the tensile steel reinforcing bars. Due to corrosion, the steel reinforcement became more susceptible to fatigue failure than the reinforcement in uncorroded beams. When strengthened in shear using FRP, the fatigue life increased by about 8 percent above that of the unrepaired specimen with the same mass loss. As corrosion progressed, the average rate of reduction in fatigue life was about 1.2 percent per 1 percent mass loss, whereas the corresponding rate for the unrepaired specimens was 1.5 percent per 1 percent mass loss for the unrepaired specimens. The increase in fatigue life directly after FRP repair and the decrease in the rate of reduction in fatigue life with further corrosion could be due to normal data scatter. Masoud (2002) could not conclude that FRP wrapping enhanced the fatigue life.

The test results of Masoud are shown in Figure 2.13. For the specimen repaired in combined shear and flexure for 5 percent mass loss, the fatigue life was 2.1 times that of the unrepaired specimen at the same corrosion level. With the progress of corrosion, the rate of reduction in fatigue life was 1.1 percent per 1 percent mass loss. This is smaller than the rate observed for the unrepaired specimens, but the difference falls within the scatter expected in fatigue

results. Hence, in the short term, the fatigue life can be significantly increased when FRP sheets are bonded to the soffit of beam. However, in the long term, FRP repair may not greatly affect the fatigue life.

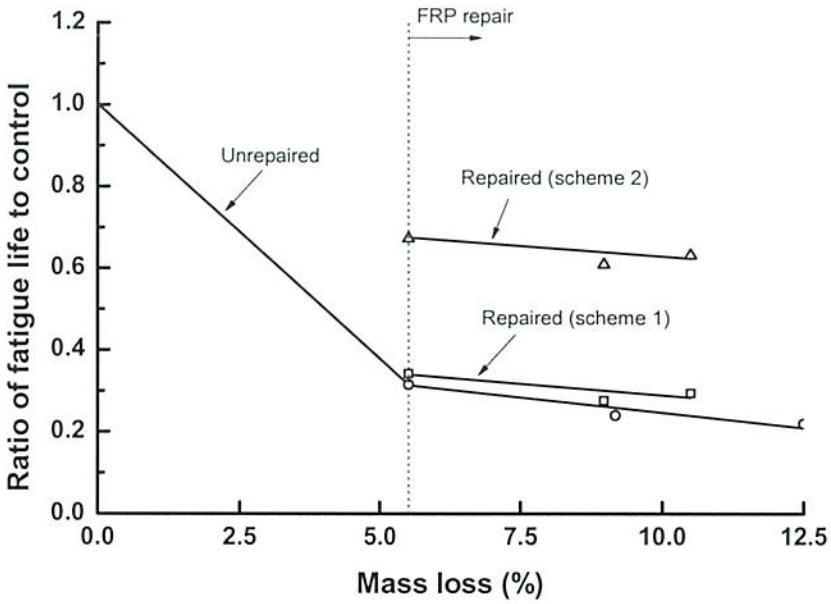

Figure 2.13 – Ratio of fatigue life of test specimens to control versus mass loss by Masoud (2002).

2.7 Fatigue behaviour of FRP-to-concrete bond

Bizindavyi et al. (2003) reported an experimental investigation of FRP-to-concrete bonded joints subjected to fatigue using single-lap joint tests. Two types of FRP laminates were used in their study; thirteen specimens were prepared using GFRP laminates and 33 specimens were prepared using CFRP laminates. Each test was performed under a constant amplitude sinusoidal loading at 1 Hz loading rate. The test parameters were the applied shear stress levels, layers of FRP laminates and joint dimensions.

During testing, three distinct phases of crack propagation were identified, shown in Figure 2.14. The first phase occurs over the region I, near the loaded end of the specimen, during the initial 10 to 15 percent of the specimen life. Formation of a crack occurs at this phase within the concrete. Crack propagation then progresses gradually in a shearing mode within region II, along the concrete-adhesive interface, during 50 to 75 percent of the specimen life. Finally, for the remaining of the specimen life, the crack propagates until failure occurs.

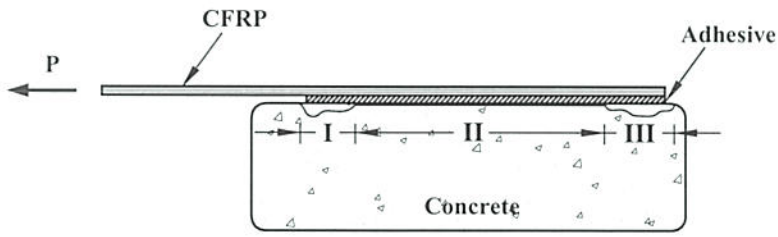

Figure 2.14 – Phases of crack propagation observed by Bizindavyi et al. (2003).

Three types of failure modes were observed: failure of the FRP laminate outside the bonded region (Failure 1), failure by simultaneous rupture of the FRP laminate and shearing of the concrete (Failure 2), and failure due to shearing of the concrete (Failure 3). Failure modes 1 and 2 were observed in FRP-to-concrete joints subjected to high cyclic stress levels, whereas failure mode 3 was observed in cases where joints were submitted to moderate and low stress levels. At the same cyclic stress range, higher maximum FRP-concrete bond slip values were obtained on the shorter GFRP-to-concrete joints than the longer ones, thus having shorter fatigue lives. For the same bonded area and cyclic bond stress ranges, the fatigue lives for the wider specimens were significantly greater than those for the narrower and longer joints. The presence of a non-zero minimum load during cyclic loading caused specimens to have a significantly shorter fatigue life than those with zero minimum loads for the same stress range. From the test data, the fatigue life curves were expressed as

$$\ln(\Delta\tau_{ave}) = a - c\ln(N_f) \tag{2.2}$$

where $\Delta\tau_{ave}$ is the cyclic mean bond stress range, N_f is the number of cycles to failure, and a and c are constants ranging from 0.08 to 1.06 and 0.041 to 0.095, respectively. Figure 2.15 shows the test results and curves from Eq. 2.2.

Bizindavyi et al. (2003) observed that as the number of load cycles increased, the FRP-concrete bond slip increased (Figure 2.16). Also, the higher the applied cyclic stress, the greater was the slip and the shorter was the fatigue life of the bonded joint.

Ferrier et al. (2005) tested six single-lap joints, shown in Figure 2.17. One test specimen acted as the control and was loaded statically until failure. It failed at a shear stress ($\tau_{ave,f}$) of 1.18 MPa. The remaining specimens were tested in fatigue to failure using different maximum stress levels, as shown in Table 2.6.

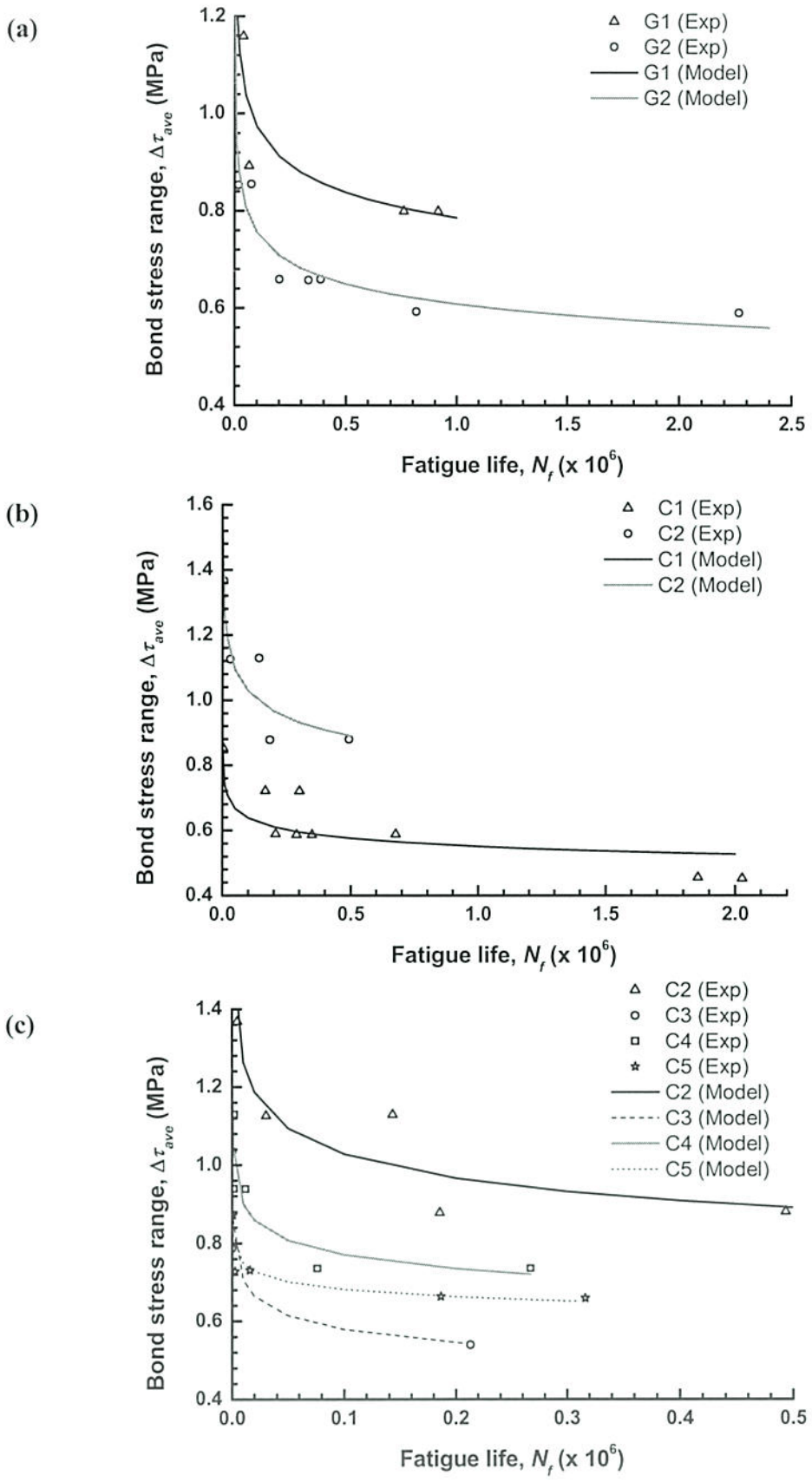

Figure 2.15 – Fatigue life ($\Delta\tau_{ave}$ - N_f) curves for specimen series (a) G1 and G2 (b) C1 and C2 (c) C2, C3, C4 and C5 by Bizindavyi (2003).

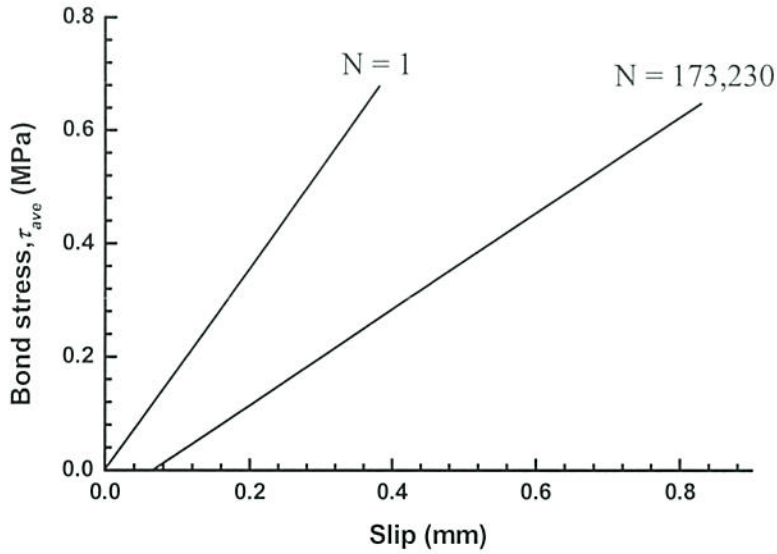

Figure 2.16 – Typical cyclic bond stress-slip relationship for a CFRP-concrete joint by Bizindavyi et al. (2003).

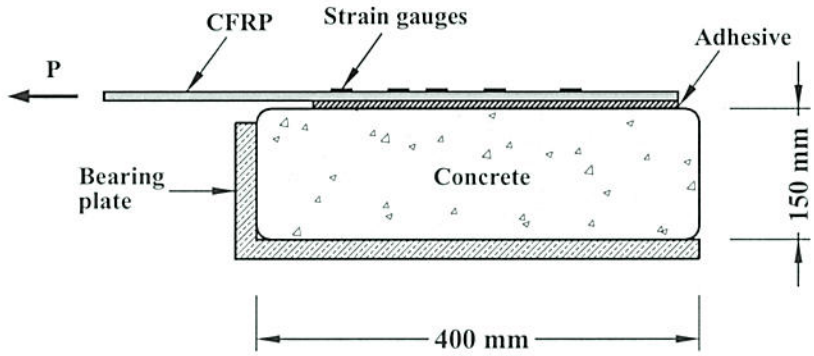

Figure 2.17 – Single-lap joint test of Ferrier et al. (2005)

Table 2.6– Single-lap joint test result of Ferrier et al. (2005).

Specimen	Failure cycle	$\tau_{ave,max}$ (MPa)	$\frac{\tau_{ave,max}}{\tau_{ave,f}}$
1	2,450	0.78	0.66
2	6,700	0.74	0.63
3	25,670	0.69	0.59
4	135,000	0.64	0.54
5	1,000,000	0.57	0.50

Ferrier et al. (2005) also conducted double-lap shear tests on CFRP-to-concrete bonded joints (Figure 2.18), using three types of adhesive (A, B and C). The control specimen failed statically at a shear stress of 1.4 MPa. The remaining three specimens were loaded in fatigue at 1 Hz. The specimens were tested using different cyclic load ranges (0.10 MPa to 1.10 MPa, 0.10 MPa to 0.90 MPa and 0.10 MPa to 0.60 MPa). Failure of the joint was observed as debonding of the composite plate. Their results show that there is an approximate linear relationship between the maximum shear stress, $\tau_{ave,max}$, and $\log N_f$ as given by

$$\tau_{ave,max} = m\log(N_f) + n \tag{2.3}$$

where the fitting coefficients, m and n are given in Table 2.7. The $\tau_{ave,max}$ - N_f curve from the test data revealed that the shear stress should be limited to 0.80 MPa to have a fatigue life of 10 million cycles at 1 Hz frequency.

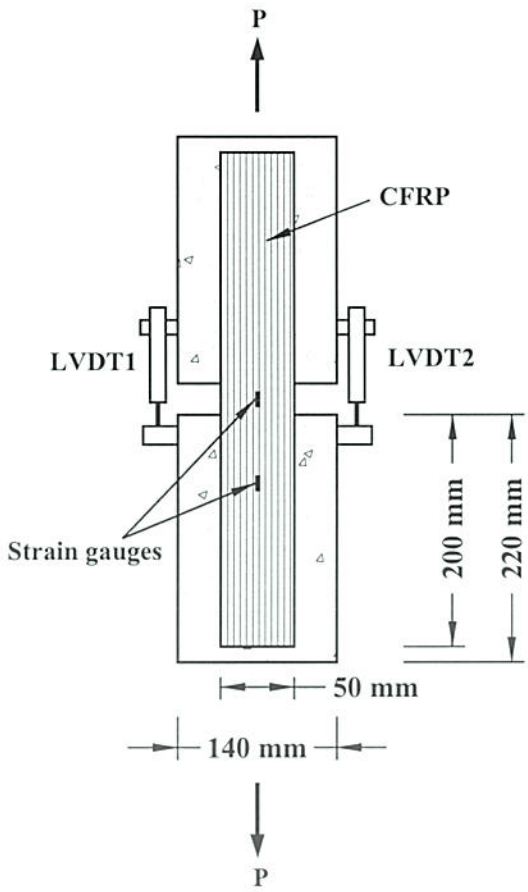

Figure 2.18 - Double-lap joint test of Ferrier (2005)

Table 2.7 – Parameters to define Eq. 2.3.

Adhesive	Parameter	
	m	n
A (double-lap test)	-0.037	1.000
B (double-lap test)	-0.033	0.991
B (single-lap test)	-0.032	0.988
C (double-lap test)	-0.032	1.009

Dai et al. (2005) conducted nine double-lap joint tests under fatigue using the test system shown in Figure 2.19. The test system exerted direct tension in CFRP and a direct shear at the CFRP-concrete interface while avoiding eccentric loading effects. The test parameters and results are shown in Table 2.8 where f_c is the concrete compressive strength and s_{max} is the slip at the loaded end just prior to failure. For the specimens with no frost damage, failure was by debonding of the FRP laminate from the concrete (FP). The specimens with frost damage failed by delamination of the concrete cover (CD). The frost damage changed the strength of concrete, weakening the bond between the reinforcing steel and the concrete. This, in turn, resulted in a cover delamination failure mode.

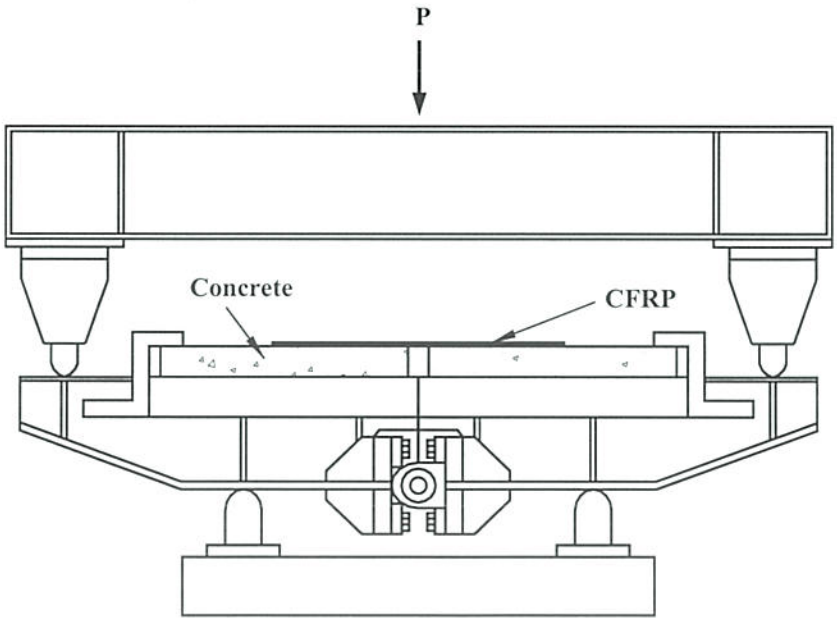

Figure 2.19 – Test system by Dai et al. (2005)

Table 2.8 – Test parameters and results of Dai et al. (2005).

Specimen	RDEM (%)	$\tau_{ave,max}$ (MPa)	f_c (MPa)	$\frac{\tau_{ave,max}}{\tau_{ave,f}}$	s_{max} (mm)	Failure cycle	Failure mode
S1-1	100 (0%	2.0	34.8	0.73	>0.41	285	FP
S1-2	frost	1.7		0.64	>0.48	23,704	FP
S1-3	damage)	1.4		0.51	>0.37	1,495,810	FP
S2-1	70	1.9	23.4	0.67	>0.34	5,710	CD
S2-2		1.4		0.50	>0.46	>2,000,000	CD
S3-1	85	2.1	34.1	0.78	>0.27	7,363	CD
S3-2		1.7		0.63	>0.31	83,858	CD
S3-3		1.4		0.52	>0.37	>2,000,000	CD
S4-3	68	1.2	25.7	0.60	>0.43	1,425,729	CD

A typical bond stress-slip relationship of CFRP-concrete joints, which was observed at a same location but under different loading cycles, is shown in Figure 2.20. The local slip increased gradually with the fatigue cycles. Along with the increase of local slip, the local bond stress reached peak value first and then degraded gradually. After a certain number of fatigue cycles, the local bond stress became small, implying the occurrence of local debonding.

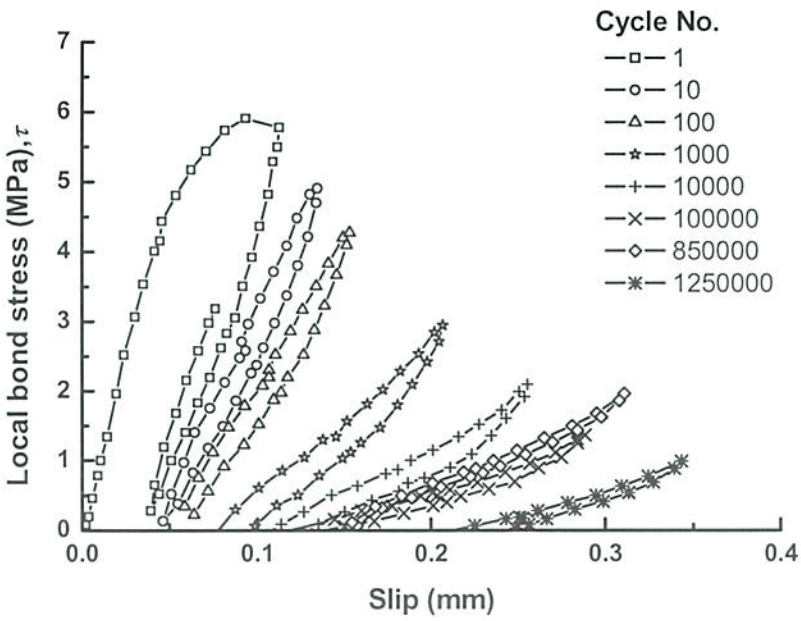

Figure 2.20 - A typical fatigue local τ -s curve of CFRP-concrete joints by Dai et al. (2005).

Figure 2.21 shows the average bond stress-slip curves for specimens S1-1 and S1-3, which were tested with $\tau_{ave,max}/\tau_{ave,f}$ of 0.73 and 0.51, respectively. The average bond stress-slip curve for Specimen S1-3 shows some nonlinearity at the first fatigue cycle but not as significant as that in Specimen S1-1. The rate of increase of slip with the number of fatigue cycles was significantly lower compared to that measured in Specimen S1-1. Therefore, the fatigue life of CFRP-concrete bonded joints is reduced with increasing bond stress levels.

As to the influence of initial frost damage, Dai et al. (2005) reported that the initial damage did not shorten the fatigue life of CFRP-to-concrete joints for the same relative tensile stress level, that is the ratio $\tau_{ave,max}/\tau_{ave,f}$ was kept as constant in the FRP sheets.

Ko and Sato (2007) tested 36 double-lap joint tests in fatigue using three experimental parameters; the type of FRP (aramid, carbon and polyacetal), layers of FRP (single and double layers), and the loading stress range. From the cyclic loading tests, the bond stress-slip relationship was observed to have a tension-softening-like curve (similar to the observation by Dai et al., 2005). The Popovic's (1973) equation was used to represent the relationship and is shown in Figure 2.22. The residual slip remained after the unloading, and the unloading/reloading stiffness tended to decrease as the slip at the unloading plateau increased. The model is defined by seven empirical parameters; the maximum bond stress τ_{max}, the corresponding slip s_{max}, curve characteristic constant a, the unloading stiffness K, the ultimate slip s_u, the friction stress τ_{fp} and the negative friction stress τ_{fn}. A linear approximation was adopted for the unload/reload path.

The fitting formula of the relationship between the unloading stiffness K, and the unloading slip, s*, was proposed as

$$K = C_2 s^{*C_3} \tag{2.4}$$

and is shown in Figure 2.23. Based on their results, Ko and Sato determined the parameters that define Figure 2.22 as those listed in Table 2.9. The correlative factor R^2 ranged from 0.42 to 0.86.

Yun et al. (2008) studied the performance of five FRP bonding systems under static and fatigue loading using double-lap joint tests with one of the bonding systems tested being externally-bonded FRP. All specimens were subjected to fatigue at 5 Hz and the test parameters and results are shown in Table 2.10.

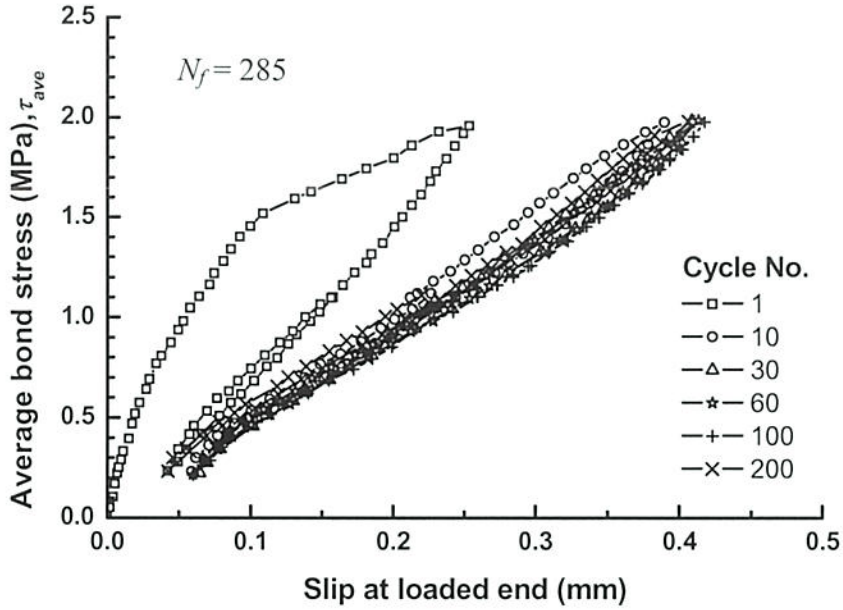

(a)

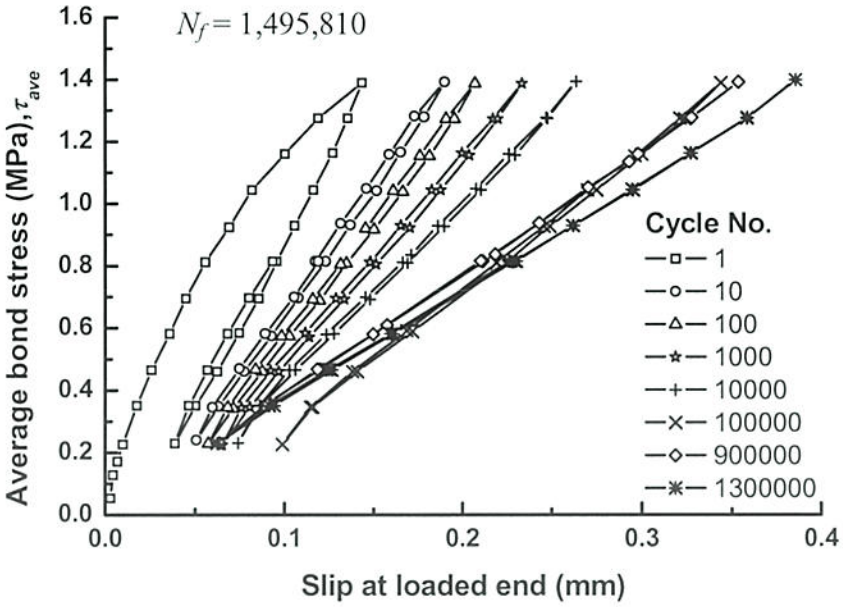

(b)

Figure 2.21 - Average τ_{ave}-s curves of CFRP-concrete joints under fatigue loading by Dai et al. (2005) for (a) Specimen S1-1 and (b) Specimen S1-3.

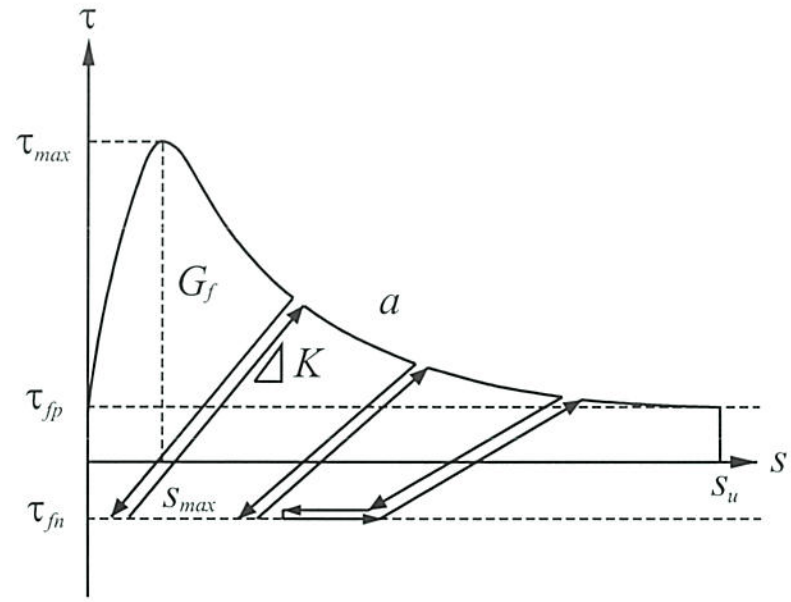

Figure 2.22 – Cyclic hysteresis model of bond stress-slip relationship by Ko and Sato (2007).

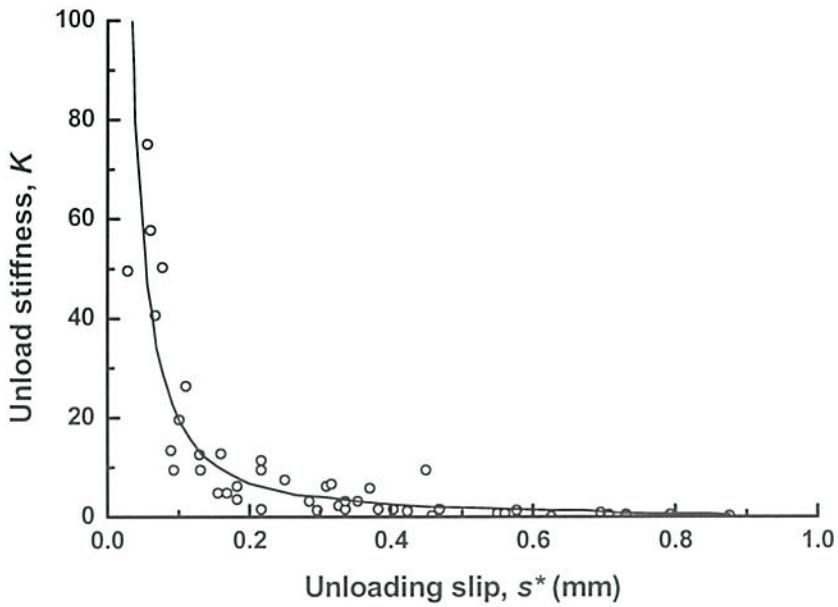

Figure 2.23 – Typical relationship between unloading stiffness, K and slip at unloading, s^* by Ko and Sato (2007).

Table 2.9 – Constants for bond stress-slip relationship, after Ko and Sato (2007).

Constant	Range of values
C_2	0.35 – 7.60
C_3	(-1.90) – (-0.93)
τ_{max}	1.73 – 3.83
s_{max}	0.01 – 0.19
s_u	0.96 – 7.41
a	1.7 – 6.4
τ_{fp}	0.02 – 0.45
τ_{fn}	(-1.12) – (-0.04)

Table 2.10– Test parameters and results of Yun et al. (2008).

Specimen	f_c (MPa)	Loading regime	$\frac{\tau_{ave,min}}{\tau_{ave,f}}$	$\frac{\tau_{ave,max}}{\tau_{ave,f}}$	$\frac{\Delta\tau_{ave}}{\tau_{ave,f}}$	Failure cycle
M-EB	40.6	Static	-	-	-	-
F-EBA	43.5	Fatigue	0.10	0.45	0.35	>2,000,000
F-EB-B	43.9	Fatigue	0.23	0.60	0.37	>2,000,000

The externally bonded specimens of Yun et al. did not fail after 2 million cycles and were subsequently loaded statically to failure. Failure was by debonding of the FRP laminate together with a thin layer of concrete.

Figure 2.24 shows the load versus slip curves at loading intervals for the specimens. Under the low-level fatigue loading of specimen F-EB-A, the slopes of the early loops slightly decrease in the early cycles and then remain unchanged thereafter, which indicates a slight reduction in the bond stiffness at the beginning that does not then deteriorate further in the later cycles. However, under the high-level fatigue loading of specimen F-EB-B, the slopes of the loops gradually decrease continuously until the end of the tests, indicating a continuous degradation in the bond stiffness. For specimen F-EB-B, which had a high load range, the areas enclosed by the loading and unloading curves at the 100th and 1,000th cycles are very small, which indicates an insignificant dissipation of energy due to the small plastic deformation (micro-cracking) of the bond at the loaded end after the first cycle. After 10,000 cycles, the areas enclosed by the loops increase gradually, indicating increasing energy dissipation as a result of the bond deterioration.

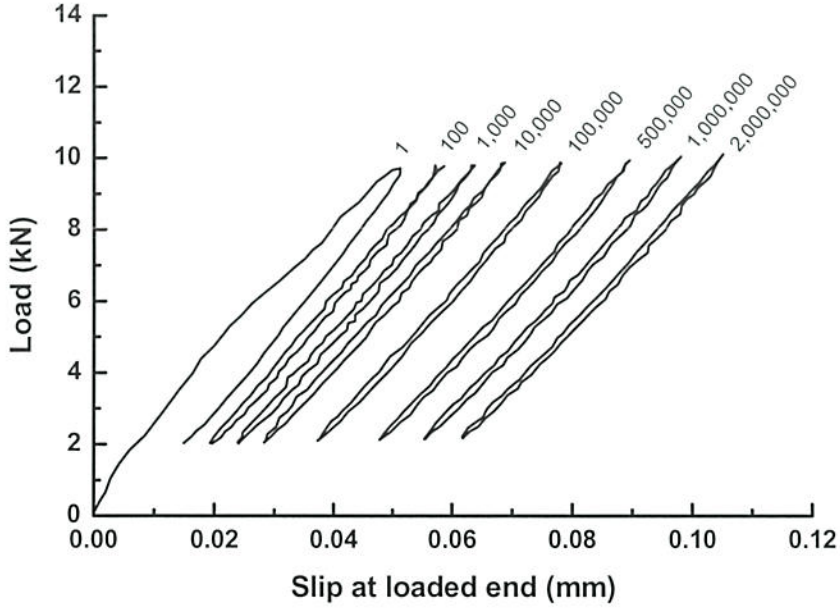

(a)

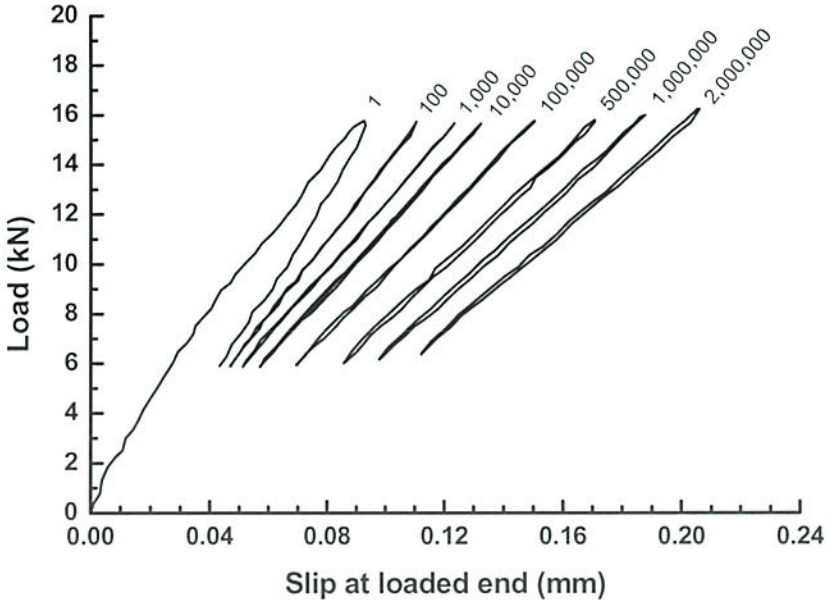

(b)

Figure 2.24 – Load versus slip curves of CFRP-concrete joints under fatigue loading by Yun et al. (2008) for (a) Specimen F-EB-A and (b) Specimen F-EB-B.

The slip versus number of cycles at both the maximum and minimum stress levels is shown in Figure 2.25. Initially, a significant increase of slip was observed between the 10th cycle and the 100,000th cycle, which was then followed by a mild growth region where the slip increased slowly until the last cycle.

Figure 2.26 shows the strain in the FRP laminate during cyclic testing, taken from strain gauges placed on the laminate at three distances away from the loaded end (10 mm, 20 mm and 50 mm). In most cases, the strain increased with the number of cycles. After 1,000 cycles, the strain at 20 mm from the FRP end in Specimen F-EB-B was less than the strain at 10 mm. This indicated a significant loss in bond stress between the 10 mm and 20 mm positions after 1000 load cycles.

After the fatigue tests, the test specimens were loaded statically to failure. As shown in Figure 2.27, the load-slip response of Specimen F-EB-A is almost identical to that of Specimen M-EB, indicating that low-level fatigue loading did not cause significant damage to the specimen and did not affect the overall bond performance. Specimen F-EB-B, which was subjected to higher stress levels, showed a reduction in bond stiffness.

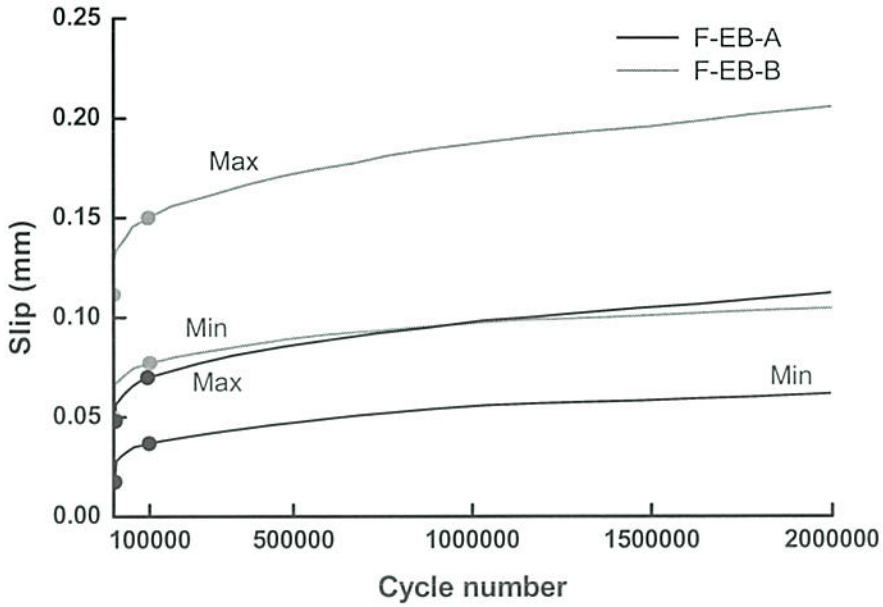

Figure 2.25 – Development of slip during cyclic loading by Yun et al. (2008).

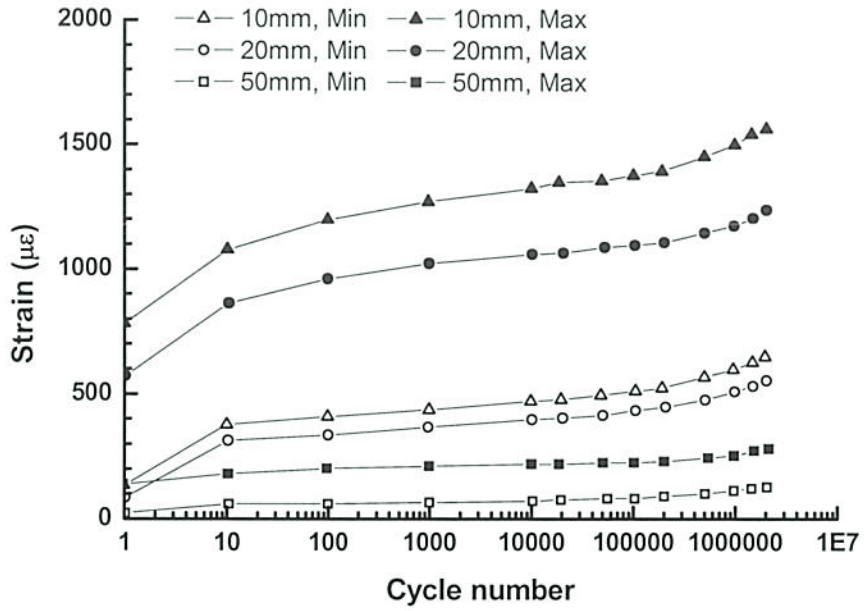

(a)

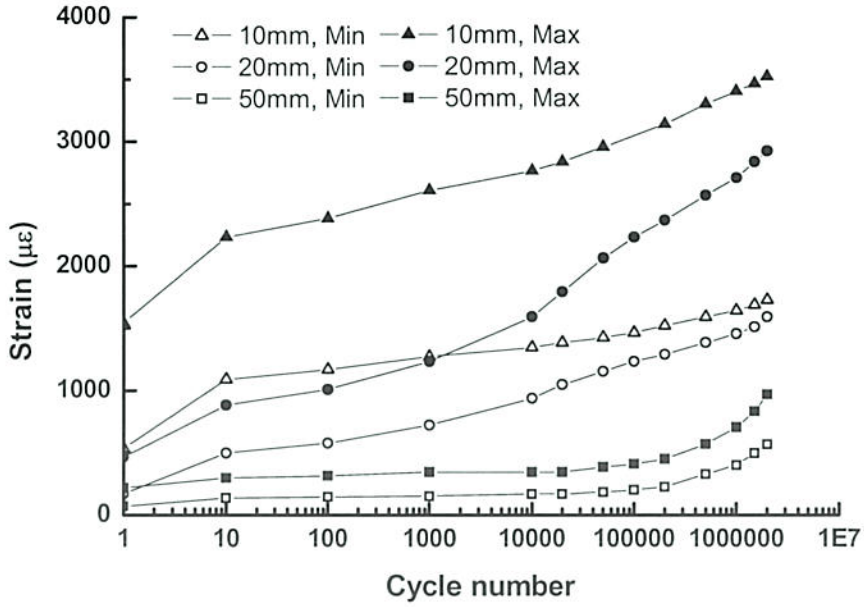

(b)

Figure 2.26 – Strain in FRP taken from strain gauges at distances from the loaded end of (a) Specimen F-EB-A and (b) Specimen F-EB-B by Yun et al. (2008).

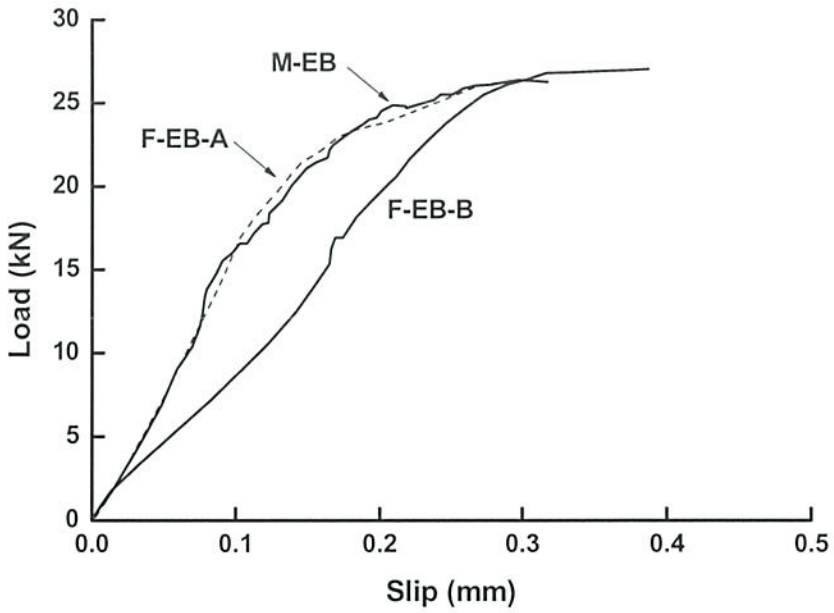

Figure 2.27 – Load-slip curves of test specimens tested to failure after 2 million load cycles.

2.8 Constitutive relationships for RC elements

2.8.1 Concrete

The stress-strain response of concrete varies with the number of load repetitions (ACI, 1974, Neville, 1996 and Holmen, 1982). It starts out with the usual concave shape, quickly transitions to a straight line, then gradually moves to a characteristic convex shape. Test observations indicate that the closer the concrete is to failure, the more convex its stress-strain response.

According to Jun and Stang (1998), the response of concrete under cyclic loading can be approximately enveloped by the quasi-static loading as shown in Figure 2.28a. For the case of a constant stress amplitude fatigue loading, the quasi-brittle response can also be used as a failure criterion, as shown in Figure 2.28b. The failure of concrete under cyclic loading occurs when the strain in the concrete reaches the strain corresponding to the cyclic stress on the descending branch of the quasi-static stress-strain curve.

In tests of Holmen (1982), it was observed that the maximum strain in concrete in compression and under cyclic loading follows three distinct stages; a rapid increase from 0 to about 10 percent of the fatigue life (Stage I), a uniform increase from 10 percent to approximately 80 percent of the fatigue life (Stage II) followed by a rapid increase to failure. Holmen (1982) proposed that the first and second stages be described by

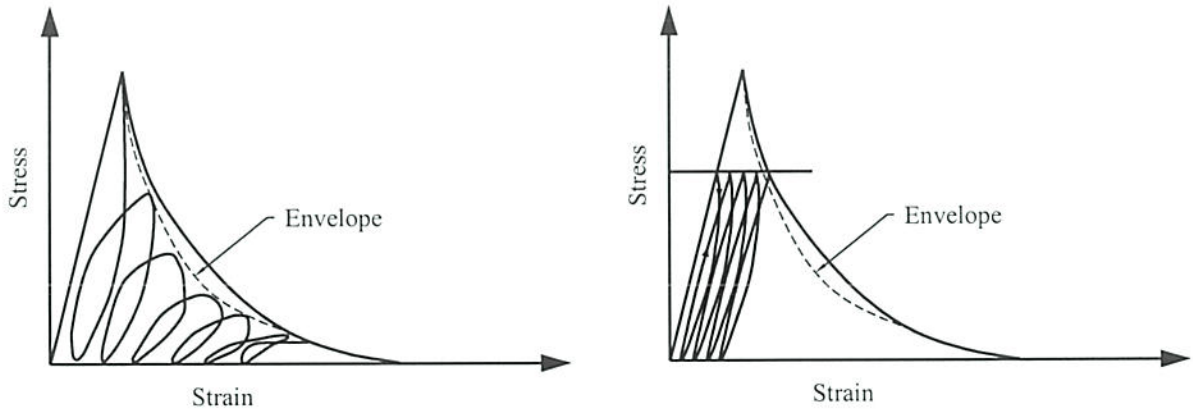

(a) **(b)**

Figure 2.28 – Typical stress-strain relation for quasi-static cyclic (a) constant strain amplitude response and (b) constant stress amplitude response, by Jun and Stang (1998).

Stage I: $$\varepsilon_{max} = \frac{1}{E_{sec}} \left| S_{max} + 3.18\left(1.183 - S_{max}\right)\left(N/N_f\right)^{0.5} \right| + 0.413\times10^{-3} S_c^{1.184} \ln\left(t+1\right) \quad (2.5)$$

Stage II: $$\varepsilon_{max} = \frac{1.11}{E_{sec}} \left| 1 + 0.677\left(N/N_f\right) \right| + 0.413\times10^{-3} S_c^{1.184} \ln\left(t+1\right) \quad (2.6)$$

where ε_{max} is the maximum strain (Figure 2.29a); E_{sec} is the secant modulus at the first cycle, S_{max} is the ratio of maximum stress to concrete strength; S_c is the characteristic stress level and is given as S_m + RMS; S_m is the mean stress ratio and is equal to $0.5\left(S_{min} + S_{max}\right)$; S_{min} is the ratio of minimum stress to concrete strength; N is the number of load cycles; N_f is the number of load cycles to failure for a specified probability of failure; t is the duration of the alternating load (in hours), RMS is the root mean square value of the stress ratio. For a sinusoidal loading,

$$RMS = \left(S_{min} + S_{max}\right)/8^{0.5} \quad (2.7)$$

The secant modulus after the first cycle, E_N is reduced throughout the fatigue life according to S_{max}, shown in Figure 2.29b.

In estimating the fatigue life, N_f of concrete, several proposals are available in literature and are summarized in Table 2.11.

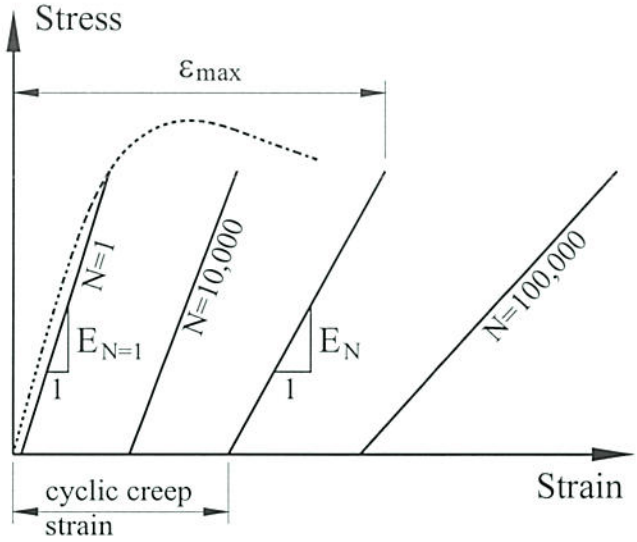

(a)

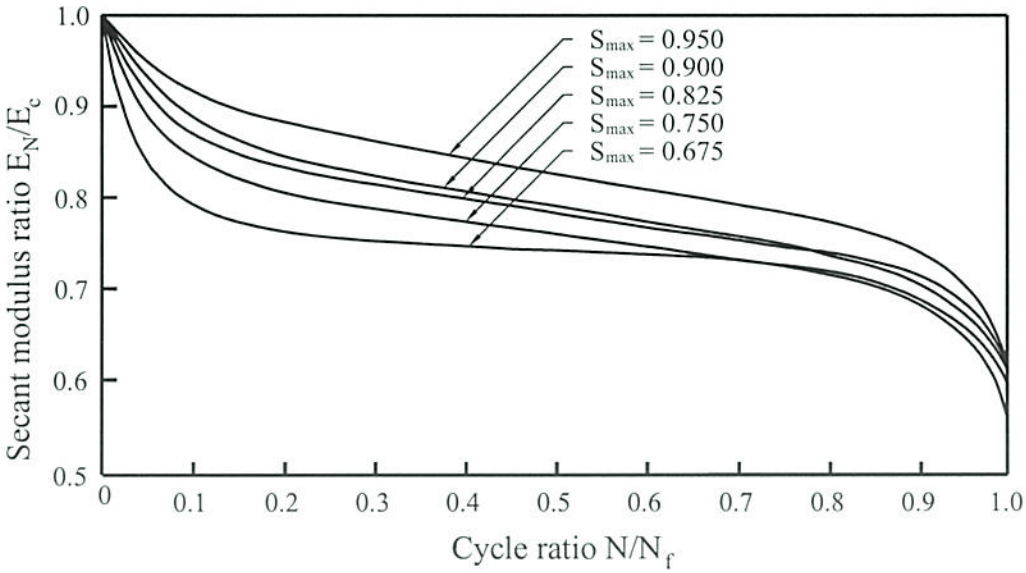

(b)

Figure 2.29 – (a) Constitutive model for concrete subjected to fatigue loading and (b) Reduction of secant modulus according to load cycle ratio and S_{max} by Holmen (1982).

Table 2.11 – Models to estimate concrete failure cycle, N_f.

Model	Expression#
JSCE (1965)	$\log N_f = 15\left[1-\frac{(\sigma_{max}-\sigma_{min})}{\left(0.9K^{'}f_c^{'}-\sigma_{min}\right)}\right]$
Aas-Jacobson (1979)	$\log N_f = \frac{1}{\beta_f}\left[\frac{1-\left(\sigma_{max}/f_c^{'}\right)}{1-(\sigma_{max}/\sigma_{min})}\right]$
Hsu (1981)	$\log N_f = \frac{1-0.0294\log T_p-\sigma_{max}/f_r}{0.0662\left[1-0.556(\sigma_{min}/\sigma_{max})\right]}$
Kakuta et al. (1982)	$\log N_f = 17\left[1-\frac{(\sigma_{max}-\sigma_{min})/f_c^{'}}{1-\left(\sigma_{min}/f_c^{'}\right)}\right]$
Waagard (1982)	$\log N_f = 10\left[\left\{1-\frac{\sigma_{max}}{\alpha_g\left(f_c^{'}/\gamma\right)}\right\}\Big/\left\{1-\frac{\sigma_{min}}{\alpha_g\left(f_c^{'}/\gamma\right)}\right\}\right]$
CEB-FIP (1988)	For $0 \le S_{min} \le 0.8$, $\log N_1 = \left(12+16S_{min}+8S_{min}{}^2\right)(1-S_{max})$ $\log N_2 = 0.2\log N_1(\log N_1-1)$ $\log N_3 = \log N_2(0.3-0.375S_{min})/\Delta S_c$ If $\log N_1 \le 6$, then $\log N_f = \log N_1$ If $\log N_1 > 6$ and $\Delta S_c \ge 0.3-0.375S_{min}$, then $\log N_f = \log N_2$ If $\log N_1 > 6$ and $\Delta S_c < 0.3-0.375S_{min}$, then $\log N_f = \log N_3$

Notes: # σ_{max} is the maximum applied stress; σ_{min} is the minimum applied stress; $K^{'}$ is a coefficient ($K^{'}=0.85$); $f_c^{'}$ is the compressive strength; β_f is a statistical factor ($\beta_f = 0.064$); T_p is the period of loading (seconds per cycle); f_r is the modulus of rupture; α_g is a factor to account for flexural gradient ($1 \le \alpha_g \le 10$); γ is the partial safety factor for materials ($\gamma = 1.25$); S_{max} is the ratio of maximum stress to concrete compressive strength; S_{min} is the ratio of minimum stress to concrete compressive strength; ΔS_c is the absolute difference between S_{max} and S_{min}.

2.8.2 *Reinforcing steel*

A significant body of research has been undertaken on fatigue of reinforcing steel in air (Moss, 1980 and Tilly, 1988) and in concrete beams (Helgason and Hanson, 1974 and Moss, 1982). The fatigue failure cycle number of reinforcing steel can be expressed in the form

$$(\Delta\sigma)^a N_f = K \tag{2.8}$$

where N_f is the number of cycles to failure $\Delta\sigma$ is the stress range for a constant amplitude loading and a is the inverse of the slope on the log-log plot (as shown in Figure 2.30). The constants K and a are given in Table 2.12. In Figure 2.30, the results for reinforcing steel bars tested in air by Tilly (1988) are compared with the data collected by Moss (1980), Moss (1982) and with CEB-FIP design model (1988). The data has a significant scatter. While typically the axially-tested fatigue cycle failure values are used in new design, performance in terms of stress range is about 20 percent higher for bending in concrete than axially in air, when the results for the 16 mm bars are compared (refer Figure 2.30a). This variation can be accounted for by the influence of the concrete between cracks in reducing the tensile stress in the adjacent bar known as "tension stiffening". Thus, the probability that the critical section for fatigue coinciding with the point of maximum stress (i.e. at a crack) is reduced and the probability of failure at a given cyclic stress range is reduced.

Table 2.12 - Fatigue failure prediction parameters for Eq. 2.8.

Model	Test in	Bar diameter	N_f	a	K
CEB-FIP (1988)	concrete	$\leq$ 16 mm	$\leq 1 \times 10^6$	5.0	0.408×10^{18}
			$\geq 1 \times 10^7$	9.0	0.794×10^{27}
CEB-FIP (1988)	concrete	$\geq$ 16 mm	$\leq 1 \times 10^6$	5.0	0.105×10^{18}
			$\geq 1 \times 10^7$	9.0	0.687×10^{27}
Moss (1980)	air	16 mm	All N	9.5	0.18×10^{30}
Moss (1982)	concrete	16 mm	All N	8.7	0.11×10^{29}
Moss (1982)	concrete	32 mm and 40 mm	All N	6.2	0.76×10^{29}

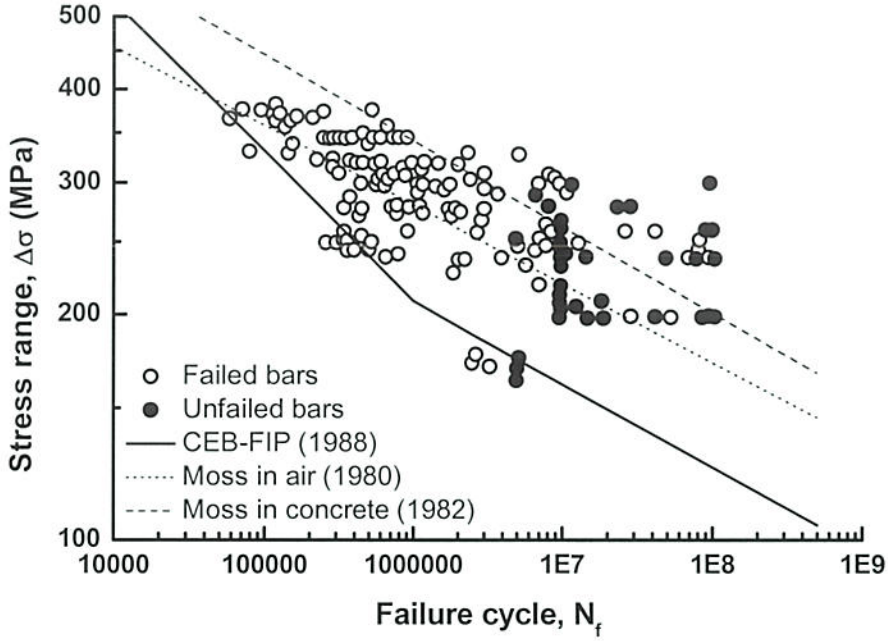

(a)

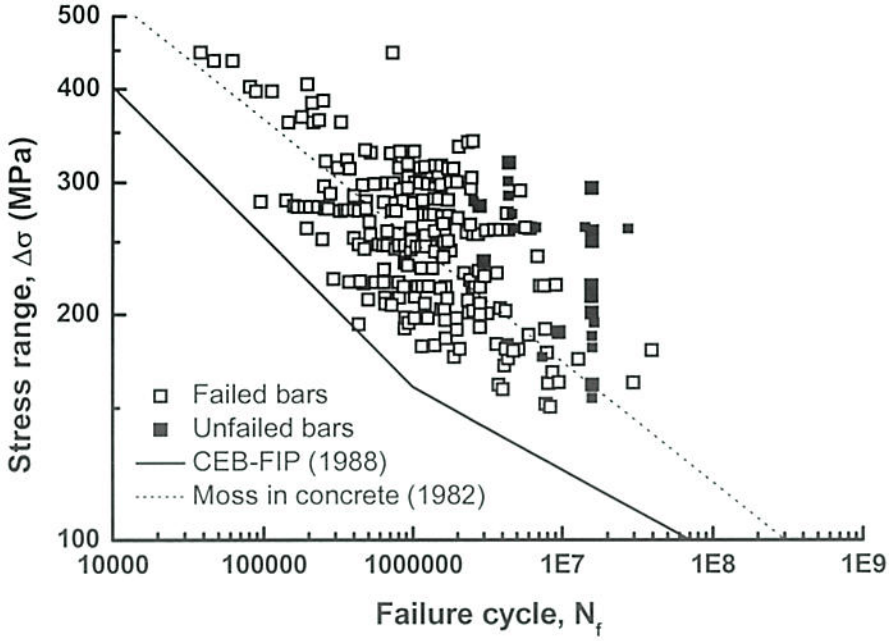

(b)

Figure 2.30 – Fatigue of reinforcing steel for bar sizes (a) 16 mm and less and (b) more than 16 mm by Tilly (1988) with Moss (1980 and 1982) and CEB-FIP (1988).

2.8.3 *Corroded reinforcing steel*

Booth et al. (1986) reported an investigation of the performance of 32 mm diameter bars immersed in seawater. Two loading frequencies were carried out, 0.1 Hz and 3 Hz of which the former gave a significantly lower fatigue life of the bars. This was attributed to the fact that more corrosion could have developed in the bar during the greater time taken for the same number of load cycles. It was recommended that when loaded at 0.1 Hz, the design curve be represented by

$$(\Delta\sigma)^{2.8} N_f = 1.1\times10^{12} \tag{2.9}$$

where $\Delta\sigma$ is the stress range applied and N_f is the number of cycles to failure.

Based on test data of Booth et al. (1986), Mallett (1991) recommended that design curve be represented by a different relationship depending on the stress range. The relationships apply to straight bars in the splash zone of marine structures susceptible to corrosion and are given by

$$(\Delta\sigma)^{6} N_f = 4.2\times10^{19} \qquad \text{for } \Delta\sigma \geq 235 \text{ MPa} \tag{2.10}$$

$$(\Delta\sigma)^{2.8} N_f = 1.1\times10^{12} \qquad \text{for } 65 \text{ MPa} \leq \Delta\sigma \leq 235 \text{ MPa} \tag{2.11}$$

$$(\Delta\sigma)^{4.8} N_f = 1.8\times10^{3} \qquad \text{for } \Delta\sigma \leq 65 \text{ MPa} \tag{2.12}$$

Figure 2.31 shows a comparison between the recommendations by Booth et al. (1986) and Mallet (1991) against the test data of Booth et al. (1986).

The behaviour of corroded reinforcing steel was modelled, numerically, by Coronelli and Gambarova (2004) for both chloride- and carbonated-induced corrosion. The finite element model reproduces the attack due to carbonation by reducing the section of each bar element. As for the consideration for pitting corrosion, an approach based on experimental results by Cairns and Millard (1999) and Castel et al. (2000) was used. Its effect on bar ductility is introduced by enforcing lower ultimate strains compared to the sound steel. The reduction factor of bar cross section α_{pit}, was taken as

$$\alpha_{pit} = \frac{\Delta A_{pit}}{A_{bar}} \tag{2.13}$$

where ΔA_{pit} is the area reduction due to pitting; and A_{bar} is the nominal bar cross section area. The ultimate strain of the corroded steel, ε'_{su} was taken as

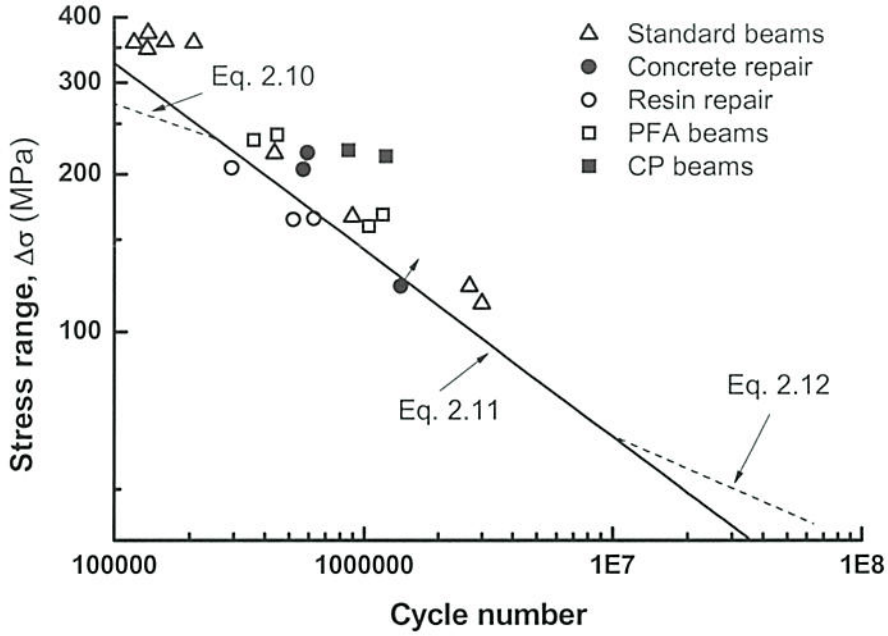

Figure 2.31 – Comparison between test data of Booth et al. (1996) and Eqs 2.10 to 2.12.

$$\varepsilon'_{su} = \varepsilon_{sy} + \left(\varepsilon_{su} - \varepsilon_{sy}\right)\left(1 - \frac{\alpha_{pit}}{\alpha_{pit}^{max}}\right) \qquad \text{for } \alpha_{pit} < \alpha_{pit}^{max} \tag{2.14}$$

where ε_{su} is the ultimate strain of the sound steel, ε_{sy} is the yield strain of the sound steel and α_{pit}^{max} is the maximum percent of bar cross section reduction valued either 0.5 (Cairns and Millard, 1999) or 0.1 (Castel et al., 2000).

2.9 Numerical modelling of FRP-strengthened RC beams in fatigue

El-Tawil et al. (2001) used a fibre section technique to compute the moment-curvature response of a reinforced concrete sections strengthened with CFRP. A fibre section analysis of a composite cross section entails discretisation of the section into many small layers (fibres) for which the constitutive models are based on uniaxial stress-strain relationships. Each region represents a fibre of material running longitudinally along the member and can be assigned one of the several constitutive models representing concrete, CFRP, or steel reinforcement.

El-Tawil modelled a T-beam specimen used in their experiments to verify their model using the mesh shown in Figure 2.32. The response of the FRP was assumed to be elastic-perfectly

brittle with perfect bond between the FRP and concrete. The reinforcing steel was modelled as bilinear with a post-yield strain hardening of 1 percent. It was assumed that the modulus of elasticities of the reinforcing steel and of the FRP remained unchanged during the cyclic loading. Perfect bond was taken between the FRP, and the reinforcing steel, with the adjacent concrete. For the concrete, the fatigue response was based on the linear stress-strain relationship of Holmen (1982), as described above. Based on calibration to test results in Bennet and Raju (1971) and Holmen (1982), the secant modulus of at N cycles, E_N was taken as

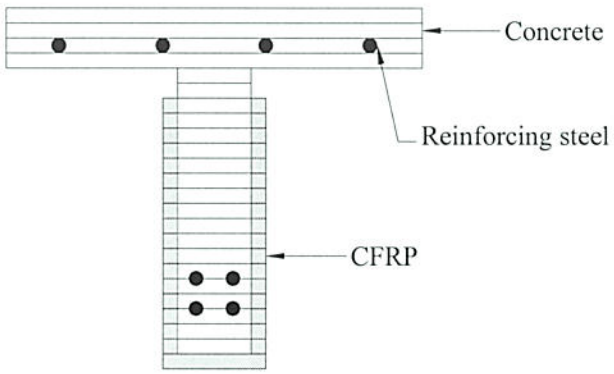

Figure 2.32 - Fibre section discretization of a reinforced concrete section strengthened with CFRP laminates by El-Tahwil et al. (2001).

$$E_N = \left(1 - 0.33\, N/N_f\right) E_{sec} \tag{2.15}$$

The concrete was taken to have no tensile strength.

The El-tawil et al. model was implemented into a computer program and computed in blocks of 10,000 cycles, after which the concrete constitutive model was updated. Examples of the results are shown in Figures 2.33 and 2.34. The model results generally compare well with the test data favourably for the first two stages of fatigue.

Based on an analytical model by Balaguru and Shah (1982), Papakonstantinou et al. (2002) developed a numerical model incorporating cyclic creep of concrete and degradation of flexural stiffness of reinforced concrete beams strengthened with GFRP. The model was then used to calculate the increase in deflection of eight GFRP-strengthened beams and proved capable of predicting the deflection increase in reinforced concrete beams subjected to fatigue. Perfect bond was assumed between both the FRP and the reinforcing steel with the concrete.

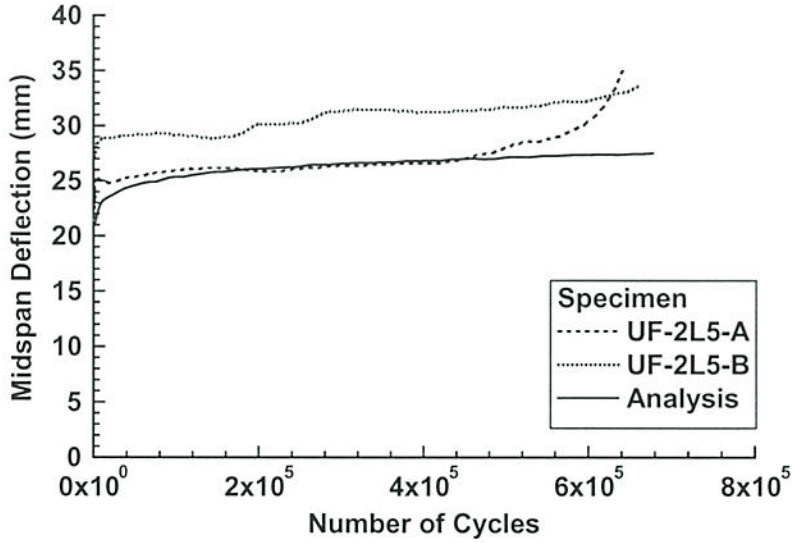

Figure 2.33 - Comparison model results with test data of soffit repaired beam with 2 CFRP layers from Shahawy and Beitelman (2000) by El-Tahwil et al. (2001).

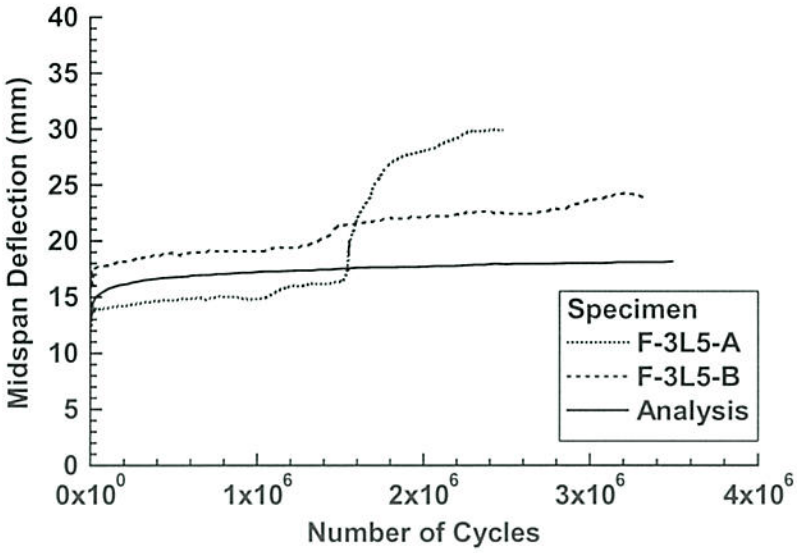

Figure 2.34 - Comparison model results with test data of soffit repaired beam with 3 CFRP layers from Shahawy and Beitelman (1999) by El-Tahwil et al. (2001).

A comparison of the Papakonstantinou et al. model versus test results is presented in Figure 2.35. It is seen that a reasonable correlation exists at the point where the model coincides with the number of cycles at failure. The model, however, is not capable of predicting the number of cycles to failure.

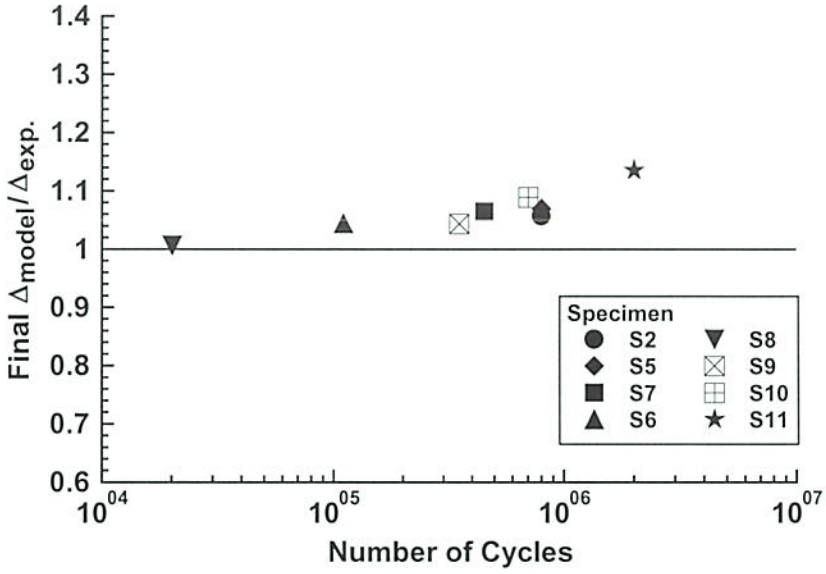

Figure 2.35 - Ratio of final mid-span experimental deflection

2.10 Concluding Remarks

This literature review has indicated that a significant improvement in the fatigue performance of reinforced concrete beams can be obtained when strengthened or repaired with FRPs. All research groups generally agree that the fatigue life of a reinforced concrete beam is improved significantly when strengthened with FRPs. The deflection of a FRP-strengthened beam is also decreased.

Many research groups have conducted experiments to investigate the behaviour of reinforced concrete beams strengthened with FRP composites with varying test variables. However, out of all the experiments documented, only a third of them tested reinforced concrete beams that were at least 4 m in length. The remaining of the experiments used small-scaled models; some as short as 700 mm (Wu et al., 2003).

In the field, concrete members of a deteriorating structure can be significantly damaged before the repair is implemented. However, in the experiments, most of the test specimens were newly cast specifically for testing purposes. In only a few experiments were the test specimens subjected to a level of pre-loading to simulate a damaged member. Only two studies have investigated the fatigue performance of corroded reinforced concrete beams repaired using FRPs. In both studies, the FRP repair could not restore the fatigue life of the corroded beams to their original, undamaged state.

The conventional repair for a corroded concrete member, in a deteriorated structure, is by replacing the damaged concrete with repair materials such as epoxy mortar. A few studies, such as Pong (2001) and Maaddway (2004), have investigated the behaviour of such repaired concrete member further repaired with FRPs. However, none of those studies looked into the fatigue performance of such members. This, together with the issue of specimen size, is the basis for further work in this thesis.

3 EXPERIMENTAL PROGRAM

3.1 Introduction

Numerous experiments have been reported in literature that shows the advantages of using FRP to repair concrete structures, both under static and fatigue loading. In the latter, the fatigue strength of the repaired structure is improved, which is important when rehabilitating damaged structures due to corrosion. However, it was also shown that tests from research groups are often incomplete in their data collection or unrepresentative of the actual structure due to sizing. This is important as size may be a major influence on the fatigue strength of a structure.

In this research, twelve simply supported reinforced concrete beams were prepared and tested to investigate the behaviour of FRP-repaired beams that had been subjected to extensive corrosion and loaded in fatigue. The specimens represent a variety of beams ranging in cross section dimensions (88 mm x 175 mm to 350 mm x 700 mm) and with varying spans (1500 mm to 6000 mm) to investigate the influence of the size effect. Extensive strain measurements of the FRP and concrete surfaces were recorded throughout the test.

3.2 Specimen details and conditions

The dimensions and details of the beams are shown in Figure 3.1 and Tables 3.1 to 3.2. These beams are grouped into four series and designated as Series A, B, C and D with spans ranging from 1500 mm to 6000 mm long. All beams had the same tensile and compressive reinforcement ratios of 0.8 and 0.4 percent, respectively. Series A, B, C and D were different in size with a ratio of dimensions of 1:2:4:1.

Three beams were tested in each series; one control specimen that was not corroded or repaired, one specimen that was corroded and then repaired using an epoxy based repair system and one that was corroded and then repaired using both the epoxy repair and FRP systems. The corroded specimens were pre-cracked and kept under load during a period of accelerated corrosion. Holding the specimen under load allowed the cracks to remain open during the corrosion process with the target mass loss of 15 percent of the tensile reinforcement. Prior to the accelerated corrosion process, the beams were pre-loaded to 60 percent of their theoretical failure load to develop the cracks. During the accelerated corrosion process, the beams were subjected to corrosion while under a sustained load of approximately 30 percent of their failure load. Once the target mass loss was achieved, the beams were unloaded and repaired with structural repair mortar. One beam from each series was further repaired at the soffit with CFRP and left to cure before testing.

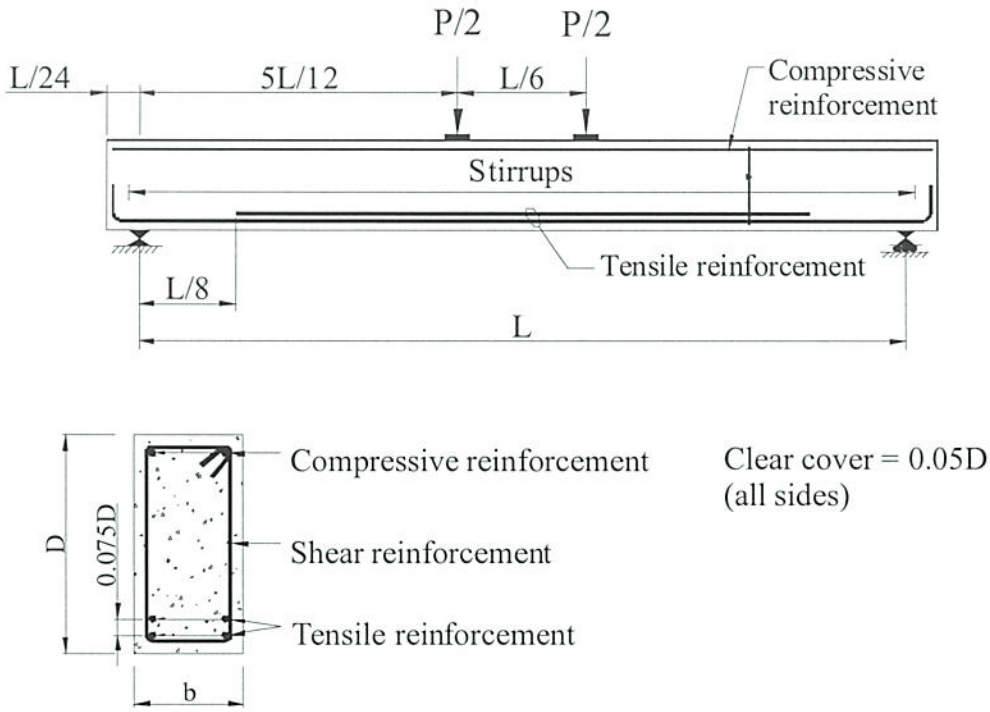

Figure 3.1 - Details of beams.

Table 3.1 – Specimen details.

Specimen	Dimension (mm)		
	Span, L	**Depth, D**	**Breadth, b**
A1, A2, A3	1500	175	88
B1, B2, B3	3000	350	175
C1, C2, C3	6000	700	350
D1, D2, D3	1500	175	88

Table 3.2 - Specimen conditions.

Specimen	Corroded	Mortar repaired	FRP repaired
A1, B1, C1, D1	No	No	No
A2, B2, C2, D2	Yes	No	Yes
A3, B3, C3, D3	Yes	Yes	Yes

All beams were tested under a fatigue loading at 1 Hz using a sinusoidal wave load-time history with the same stress range of between 20 and 60 percent of the theoretical failure load of the control beam. Beams A1, D1 and D3 were stopped at 2 million cycles and then loaded monotonically to failure. The loading histories both prior to and after repair, for all beams are given in Figure 3.2.

3.3 Materials

3.3.1 Reinforcing steel

The reinforcement details for each test series are presented in Table 3.3 and the stress-strain curves in Figure 3.3. For beams in Series A, the reinforcement used were of nominal 400 MPa grade, hot rolled, deformed bars of 6 mm diameter for the compressive, tensile and shear reinforcement.

For beams in Series B and C, the reinforcement was fabricated from nominally 500 MPa grade, hot rolled, deformed bars. Bar diameter of 12 mm were used for all reinforcement for beams in Series B and the shear reinforcement of beams in Series C. The compressive and tensile reinforcement in Series C was 24 mm diameter.

The reinforcement for beams in Series D were fabricated from nominally 600 MPa grade, round bars of 6 mm diameter bars for the compressive and tensile reinforcement. The shear reinforcement was the same as for beams in Series A.

3.3.2 Concrete

For Series A, B and C, the concrete was supplied by a local ready-mix supplier with a maximum aggregate size of 10 mm. The beams with corroded bars had a middle zone at the lower level of the specimen and for one third of the beam length. In this region, the concrete was salted. Hence, two concrete mixes were used from two concrete trucks from the same supplier. The first mix contained the normal, unsalted, concrete with 270 kg/m^3 of cement and a water-cement ratio of 0.68. The concrete was nominally 20 MPa. The second mix for the salted concrete contained the same mix, but with a lower water-cement ratio of 0.48. Prior to casting of the salted concrete mix, salted water that was prepared the previous day was added into the mix with a resulting water-cement ratio of 0.68. The salt added into the water was 3 percent by weight of the cement in the mix. Beams of Series D were cast in the concrete laboratory using a design mix targeted at achieving a mean compressive strength (f_{cm}) of 30 MPa.

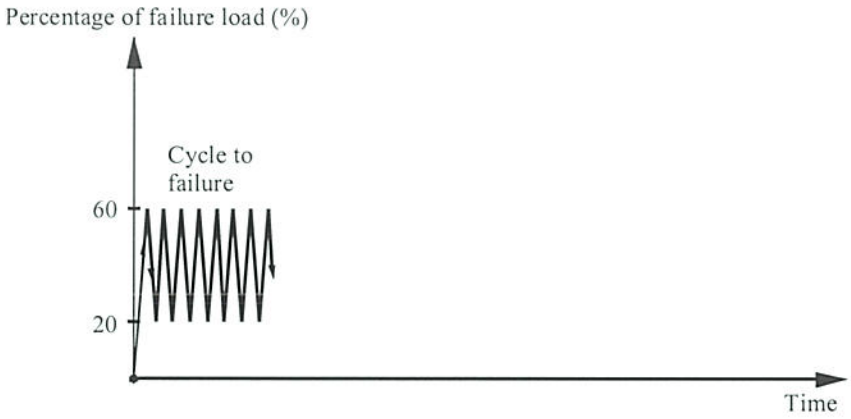

(a)

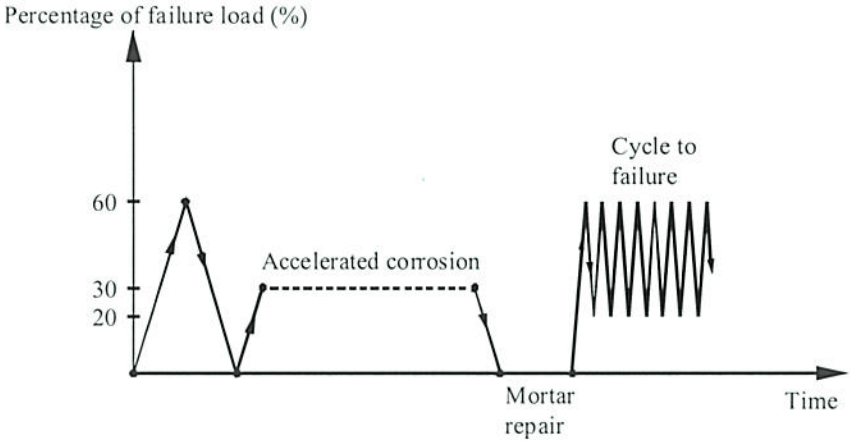

(b)

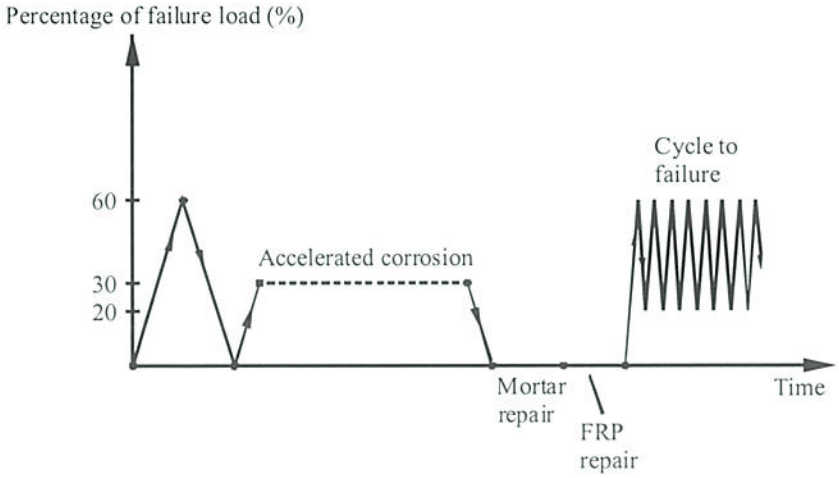

(c)

Figure 3.2 - Loading procedure for: (a) beams A1, B1, C1 and D1, (b) beams A2, B2, C2 and D2, (b) beams A3, B3, C3 and D3.

Table 3.3 – Details of reinforcement.

Specimen	Steel Reinforcement		
	Tensile	Compressive	Shear
A1, A2, A3	4 x 6mm Ø	2 x 6mm Ø	2 x 6mm Ø @75 c/c
B1, B2, B3	4 x 12mm Ø	2 x 12mm Ø	2 x 12mm Ø @100 c/c
C1, C2, C3	4 x 24mm Ø	2 x 24mm Ø	2 x 12mm Ø @150 c/c
D1, D2, D3	4 x 6mm Ø	2 x 6mm Ø	2 x 6mm Ø @75 c/c

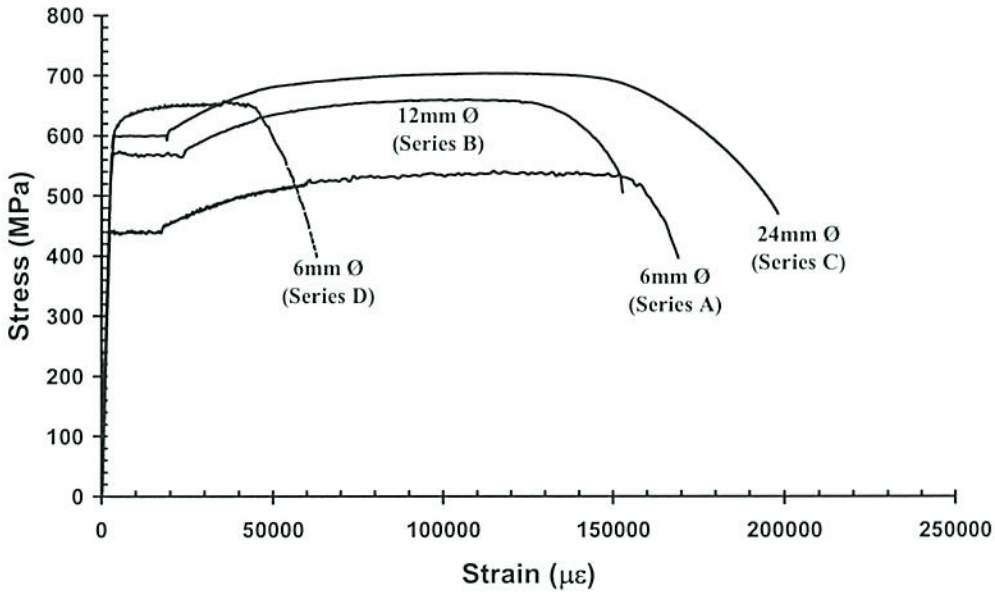

Figure 3.3 - Material properties for steel reinforcement.

The actual mean compressive strength (f_{cm}) results were obtained from the average of at least three cylinders tested in conjunction with the test beams (at a rate of 20 MPa/min) with the results given in Table 3.4 and Figure 3.4. The cylinders were demoulded after 24 hours and kept and cured at ambient temperature under hessian and plastic together with the beam specimens. All of the cylinders and specimens were watered twice a day for 28 days. The formwork for the beam specimens was stripped at approximately 7 days after casting.

Concrete cylinders were tested periodically during the testing program in accordance with the Australian Standard AS1012.9 (1999) for compression, AS1012.10 (2000) for indirect tension, AS1012.11 (2000) for flexural tension and AS1012.17 (1997) for elastic modulus. The results of the cylinder tests for each test series are given in Tables 3.5 to 3.11.

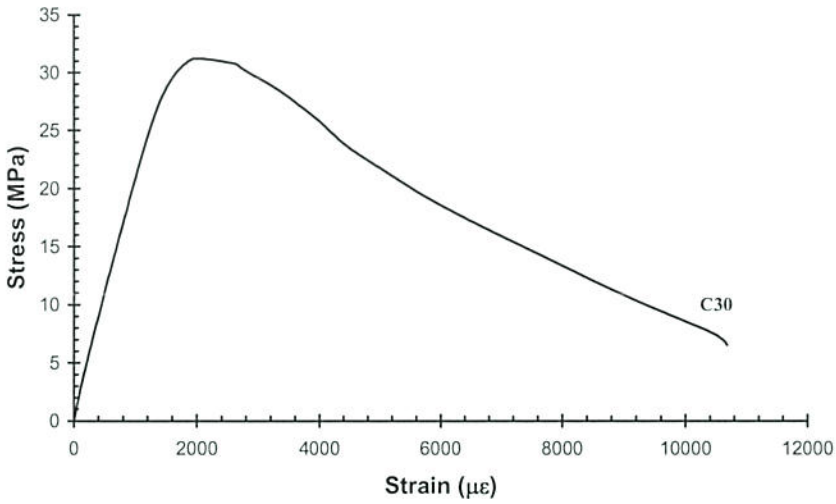

Figure 3.4 – Stress versus strain curves for concrete.

Table 3.4 – Material properties for concrete.

Specimen in Series	Unsalted concrete				Salted concrete			
	f_{cm} (MPa)	E_o (MPa)	f_t (MPa)		f_{cm} (MPa)	E_o (MPa)	f_t (MPa)	
			Flexure test	Brazil test			Flexure test	Brazil test
A, B & C	30	26050	-	2.95	11	15470	2.19	1.27
D	46	-	-	-	40	-	-	-

Table 3.5 – Mean cylinder strength for beam specimens in Series A, B and C.

Day after casting	Mean cylinder strength in MPa (No. of cylinders tested)	
	Unsalted concrete	Salted concrete
7	18.6 (2) #	7.3 (2) #
14	23.3 (2) #	8.6 (2) #
21	24.8 (2) #	8.9 (2) #
28	29.6 (2) #	9.3 (2) #
28	29.1 (1) *	8.9 (1) *
464	31.8 (1) #	12.9 (2) #
647	34.3 (3) #	-

Notes: # 150 mm x 300 mm diameter cylinder

* 100 mm x 200 mm diameter cylinder

Table 3.6 – Mean cylinder strength for beam specimens in Series D.

Day after casting	Mean cylinder strength in MPa (No. of cylinders tested)	
	Unsalted concrete	Salted concrete
29	46.8 (3) *	39.6 (2) *

Note:* 100 mm x 200 mm diameter cylinder

Table 3.7 – Indirect tensile strength (Brazil test) results for beam specimens in Series A, B and C.

Day after casting	Mean cylinder strength in MPa (No. of cylinders tested)	
	Unsalted concrete	Salted concrete
28	2.95 (2) *	1.27 (2) *

Note:* 100 mm x 200 mm diameter cylinder

Table 3.8 – Indirect tensile strength (Brazil test) for beam specimens in Series D.

Day after casting	Tensile strength in MPa (No. of cylinders tested)	
	Unsalted concrete	Salted concrete
28	-	2.19 (2)^

Note:^ 100 mm x 100 mm x 500 mm prism

Table 3.9 – Flexural tensile strength for beam specimens in Series A, B and C.

Day after casting	Tensile strength in MPa (No. of prisms tested) 100 mm x 100 mm x 500 mm	
	Unsalted concrete	Salted concrete
28	-	2.19 (2)^

Note:^ 100 mm x 100 mm x 500 mm prism

Table 3.10 – Flexural tensile strength for beam specimens in Series D.

Day after casting	Tensile strength in MPa (No. of prisms tested) 100 mm x 100 mm x 500 mm	
	Unsalted concrete	Salted concrete
28	-	2.19 (2)

Table 3.11 – Modulus of Elasticity for beam specimens.

Specimen in Series	Day after casting	Modulus of Elasticity in MPa (No. of cylinders tested)	
		Unsalted concrete	Salted concrete
A, B & C	28	26435 (1) *	15200 (1) *
A, B & C	28	25860 (2) #	15600 (2) #
D			

Notes:# 150 mm x 300 mm diameter cylinder; * 100 mm x 200 mm diameter cylinder

3.3.3 Repair mortar

The mortar EMACO S66® was used to repair the beams after the weak, salted, concrete had been removed from the specimen. It is a cementitious pourable shrinkage compensated structural repair mortar, shown in its dry form in Figure 3.5. The mortar is packaged in bags of 20kg. For every bag of repair mortar, 2.0 L of water is added to produce the mortar mixture. Concrete cylinders and prisms were cast at the same time as the beam repairs and tested according to the Australian Standard AS1012.9 (1999) for compression, AS1012.10 (2000) for indirect tension, AS1012.11 (2000) for flexural tension and AS1012.17 (1997) for elastic modulus. The results are listed in Tables 3.12 to 3.15.

Figure 3.5– Repair mortar in dry form.

Table3.12 – Mean cylinder strength for mortar.

Day after casting	Mean cylinder strength in MPa (No. of cylinders tested)
91	67.1 (3)*
237	71.9 (2)*

Note:* 100 mm x 200 mm diameter cylinder

Table 3.13 – Indirect tensile strength (Brazil test) results for mortar.

Day after casting	Tensile strength in MPa (No. of cylinders tested)
237	6.67 (2)*

Note:* 100 mm x 200 mm diameter cylinder

Table 3.14 – Flexural tensile strength for mortar.

Day after casting	Tensile strength in MPa (No. of prisms tested)
95	5.56 (3)^

Note:^ 100 mm x 100 mm x 500 mm prism

Table 3.15 – Modulus of Elasticity for mortar.

Day after casting	Modulus of Elasticity in MPa (No. of prisms tested)
103	18900 (2)^

Note:^ 100 mm x 100 mm x 500 mm prism

3.3.4 CFRP and adhesive

The CFRP used in this project was supplied by MBrace®, and was the CFK laminate 150/2000 with a laminate thickness of 1.40 mm. The resin used for the bonding of CFRP was a two-part epoxy adhesive (MBrace® laminate adhesive). The mechanical properties of the CFRP and epoxy, as provided by the manufacturer, are presented in Table 3.16.

Table 3.16 - Mechanical properties of CFRP and adhesive as given by the manufacturer.

CFRP 150/2000	
Ultimate tensile strength	2700 MPa
Modulus of Elasticity	165 GPa
Ultimate strain	1.4%
Adhesive	
Compressive strength	> 60 MPa
Flexural strength	> 30 MPa
Specific Gravity @ 23 °C	1.5
Full Cure @ 23 °C	7 days

3.4 Preparation of specimens

3.4.1 Fabrication

Steel channel sections were used to form the formwork for beams in Series A and B whereas plywood was used for beams in Series C and D. Formwork for Series C was previously built for specimens tested in Khomwan et al. (2005) and was re-used for this test as the beams had the same dimensions.

The stirrups were fabricated according to the required size and, as corrosion was intended only to occur at the tensile reinforcing bars, the stirrups were protected from corrosion by painting with two coats of a rust preventive POR-15® paint. Prior to application of the paint, oil and grease on the surface of the stirrups were removed using the degreasing product Marine Clean®. The surface was then prepared using a primer Metal Ready®, followed by the POR-15 rust preventive paint. Electrical insulation tape was then adhered to all the corners of the painted stirrups to prevent electrical contact between the longitudinal bars and the stirrups. Figure 3.6 shows a prepared stirrup.

The bottom flexural reinforcement was bent at its ends by heating the reinforcing bars using oxy-acetylene. Heat was applied to the bar until the bar was a red colour, the bar was then bent 90 degrees and allowed to air cool. Following the bending of the bottom layer bars, the bottom and top bars were tied together with the stirrups. Finally, the upper layer of bottom reinforcing bars were cut to length and tied to the reinforcing cage. The cage was then placed in the plywood form using bar chairs to maintain cover to all sides of the specimen. Some of the reinforcement cages and the formwork for beams in Series C are shown in Figures 3.7 and 3.8, respectively.

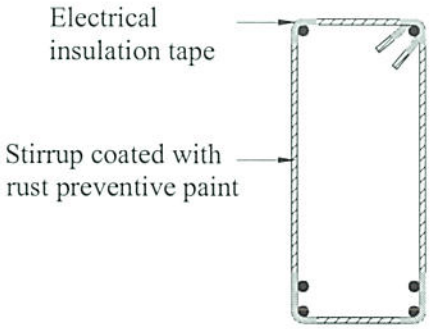

Figure 3.6 – Prepared stirrup.

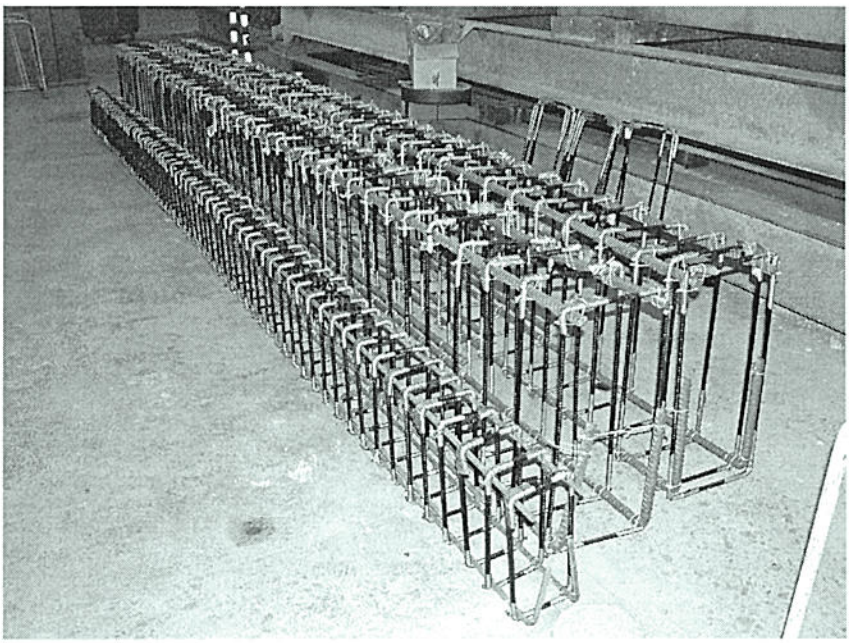

Figure 3.7 –Reinforcing cages

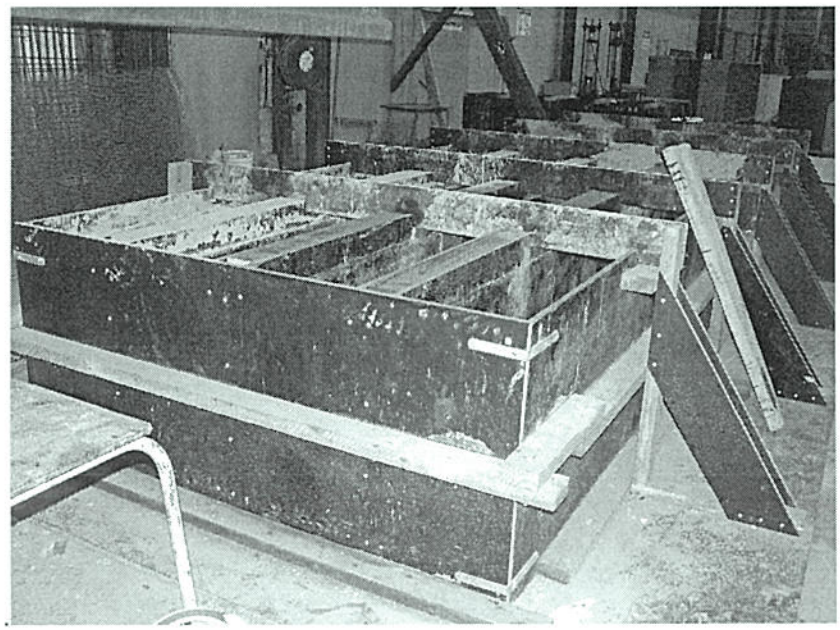

Figure 3.8 – Formwork for casting beam specimens in Series C.

3.4.2 Concrete casting

Prior to concrete pouring, dividers made out of plywood were inserted into the form at locations between the salted and unsalted concrete zones to separate the salted and unsalted concrete during pouring. The salt was added to the mix by pouring the salted water into the concrete delivery truck and mixing it for about 3 minutes. The salted concrete was then poured into the form at the middle zone of the specimen up to ⅓ of the beam height. (Figure 3.9) This was followed by pouring of the normal, unsalted concrete from the second truck. The unsalted concrete was poured at both ends of the form up until it met with the level of the salted concrete in the middle zone. The plywood dividers were then removed, the sections vibrated, and the concrete pouring continued to complete the specimens. The specimens were left to cure for at least 28 days. Figure 3.9 shows the placement of the salted and unsalted concrete within a beam specimen.

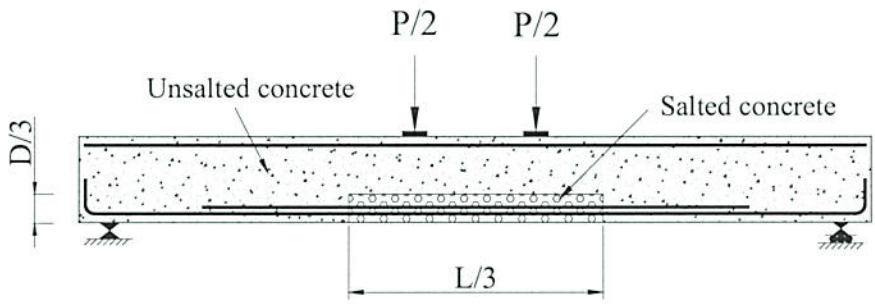

Figure 3.9 – Zones of salted and unsalted concrete in beam specimen.

3.4.3 Pre-cracking

After the specimens had cured for 28 days, the beams that had been designated for corrosion were loaded to 60 percent of their failure load in four point bending. The beams were loaded in a load control mode. Cracks were observed and the patterns were recorded on the beam. Figure 3.10 shows the cracks observed in Beam B2 during this process. The beams were then unloaded and ready for the accelerated corrosion stage.

3.4.4 Accelerated corrosion under sustained load

Two galvanised saltwater tanks were prepared in the laboratory to accommodate the corrosion specimens A2, A3, B2, B3, C2, C3, D2 and D3. The larger tank had dimensions of 1500 mm x 3000 mm x 8000 mm and accommodated the A and B series specimens with the C and D series specimens in a smaller tank of dimensions 750 mm x 1500 mm x 4000 mm. The saltwater which served as the electrolyte contained 3.5 percent by weight of sodium

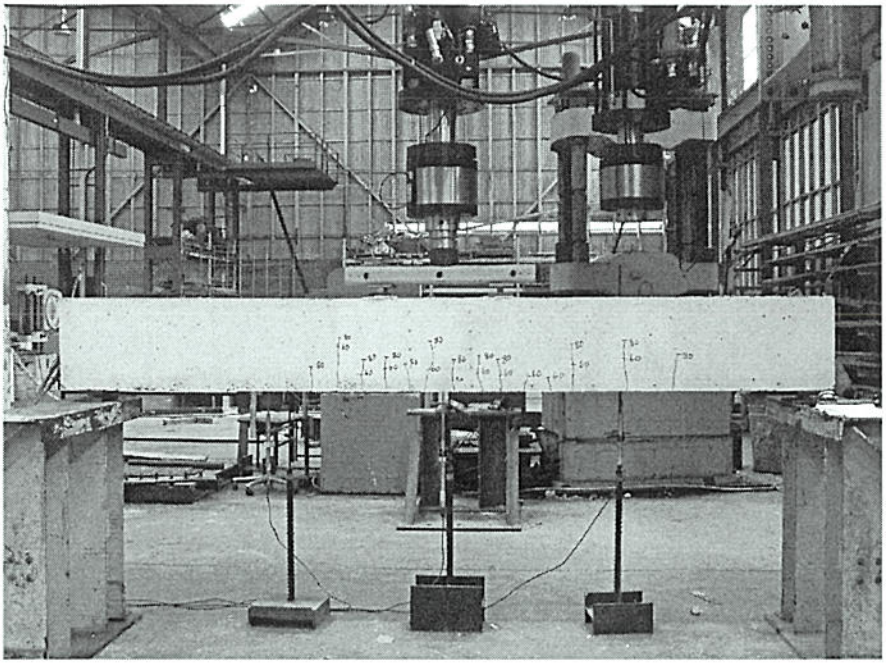

Figure 3.10 – Beam specimen B2 after pre-cracking.

chloride. During the accelerated corrosion period, the electrolyte was cycled every six hours between the two tanks to subject the specimens to wet-dry cycles. This not only simulated actual conditions of structures subjected to seawater splash zones but also provided oxygen that is essential for the corrosion process.

To accelerate the corrosion process, an electrical current was passed through the specimen with stainless steel woven wire mesh used to act as external cathodes to the specimens while the internal longitudinal steel reinforcement acted as the anode. Ideally, the surface area of a cathode relative to the anode should be larger so that corrosion would be more severe. In this test, the cathode had a surface area of approximately three times larger than that of the anode. The wire mesh was bent into a U-shaped jacket such that it encased the specimen at the soffit. The mesh was placed at the constant moment region of the beam so that corrosion was intensified in that region. A layer of foam was provided between the stainless steel mesh and the beam as a form of contact. This was required to avoid undesirable dead short circuits from occurring in the specimen. Dead short circuits can occur when there is accumulation of corrosion products between the specimen and the wire mesh, and a bridge is formed between the anode and cathode. This causes the electrical current and its associated corrosion effects to become concentrated at the location of the bridge, rendering the corrosion process ineffective.

Three external DC power supplies were used and each had a current capacity of 3 A that could be controlled in increments of 10 mA. All specimens were subjected to an induced current density of 150 $\mu A/cm^2$. The corresponding induced net current is the product of the

current density and the surface area of the longitudinal steel reinforcement and is listed in Table 3.17. In each series, the specimens were electrically connected in series so that the same current was applied to the specimens. The times required to corrode the beams to 15 percent mass loss were calculated based on mass loss prediction using Faraday's Law. The total time estimated for beams in Series A, B, C and D to meet a 15 percent mass loss were 60 days, 150 days, 380 days and 60 days, respectively.

Table 3.17 – Electrical current imposed on beam specimens.

Specimen	**Current density ($\mu A/cm^2$)**	**Induced net current (A)**
A2, A3	150	0.18
B2, B3	150	0.68
C2, C3	150	2.71
D2, D3	150	0.18

In real structures, corrosion takes place while the structure carries load and cracks are open. This acts to accelerate the corrosion process and, thus, in this test series, the specimens were maintained under a sustained load of approximately 30 percent of the ultimate failure load while the corrosion processes were taking place. For Series B and C, load was applied using hydraulic jacks and steel beam arrangements. In order to ensure that that load applied was constant throughout the corrosion process, load cells were placed between the beams and the hydraulic jacks. For Series A and D, load was applied by placing concrete blocks of the desired weight. Figures 3.11 and 3.12 show the beam specimens during the accelerated corrosion process.

The corrosion process was monitored using a rapid, non-destructive, polarization instrument named Galvapulse and the corrosion stopped when the predicted level of corrosion was achieved. At the end of the accelerated corrosion process, the beam specimens were removed from the tanks. The conditions of the beams were noted and horizontal cracks at the soffit and along the sides of the beam were observed. The cracks, which ran parallel to the tensile reinforcing bars were consistent with observations reported by other researchers (Masoud, 2002) and shown in Figure 3.13. These cracks were due to the presence of rust, which caused the area immediately surrounding the tensile bars to expand. Rust was also noticed to accumulate mostly at the flexural cracks that had formed during the pre-cracking process. Figure 3.14 shows the condition of specimen C2 at the completion of the corrosion process.

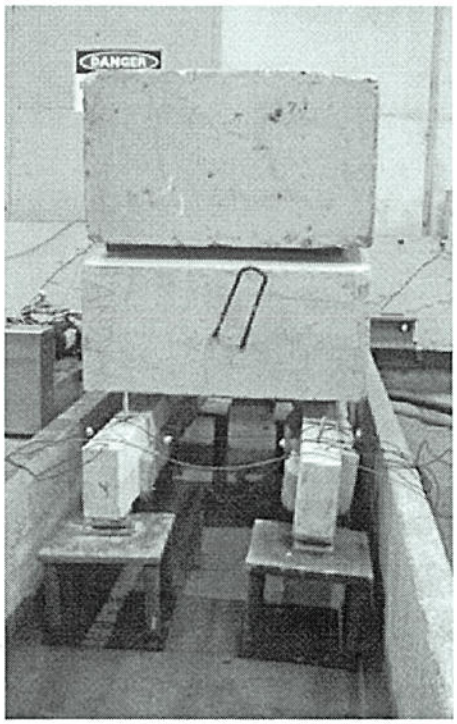

(a)

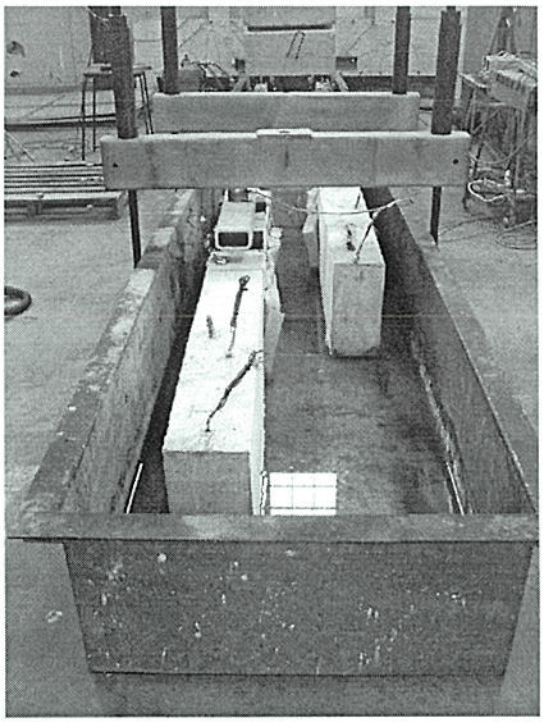

(b)

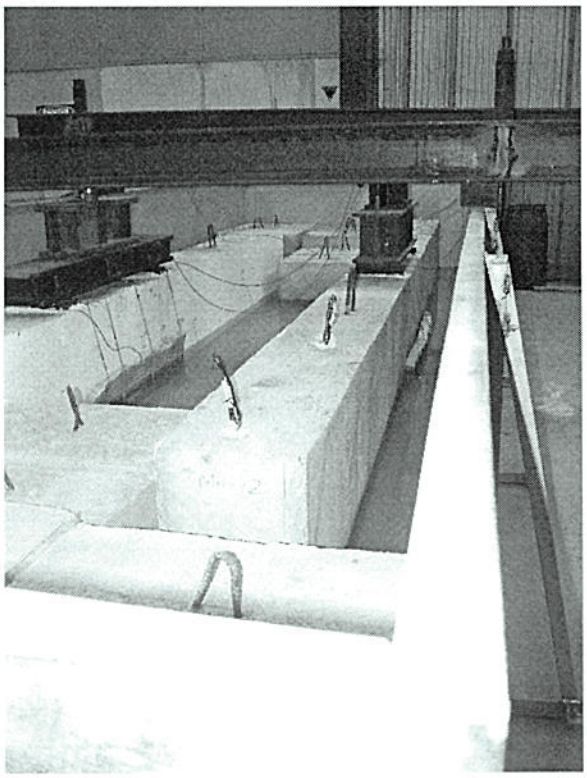

(c)

Figure 3.11 – Beam specimens during accelerated corrosion process in (a) Series A, (b) Series B and (c) Series C.

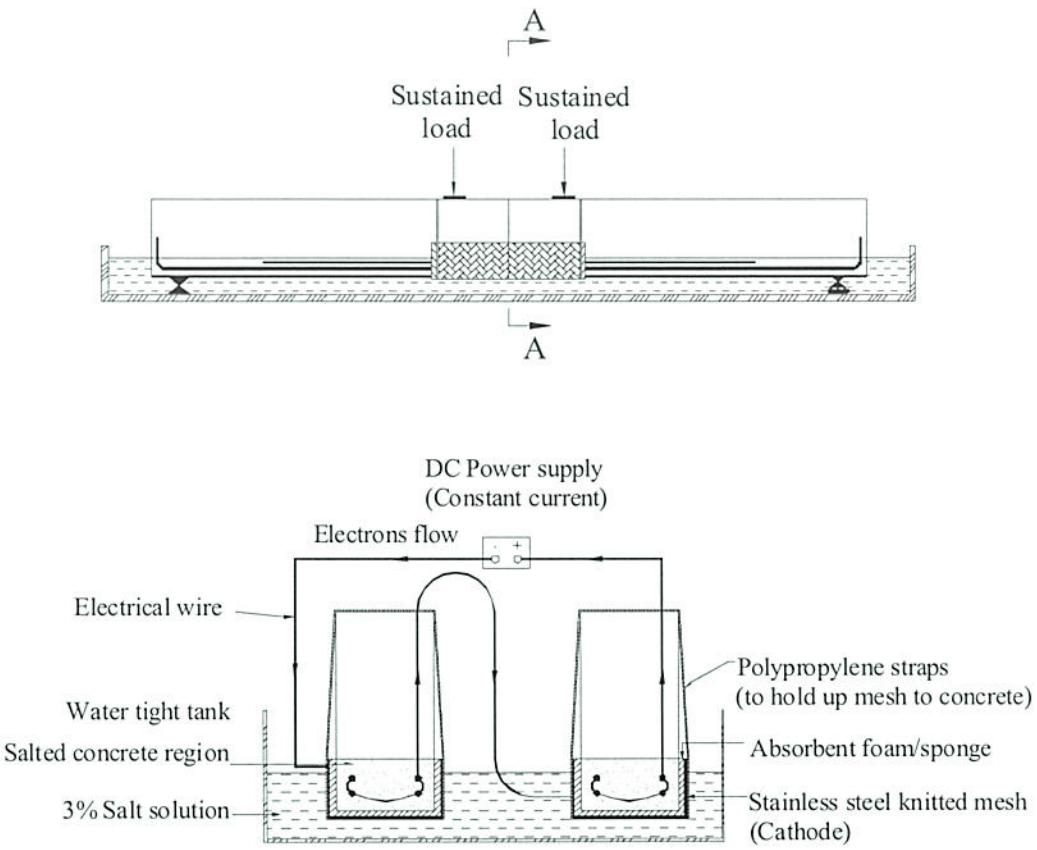

Figure 3.12 – Schematics of beam specimens during accelerated corrosion process.

Figure 3.13 – Longitudinal crack running parallel to tensile bars due to corrosion.

Figure 3.14– Condition of beam C2 after the accelerated corrosion process.

3.4.5 Mortar repair

Rust from the accelerated corrosion process had led to the deterioration of concrete at the level of the tensile reinforcing bars. Thus, just as for the repair of a beam in practice, the deteriorated concrete was removed. The concrete was carefully removed using a hammer and chisel for beams in Series A and D, and using a jackhammer for beams in Series B and C. The procedure for concrete removal was carried out according to the ICRI (1995) guidelines.

Upon removal of the deteriorated concrete, the tensile bars were observed to have severe pitting corrosion, as shown in Figure 3.15, while the stirrups did not show any signs of deterioration. Prior to casting of the repair mortar, the reinforcing bars were cleaned using a wire brush to remove the loose rust product.

The formwork for casting the mortar was made from plywood. For specimens in Series A, B and D, the beams were inverted and the formwork was provided along the sides of the

Figure 3.15 – Pitting corrosion observed on reinforcing bar in specimen of Series C.

beams. The formwork was clamped onto the beam to ensure a proper fit. Beams of Series C were laid down on their sides onto their formwork due to their large size. Figure 3.16 shows beams of Series C ready for mortar casting.

Prior to casting of the repair mortar, the concrete surface was wetted to provide a sound bond between the substrate concrete and the mortar. Bags of 20 kg repair mortar were mixed with 2.0 litres of water per bag in a concrete mixer for about 4 to 5 minutes. The mixture was then poured into the required areas with mechanical vibrators used to ensure consolidation of the mortar pour. Finally, trowels were used to smooth the surface and the specimens were left to cure for 28 days. The formwork was removed after 7 days.

3.4.6 Application of CFRP

Before the CFRP was applied to the soffit of the beams, the surfaces of the concrete were ground to remove the surface cement paste and expose the aggregates. The size of the CFRP plate applied depended on the series. All repaired beams except those in Series C required one CFRP plate each. Beams of Series C required 2 plates side by side, separated by a 5 mm gap. The CFRP plate was cut to size using a sharp knife. Table 3.18 and Figure 3.17 show the dimension and location of the CFRP plates.

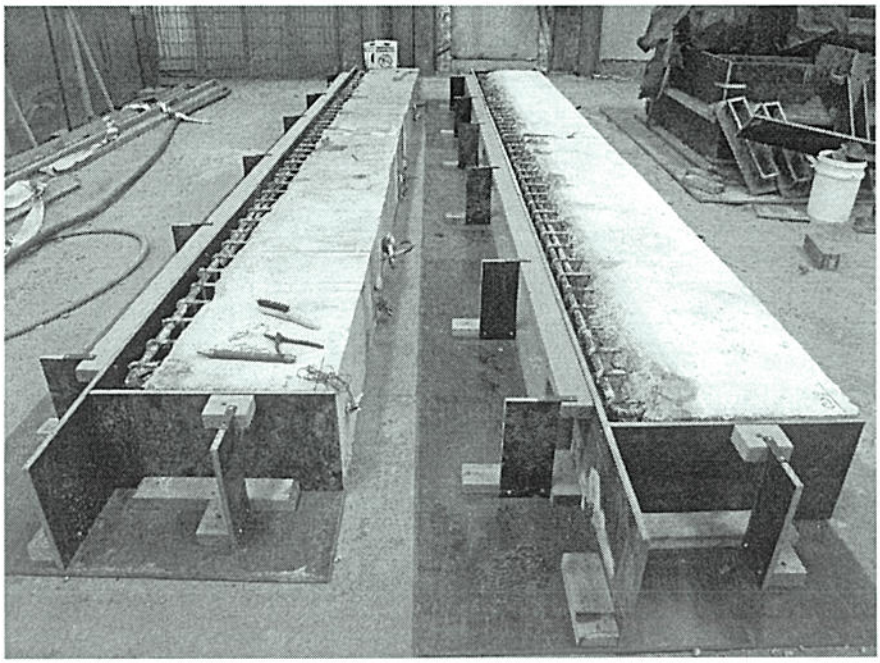

Figure 3.16 – Beam specimens in formwork ready for mortar repair.

Table 3.18 – Dimension of CFRP plate applied to beams.

Test Series	Thickness (mm)	Width (mm)	Length (mm)
A	1.4	60	1375
B	1.4	120	2750
C	1.4	2 x 120	5500
D	1.4	60	1375

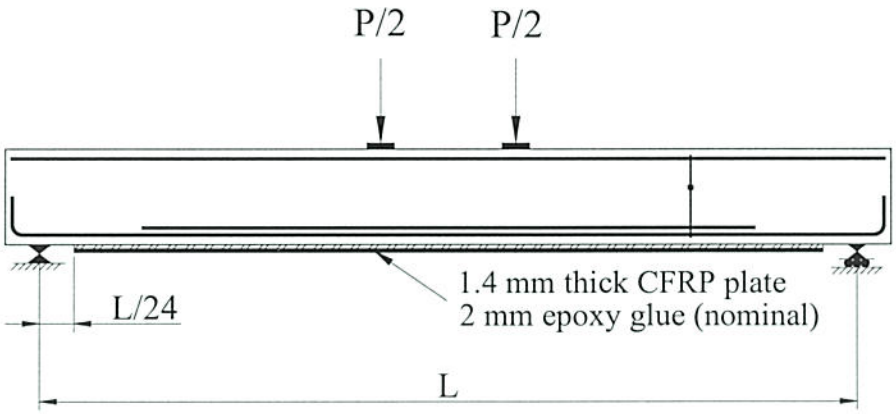

Figure 3.17 – Details of CFRP repaired beams.

The CFRP plate was prepared by cleaning it with acetone to remove any grease, oil, carbon dust or other contaminants prior to installation. After the CFRP and concrete surfaces were prepared, the MBrace® primer was mixed as per the suppliers instructions and applied to the concrete surface. The epoxy adhesive was then mixed and applied to both the CFRP and the concrete surface to a nominal thickness of 3 mm. The CFRP was subsequently applied to the soffit of the beam specimen using light pressure. The beam was left to cure at ambient temperature for at least 7 days before testing. The installation process is shown in Figures 3.18 to 3.25.

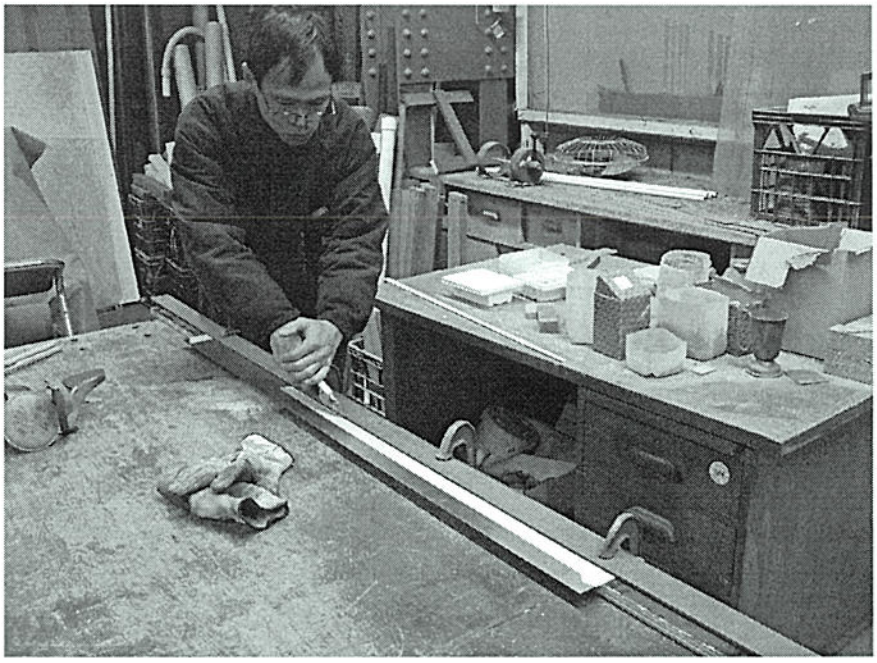

Figure 3.18 – CFRP plate cut to size.

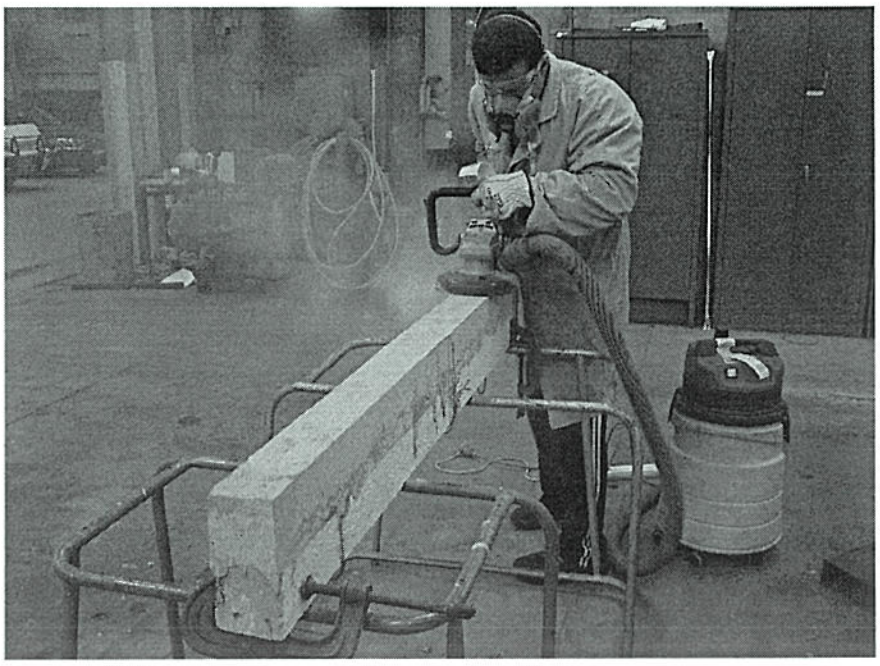

Figure 3.19 – Concrete surface preparation using concrete grinder.

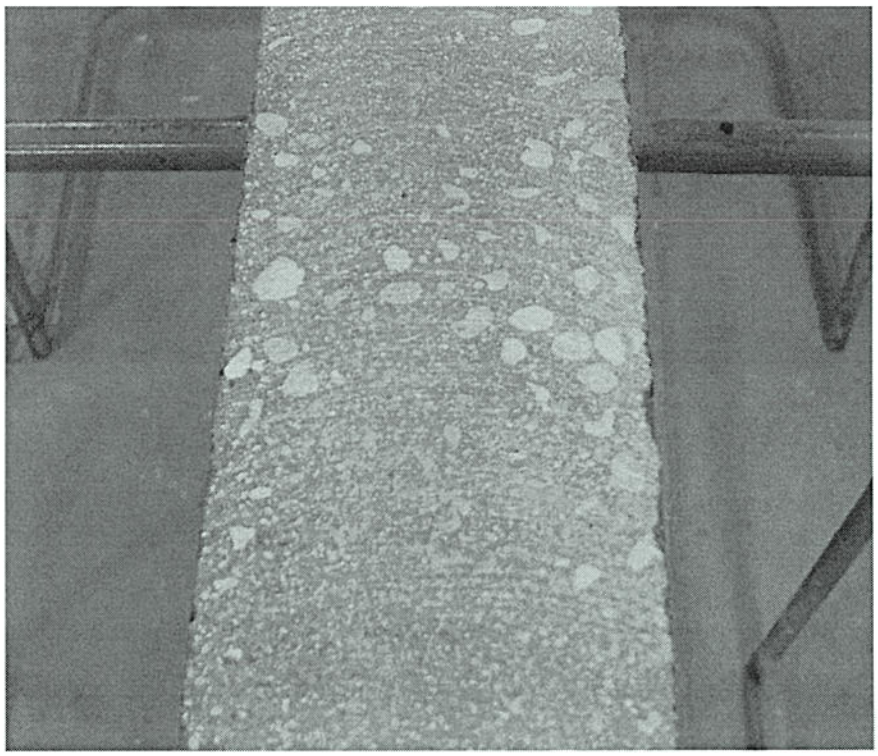

Figure 3.20 – Exposed aggregate after surface preparation.

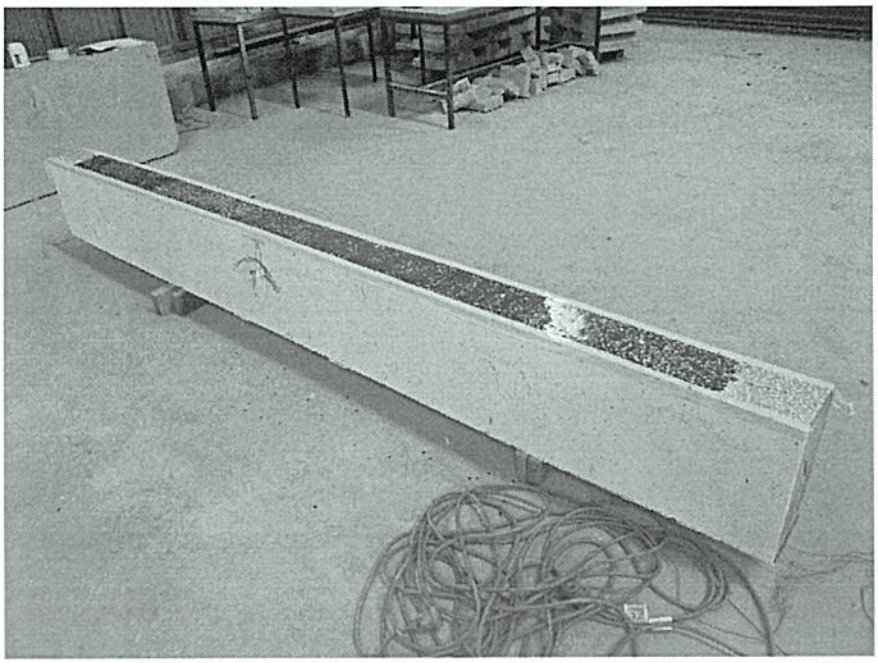

Figure 3.21 - Primer applied on concrete.

Figure 3.22 – Mixing of epoxy adhesive components.

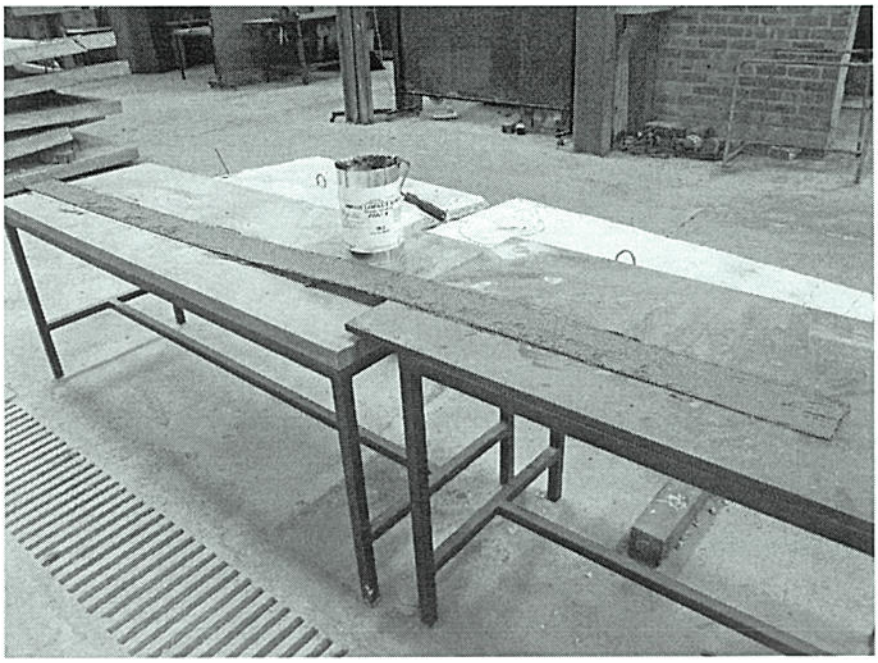

Figure 3.23 – Epoxy adhesive applied to CFRP.

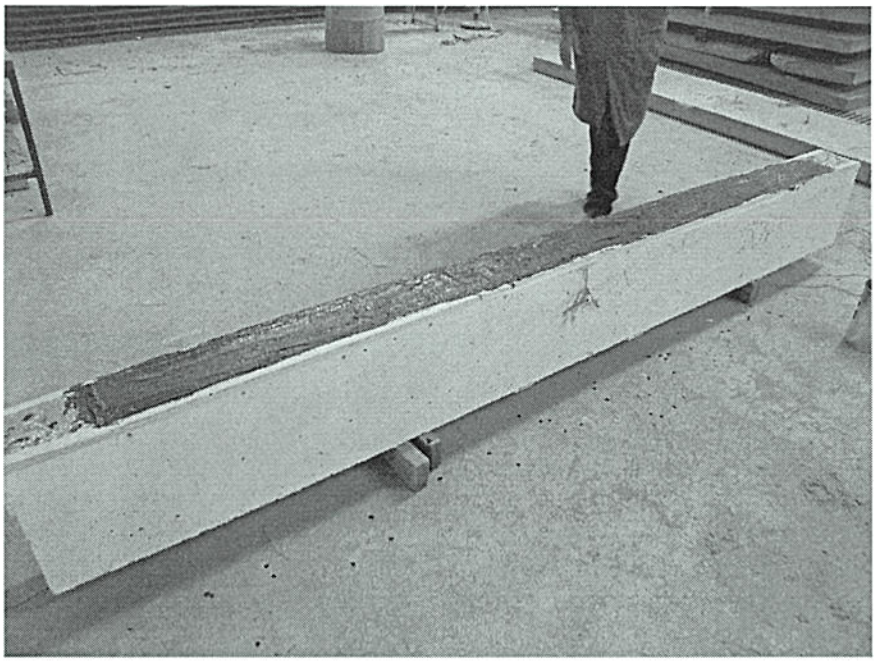

Figure 3.24 – Epoxy adhesive applied to concrete

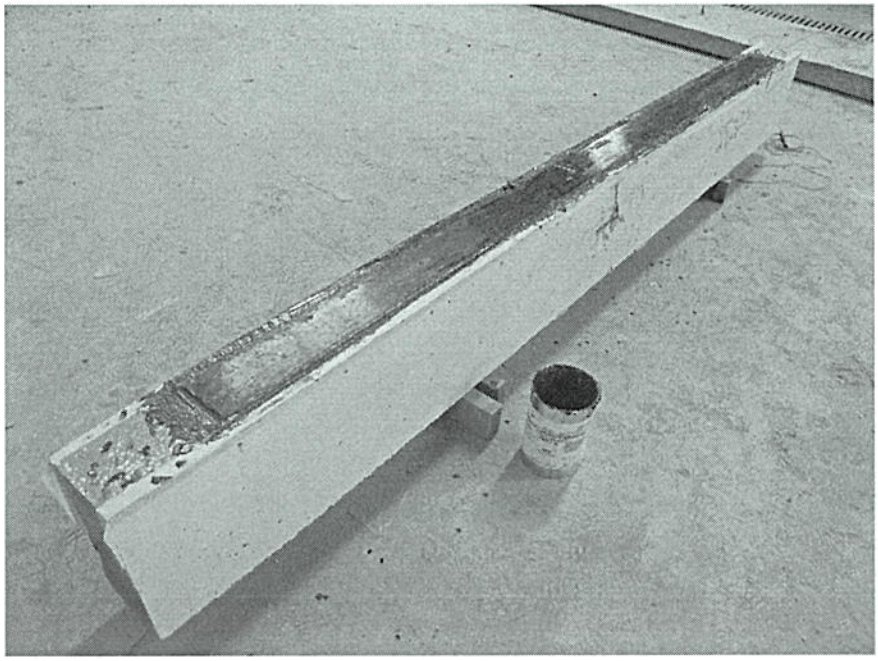

Figure 3.25 – Final installation of CFRP.

3.5 Instrumentation

3.5.1 General

The instrumentation setup involved electrical gauging and monitoring equipment. Loads, displacements, steel tensile strains and CFRP strains were measured. A computerized data-logging system was used to obtain these measurements through a Hottinger Baldwin Messtechnik (HBM) system. In addition to these measurements, concrete strains were also recorded by means of mechanical gauging at specific intervals during the testing stage.

3.5.2 Loads

All specimens were tested in four-point bending. A 600 kN capacity Instron loading actuator was used to apply the fatigue loads on specimens. In all tests, loads were measured by placing a load cell between the hydraulic jack and the beam and linked to the HBM data acquisition system.

3.5.3 Strains

Point strains were measured using electronic resistance strain gauges that had been attached to the main tensile reinforcement, before casting of the specimen for the control specimens and before casting of the repair mortar for the deteriorated specimens, and to external surfaces of the CFRP plates. For beams in Series A and D, four strain gauges (S1 to S4) were attached to the main tensile reinforcement at the mid-span (Figure 3.26). For beams in Series B and C, in addition to the four strain gauges in the mid-span, two strain gauges were attached to the tensile reinforcement under each of the load points. Hence, there were eight strain gauges for each beam (S1 to S8), shown in Figure 3.27. For the CFRP-repaired beams, 11 strain gauges were attached to the CFRP plates at intervals of $L/48$ where L is the beam span. Figure 3.28 shows the location of the strain gauges at the CFRP plate.

Average surface strains were measured at the level of the reinforcement along the beam using Demec strain gauges (Figure 3.29). Demec targets were also located at the mid-section of the specimen to measure curvatures.

Displacements were measured at the midspan of the beams using a laser displacement transducer placed under the beam that was connected to the centralised data logging system.

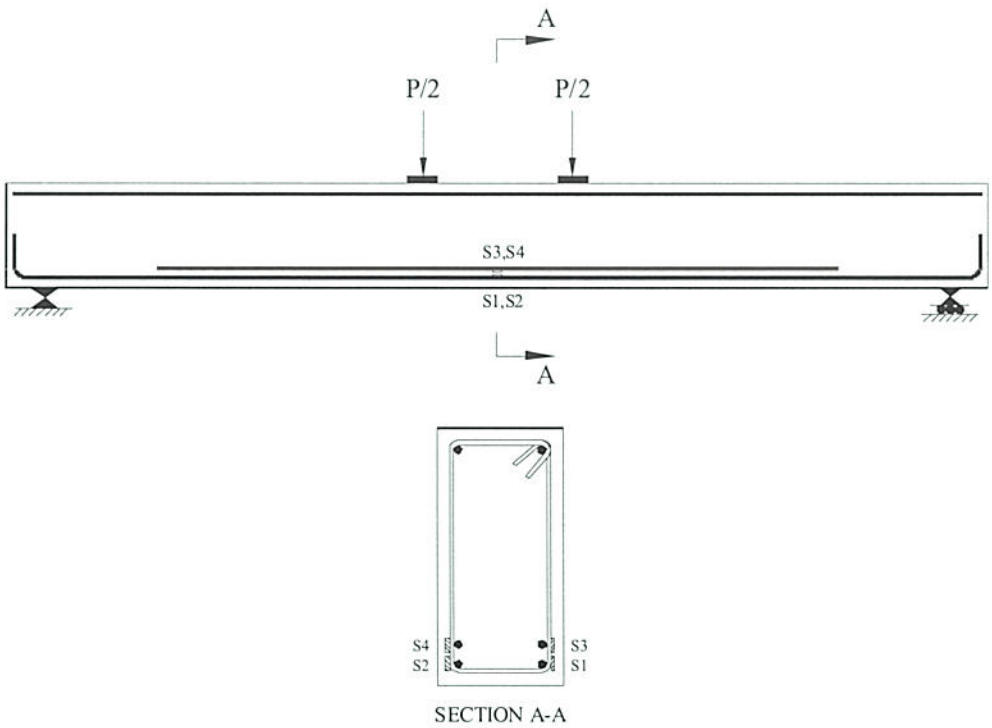

Figure 3.26 – Strain gauge locations on tensile reinforcement for control beams.

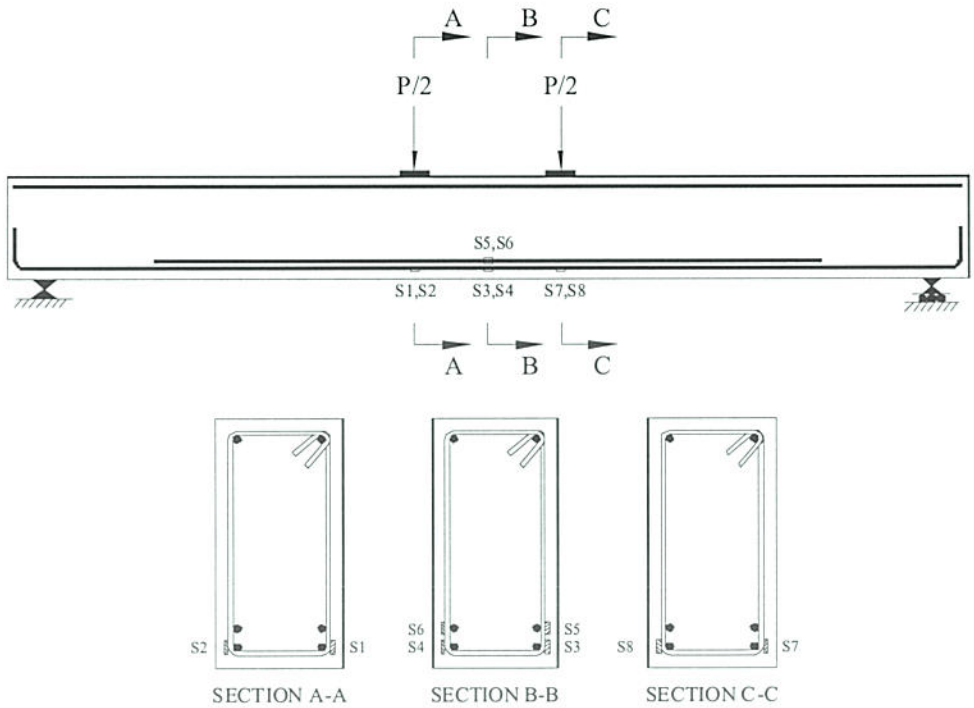

Figure 3.27 – Strain gauge locations on tensile reinforcement for corroded beams.

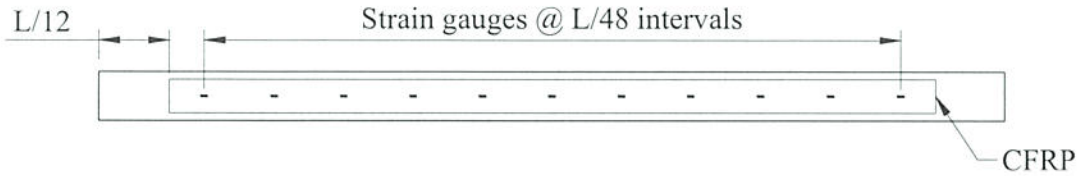

Figure 3.28 – Location of strain gauges on CFRP plate at bottom of beam.

3.6 Testing

3.6.1 Test setup and testing procedure

The beams were simply supported at each end and tested in four-point bending, as shown in Figure 3.30. Load was applied cyclically to the specimens using a sinusoidal wave loading control. The load range applied was between 20 percent and 60 percent of the theoretical failure load of the control beam at a loading rate of 1.5 Hz. The upper and lower loads for each test series are given in Table 3.19.

Prior to cycling of the load, the beams were loaded monotonically and held constant at the minimum and maximum load to record changes and take measurements. The Instron loading machine was programmed to pause at certain intervals during the cyclic loading to enable data recording and observations. These momentary pauses were more frequent during the lower cycle numbers as larger changes occur during the early cycles. After 100,000 load cycles, the testing was paused every further 100,000 cycles to record data and observations. At each stop, the load was locked off at the median load of 40 percent of the theoretical failure load. Observations of crack development on the concrete beams were then marked with a felt pen and Demec strains readings taken. Once this was completed, the cyclic loading was resumed for a period of 1 minute with the data logging set to record at a rate of 50 Hz to collect the deflection and steel and CFRP strains. Cyclic loading was then resumed without electronic data collection until the next measurement point was reached. Testing was undertaken for approximately 7 hours each day for the first 100,000 load cycles, after which the test was left to run overnight for 18.5 hours such that 100,000 load cycles was achieved each following morning. This process was repeated until the failure of the specimens or 2 million cycles, whichever occurred first.

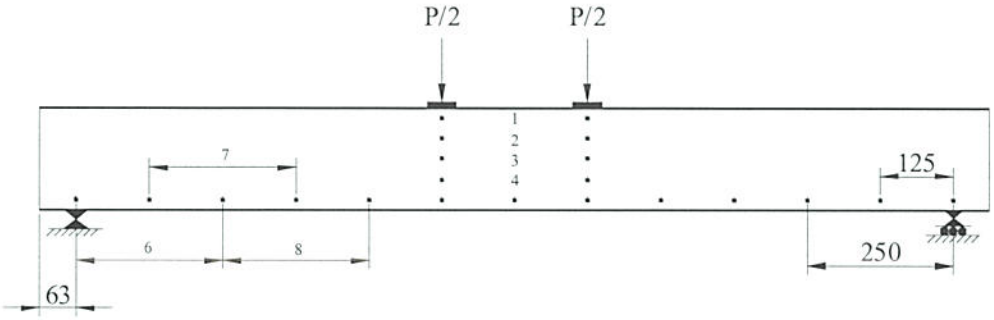

(a)

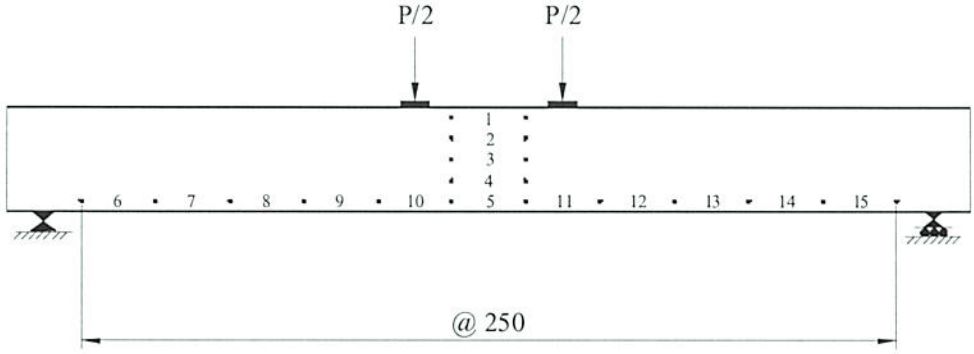

(b)

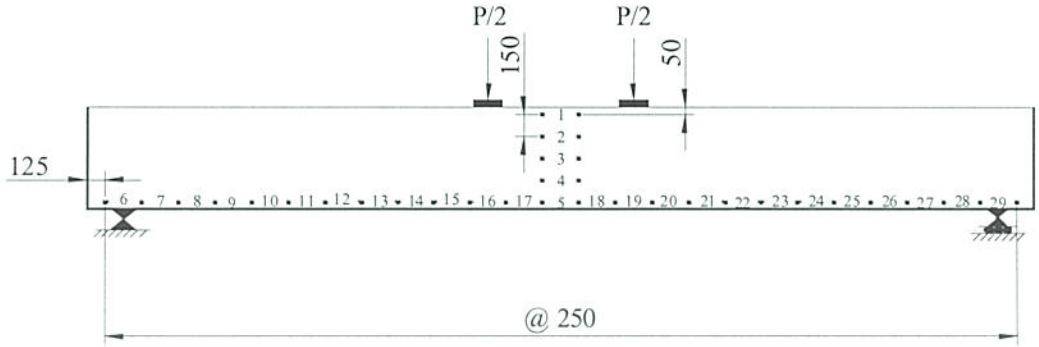

(c)

Figure 3.29 – Demec targets locations on concrete surface for beams in (a) Series A and D (b) Series B and (c) Series C.

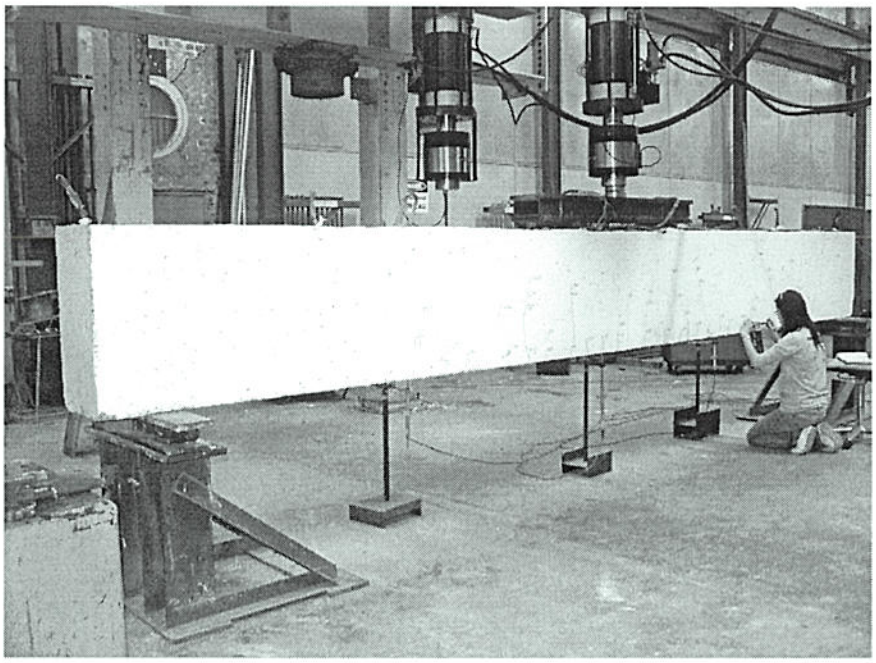

Figure 3.30 – Test setup for beam specimens.

Table 3.19 – Load ranges for test series.

Test series	Load range (kN)
A	5 – 17
B	20 – 80
C	75 – 240
D	6 – 19

4 TEST RESULTS AND OBSERVATIONS

4.1 Presentation of results

In this chapter, the experimental results are presented for the twelve test beams described in Chapter 3. The experimental results and observations are summarized in Section 4.2. The individual test result and crack patterns of each beam are given in Section 4.3. Section 4.4 gives an overall discussion of the test results. Finally, conclusions are given in Section 4.5.

4.2 Fatigue lives and failure modes

The fatigue lives and modes of failure for the twelve test beams are presented in Table 4.1 with seven beams failing by fatigue fracture of one or more of the tensile reinforcing bars. For two beams that were repaired with CFRP (beams B3 and C3), debonding of the plate was observed to occur immediately after the fracture of the tensile reinforcement. Beams D1 and D3 did not fail after 2 million cycles and were then loaded statically to failure. Beams A1 and A3 failed prematurely due to an error by the technical operator in making an adjustment to the loading system. Beam B2, severely corroded, failed before one load cycle was completed.

4.3 Beam test results

4.3.1 Specimen A1

Specimen A1 was the small-sized control beam, which was neither corroded nor repaired with CFRP. The beam was loaded monotonically up to the mean testing load of 11 kN and was then cycled between 5 kN and 17 kN at 1.5 Hz using a sinusoidal loading wave. Within 1000 load cycles, three flexural cracks had appeared in the constant moment region. Cracks grew in length up until 50,000 cycles with the primary crack measured to be 0.05 mm wide at the level of the tensile bars. The crack pattern remained the same until the load cycle reached 800,000 cycles, when the primary crack width was measured as 0.15 mm. Two flexural-shear cracks formed as cracks continued to grow until 900,000 cycles. At 1.2 million load cycles, the primary crack had grown and widened to 1.3 mm.

The mid span deflections of beam A1 at both maximum and minimum loads are shown in Figure 4.1. In the first cycle, the deflection of specimen A1 at maximum load was 1.1 mm and then increased steadily for the first 800,000 cycles. A rapid increase in deflection was

subsequently observed possibly due to a breakdown in the bond between the reinforcing bars and concrete. From 1.4 million cycles onwards, deflection remained constant at 10.3 mm and 8.9 mm during maximum and minimum loads respectively.

Table 4.1 – Loads, fatigue lives and modes of failure for test specimens.

Beam	Load range (kN)	No. of cycles	Failure mode
A1	5 – 17	> 1.2 million	Premature failure by crushing of specimen due to overload caused by testing machine breakdown.
A2	5 – 17	272,400	Fatigue fracture of tensile steel.
A3	5 – 17	> 1.2 million	Premature failure by crushing of specimen due to overload caused by testing machine breakdown.
B1	20 – 80	508,000	Fatigue fracture of tensile steel.
B2	-	0	Fracture of tensile steel, due to extensive localized corrosion.
B3	20 – 80	308,946	Fatigue fracture of tensile steel, followed immediately by CFRP debonding.
C1	75 – 240	1.705 million	Fatigue fracture of tensile steel.
C2	75 – 240	100,590	Fatigue fracture of tensile steel.
C3	75 – 240	343,695	Fatigue fracture of tensile steel, followed by immediate CFRP debonding.
D1	6 – 19	> 2 million	Loaded monotonically and failed at 32.6 kN.
D2	6 – 19	3,750	Fatigue fracture of tensile steel.
D3	6 – 19	> 2 million	Loaded monotonically and failed at 55.6 kN.

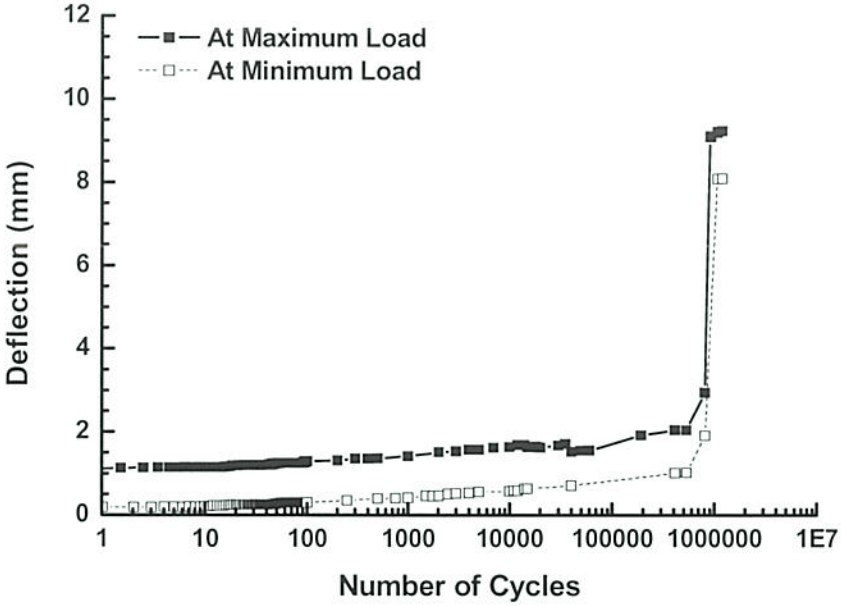

Figure 4.1 – Deflection versus number of cycles for beam A1 (at midspan).

Figure 4.2 shows the steel strain in the tensile bars during loading. The four tensile bars had steady increases in strain up until about 500,000 cycles after which the strains increased significantly to between 15,000 με and 25,000 με at 800,000 cycles. Such high strain readings (in excess of the fracture strain of the bars) are an indication of the strain gauges being faulty, after 800,000 cycles.

The concrete strains obtained using Demec gauges at the mid span and along the beam at the level of longitudinal tensile steel bars are given in Figures 4.3 and 4.4, respectively. These strain values were measured when the load was held constant at the mean load, which was 40 percent of the calculated failure load, at 11 kN. According to Figures 4.3 and 4.4, progressive failure is most pronounced when testing passed 790,000 load cycles. The beam survived another 410,000 load cycles to reach 1.2 million cycles after which it failed prematurely due to the testing machine technical error.

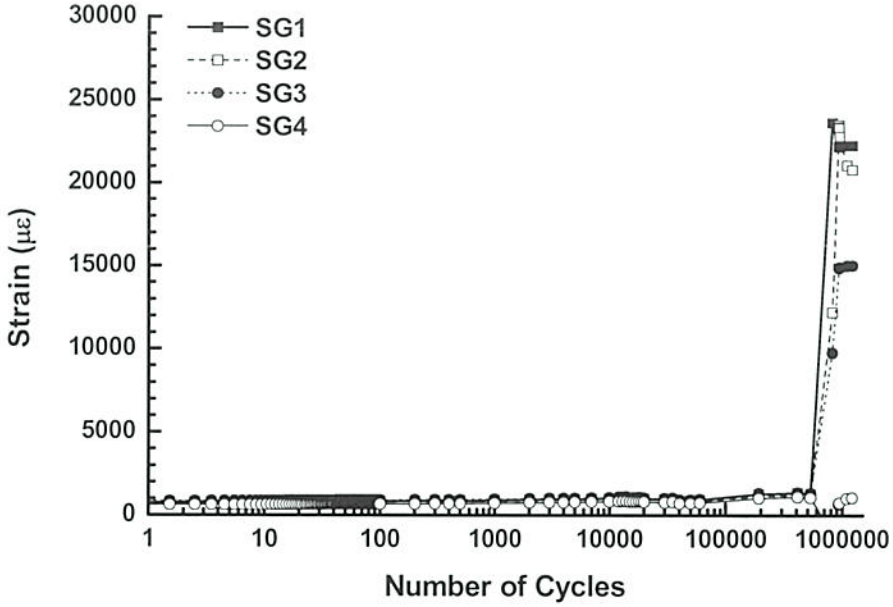

Figure 4.2 – Steel strain at midspan versus number of cycles for beam A1 taken at the maximum cyclic load of 17 kN.

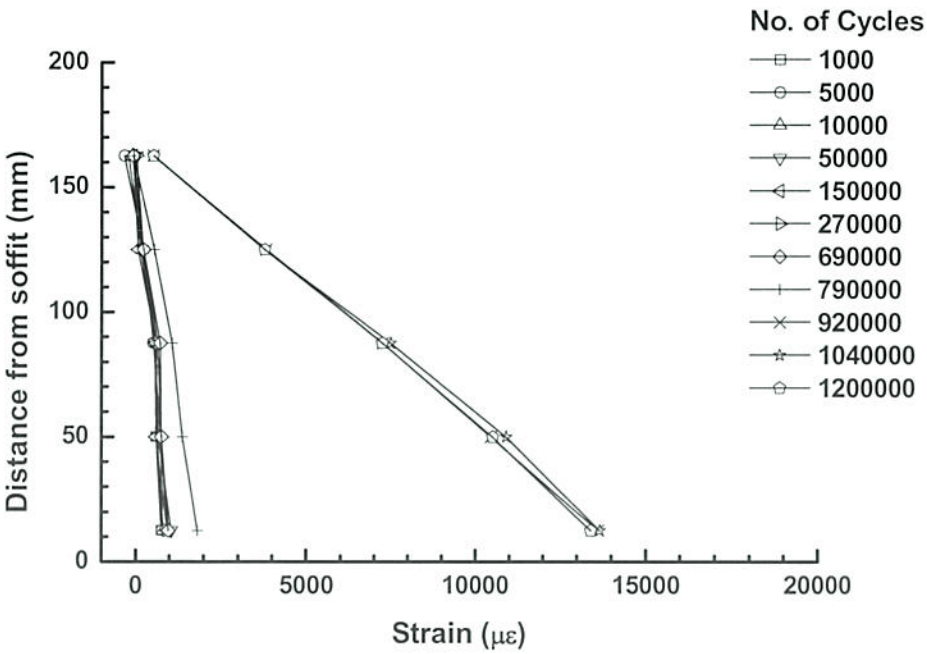

Figure 4.3 – Average strain measured using Demec gauges (at mid-span) versus distance from beam soffit for increasing load cycles for beam A1 at the mean cyclic load of 11 kN.

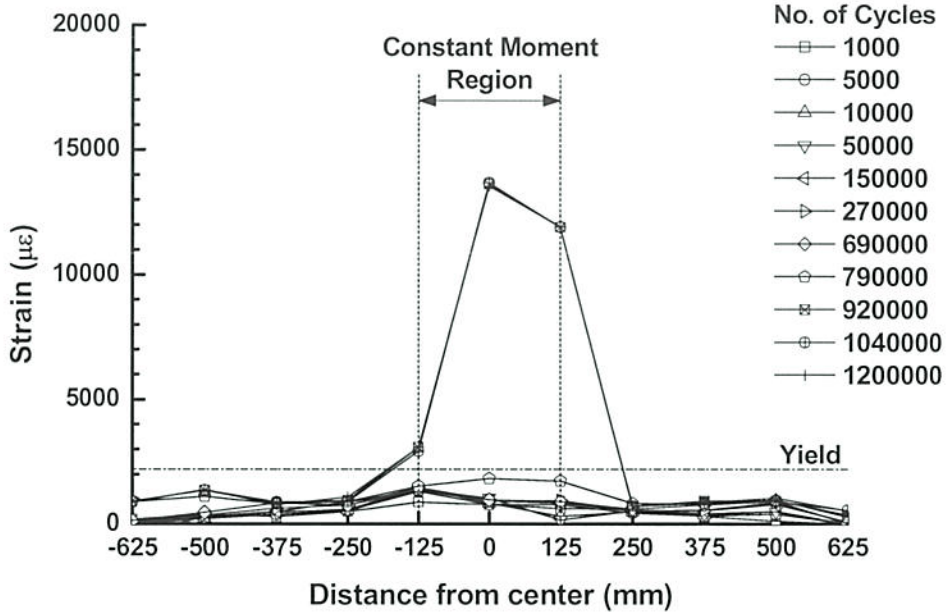

Figure 4.4 – Strain data of Demec gauges 6 to 15 along beam A1 taken at the mean cyclic load of 11 kN.

4.3.2 Specimen A2

Specimen A2 was corroded, repaired with mortar and then cyclically loaded to failure. After approximately 260 load cycles, five flexural cracks had formed. The cracks grew and new cracks formed up to approximately ⅓ the depth of the beam as the cycles increased to 1000 cycles. No further cracks formed until 10,000 cycles when a single flexural crack formed in the constant moment region. The cracks stabilised and no new cracks appeared after 10,000 cycles. At 130,000 cycles, the cracks grew slowly and steadily up to 260,000 cycles. After 260,000 cycles, crack growth was rapid at the main crack, which was directly under one of the load points. The last measured crack width was 1.27 mm at 11 kN, measured at the level of the tensile reinforcement, after 271,100 cycles. At 272,400 cycles, the beam failed by fracture of tensile steel.

Figure 4.5 shows the mid span deflections of beam A2 at maximum and minimum loads. At the first load cycle, beam A2 had a maximum deflection of 1.4 mm that was followed by a steady increase in deflection for the first 40,000 cycles. After this the deflection was almost constant at approximately 3.8 mm until just prior to failure. After 271,000 cycles, the deflection increased dramatically signalling the impending failure.

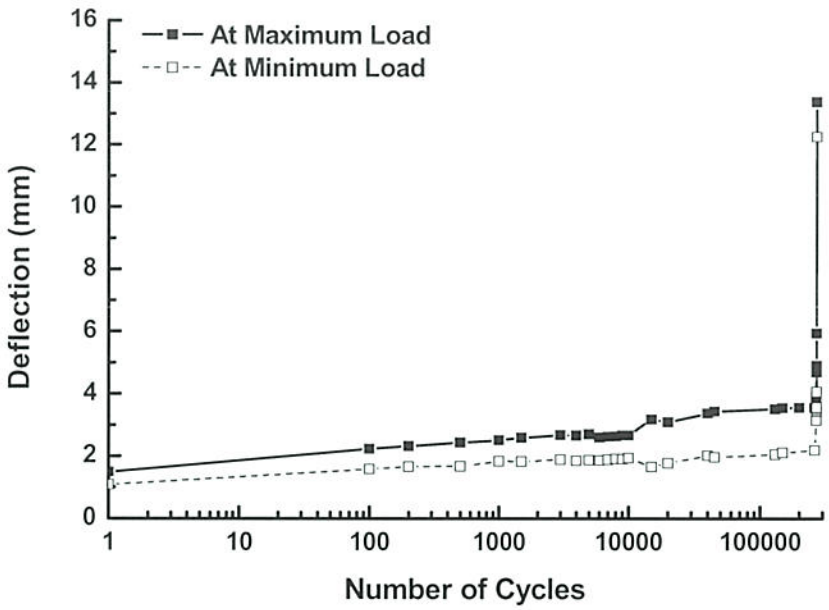

Figure 4.5 – Deflection versus number of cycles for beam A2 (at midspan).

The steel strains at midspan are shown in Figure 4.6. Consistent with the increase in deflection observed, steel strains increased at a steady rate for the first 40,000 cycles. This was followed by a reasonably constant strain until just prior to failure where changes in strain signified fracture of the tensile bars.

Figure 4.7 and Figure 4.8 show the Demec strains measured at the midspan through the section depth and along the beam at the level of tensile reinforcement, respectively. The concrete strains remained unchanged for most part of the testing stage. A significant increase in strain was observed at about 1000 cycles prior to failure, with failure occurring at 272,400 cycles under one of the load points, as shown in Figure 4.9.

4.3.3 Specimen A3

Specimen A3 was corroded, repaired with mortar and then further repaired with one strip of CFRP at the soffit. The first crack appeared after 1000 cycles at the midspan, with further cracks developing until 40,000 cycles. The cracks remained stable from 40,000 cycles to 180,000 cycles with one crack forming at 180,000 cycles and another at 286,000 cycles. The crack pattern was unchanged throughout the rest of the test. Specimen A3 was tested in parallel with specimen A1 and, as for specimen A1, at 1.21 million cycles, a problem with the jacking system overloaded the specimen causing instantaneous, uncontrolled, failure of the specimen. The widest crack measured just 0.05 mm before the failure of the jack.

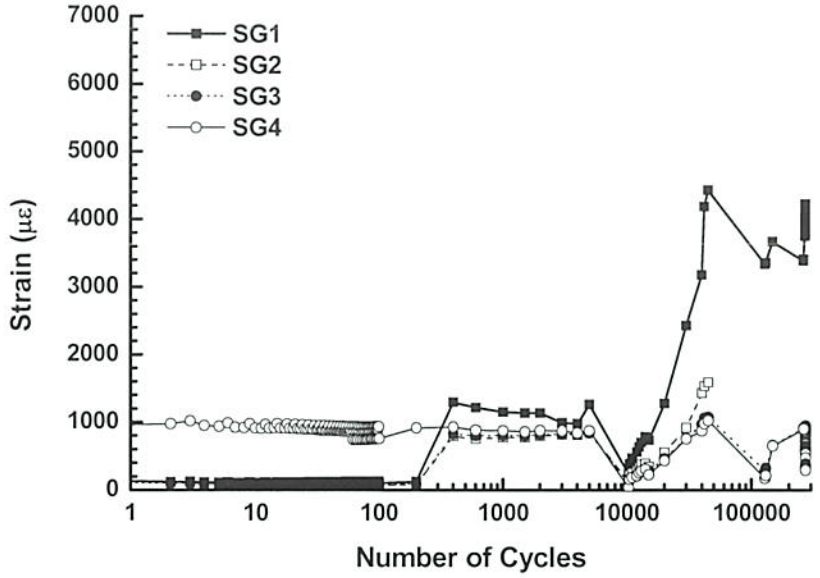

Figure 4.6 – Steel strain at midspan versus number of cycles for beam A2 taken at the maximum cyclic load of 17 kN.

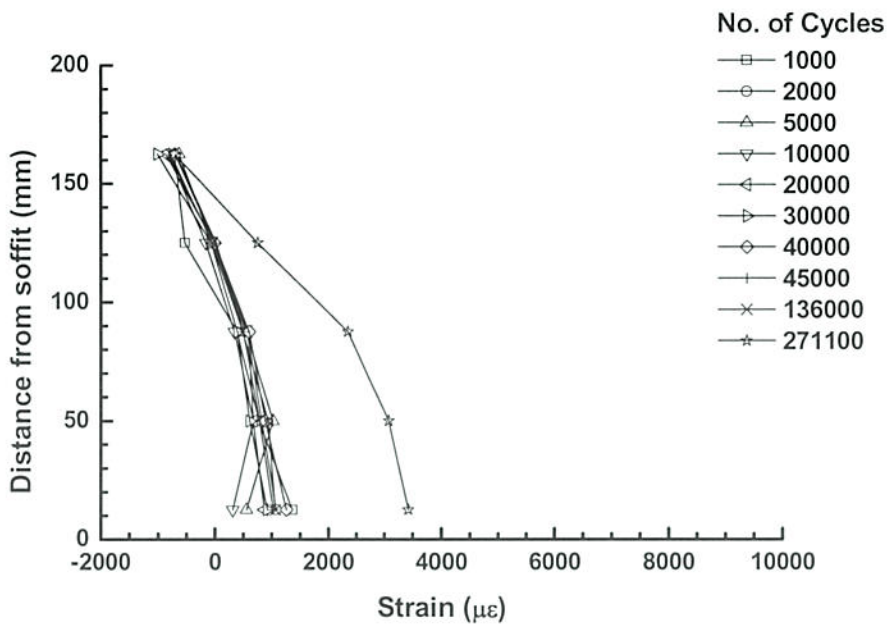

Figure 4.7 – Average strain measured using Demec gauges versus distance from beam soffit for increasing load cycles for beam A2 at the mean cyclic load of 11 kN.

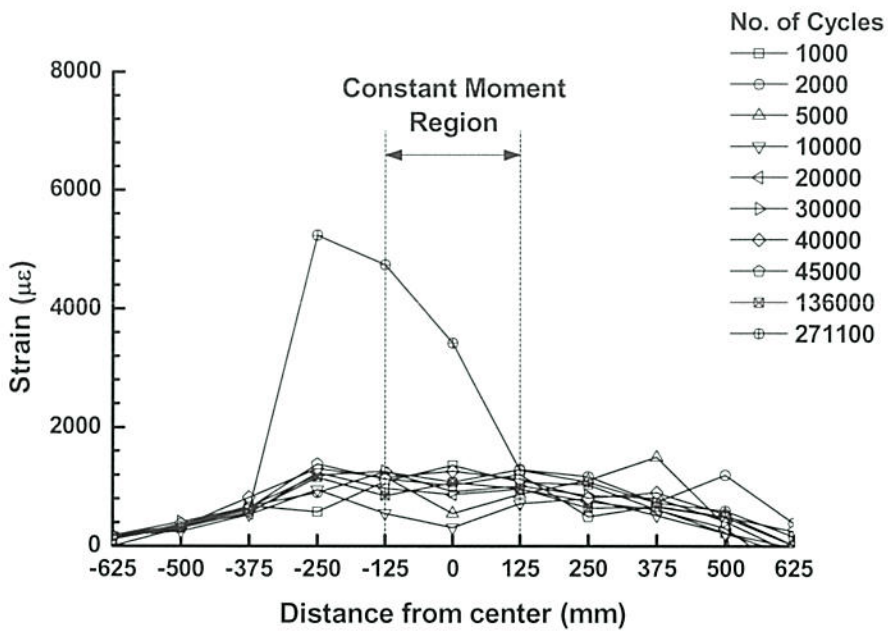

Figure 4.8 – Strain data of Demec gauges 6 to 15 along beam A2 taken at the mean cyclic load of 11 kN.

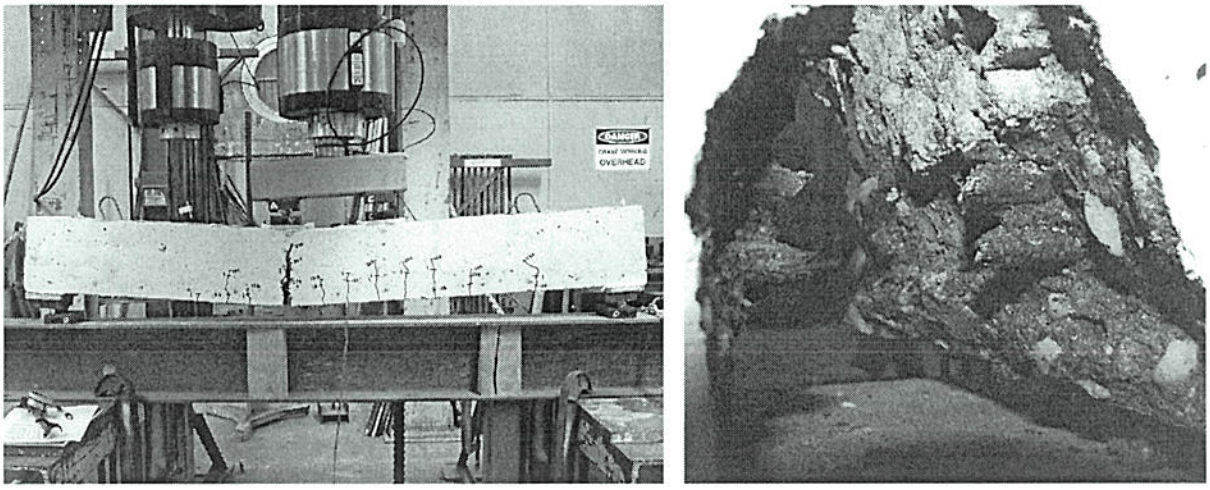

(a) (b)

Figure 4.9 – (a) Beam A2 at failure and (b) fracture of corroded tensile bars.

The mid span deflection for the test is shown in Figure 4.10. A deflection of 1.3 mm was measured at the first load cycle and then the specimen experienced a very slow and steady increase of deflection throughout the test. After 1.21 million cycles, the deflection of beam A3 was 2.1 mm.

Figure 4.11 shows the steel strains measured at midspan during maximum load at 17 kN. Strains remained relatively constant throughout the test, with the exception of one strain

gauge (SG2) showing a slight increase from 500,000 cycles onwards. The concrete strains measured at midspan and through the specimen depth, using the Demec gauge, and along the beam at the level of the tensile steel, remained relatively unchanged for the whole test, as shown in Figures 4.12 and 4.13, respectively.

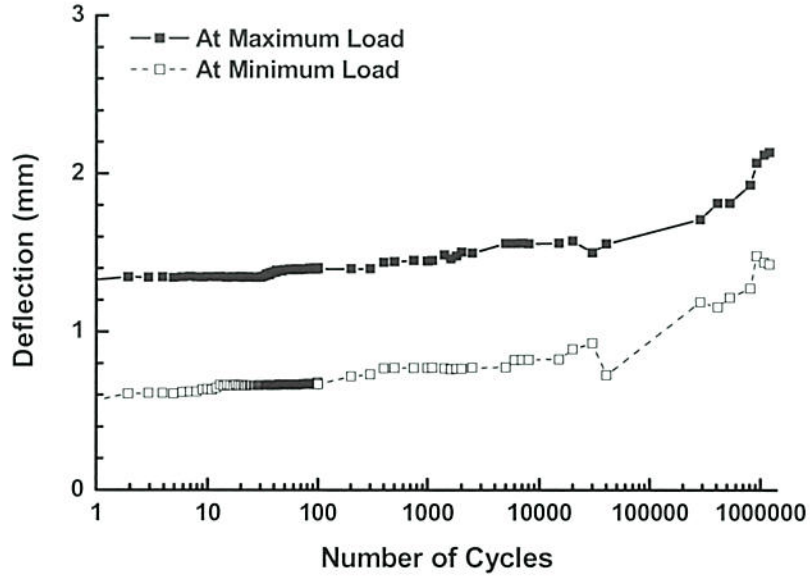

Figure 4.10 – Deflection versus number of cycles for beam A3 (at midspan).

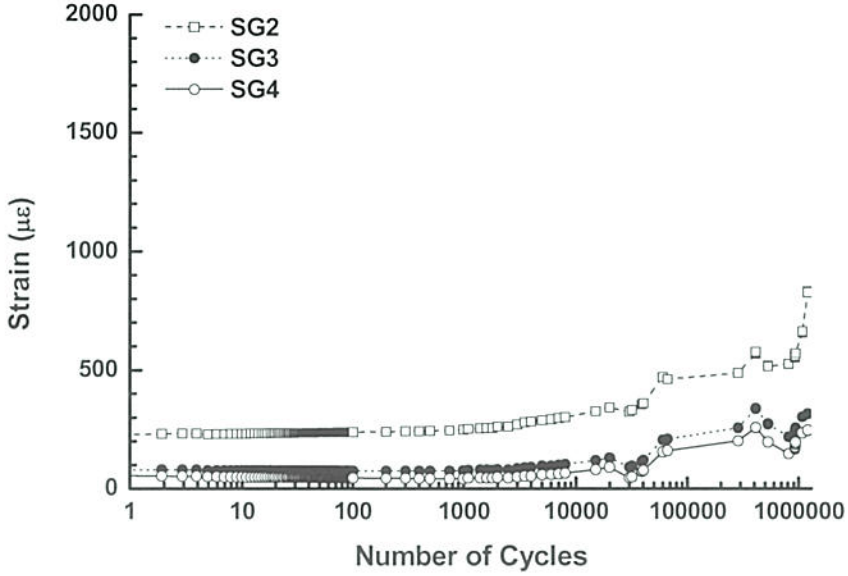

Figure 4.11 – Steel strain at midspan versus number of cycles for beam A3 taken at the maximum cyclic load of 17 kN.

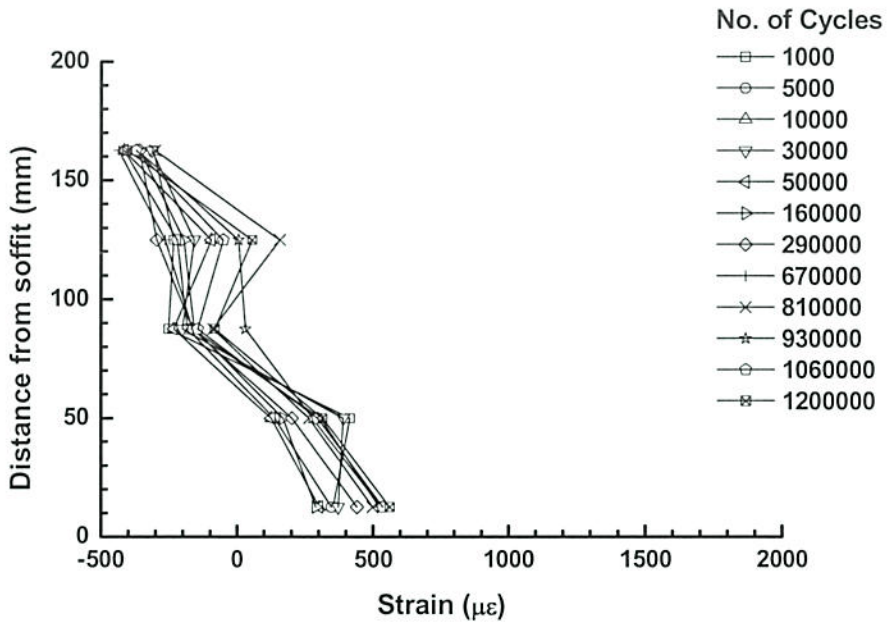

Figure 4.12 – Strain versus distance from beam soffit for increasing load cycles for beam A3 at 11 kN.

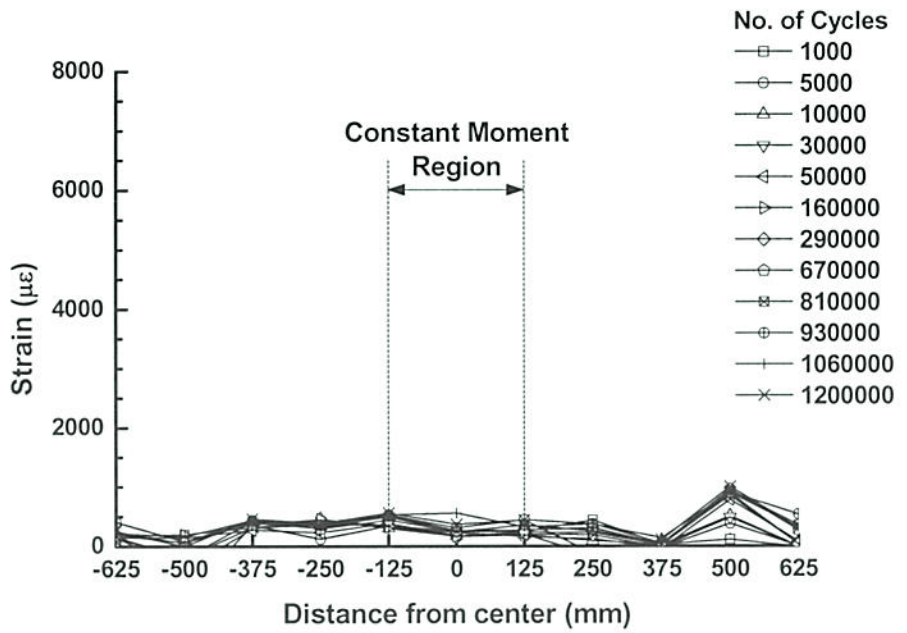

Figure 4.13 – Strain data of Demec gauges 6 to 15 along beam A3 taken at the mean cyclic load of 11 kN.

Strains the CFRP surface were recorded at 125 mm intervals using electronic strain gauges. Figure 4.14 shows the CFRP strain at the maximum load. A small but steady increase in strain is observed, with an increase in strain of 400 με after 1.2 million cycles at the midspan. There were no physical signs of debonding of the CFRP. Figure 4.15 shows the condition of beam A3 at 1.21 million cycles.

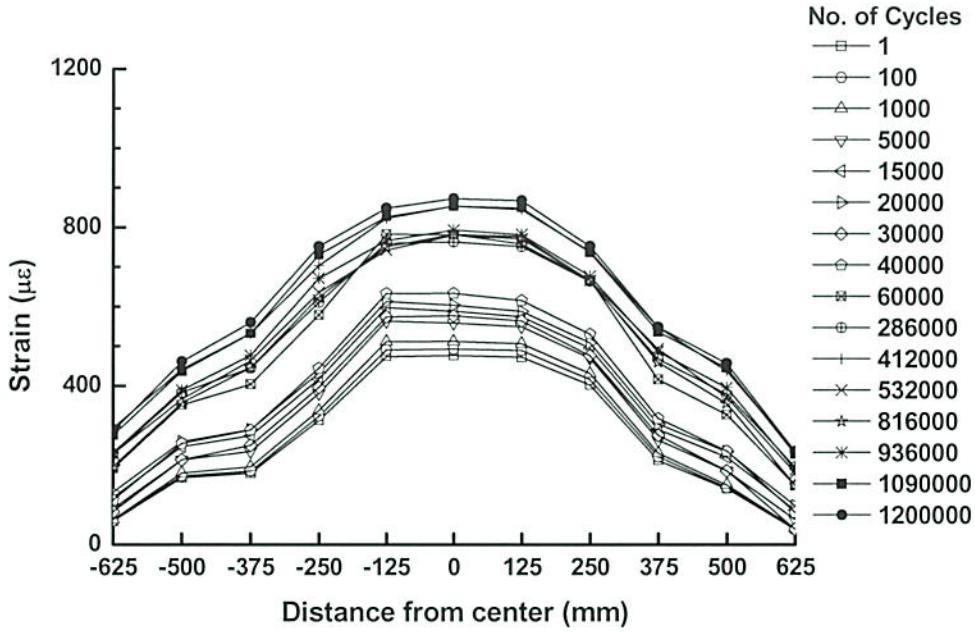

Figure 4.14 – CFRP strain along soffit of beam A3 at maximum cyclic load of 17 kN.

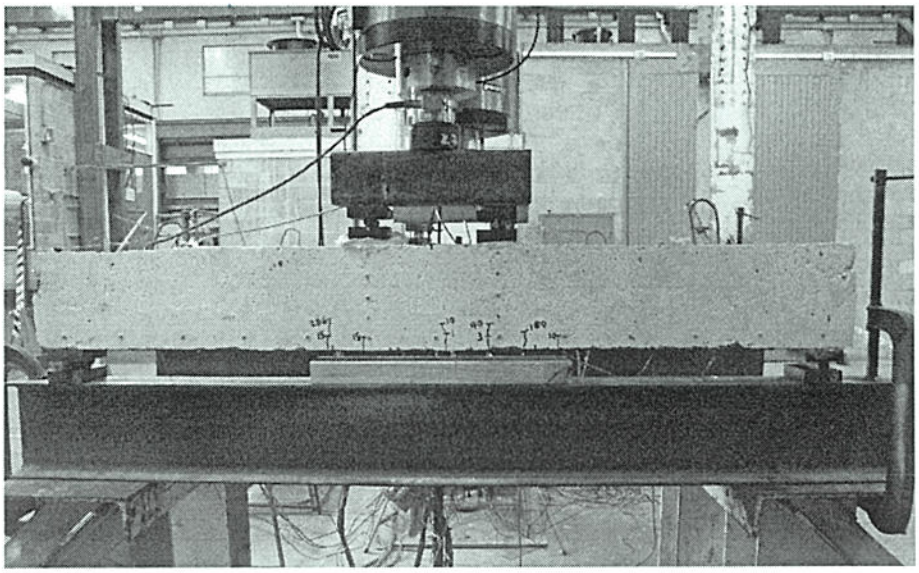

Figure 4.15 – Beam A3 at 1.21 million cycles prior to overload caused by the system failure.

4.3.4 Specimen B1

Specimen B1 was the control for the medium size beams. The beam was loaded monotonically up to the mean load of 50 kN and was then cycled between 20 kN and 80 kN at 1.5 Hz using a sinusoidal loading wave. After the first cycle, approximately 15 flexural and shear cracks appeared on the beam. The crack pattern remained unchanged until approximately 160,000 cycles, where the cracks developed further. At 508,000 cycles, a primary crack was identified as one of the cracks under the load point. This crack was the location of the eventual fracture of the bottom tensile steel bar.

Figure 4.16 shows the maximum and minimum deflections of the beam during the test. The deflection at the maximum load started out at 8.3 mm and increased steadily to 10.8 mm at about 400,000 cycles. Similarly, the deflection at minimum load began at 0.8 mm and increased to 6.0 mm at about 400,000 cycles. The last recorded maximum deflection was at 18.2 mm at 508,000 cycles, just prior to failure. Figure 4.17 shows a relatively constant strain in the tensile bars up until about 400,000 cycles when a slight drop in strain is observed in the two tensile bars at the bottom layer. Figures 4.18 and 4.19 show the Demec strain data at midspan and along the beam, respectively. Both figures show a relatively small change in strain up until just prior to failure. The failure of Beam B1 is shown in Figure 4.20.

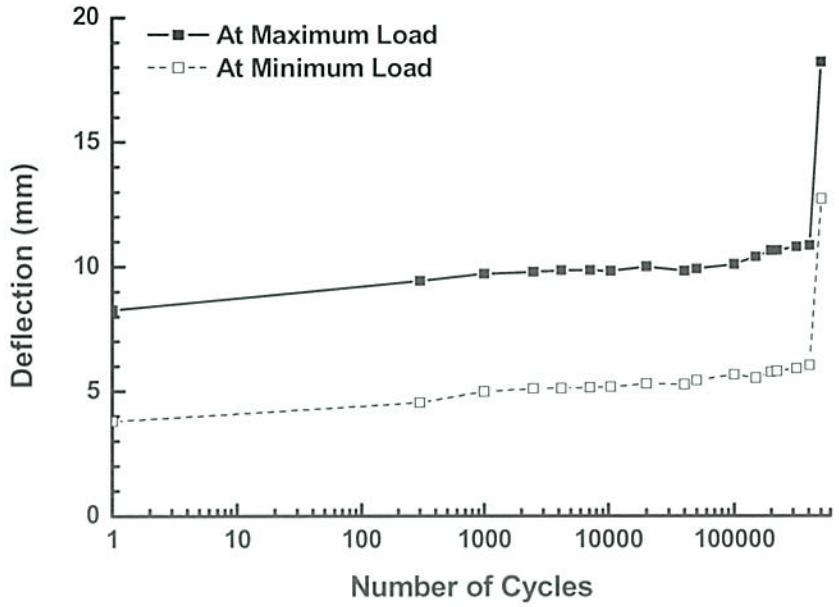

Figure 4.16 – Deflection versus number of cycles for beam B1 (at midspan).

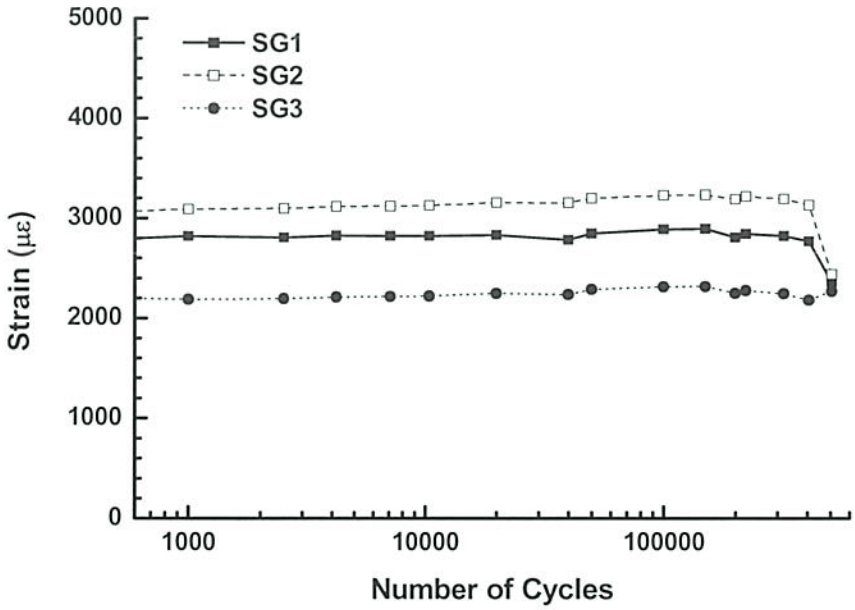

Figure 4.17 – Steel strain at midspan versus number of cycles for beam B1 taken at the maximum cyclic load of 50 kN.

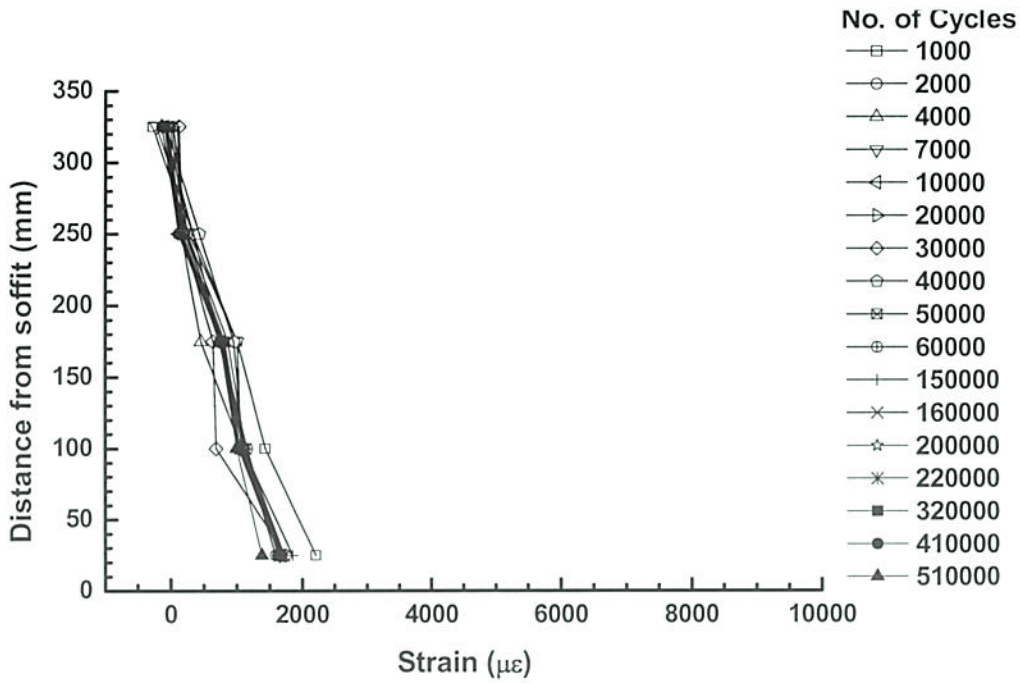

Figure 4.18 – Average strain measured using Demec gauges versus distance from beam soffit for increasing load cycles for beam B1 at the mean cyclic load of 50 kN.

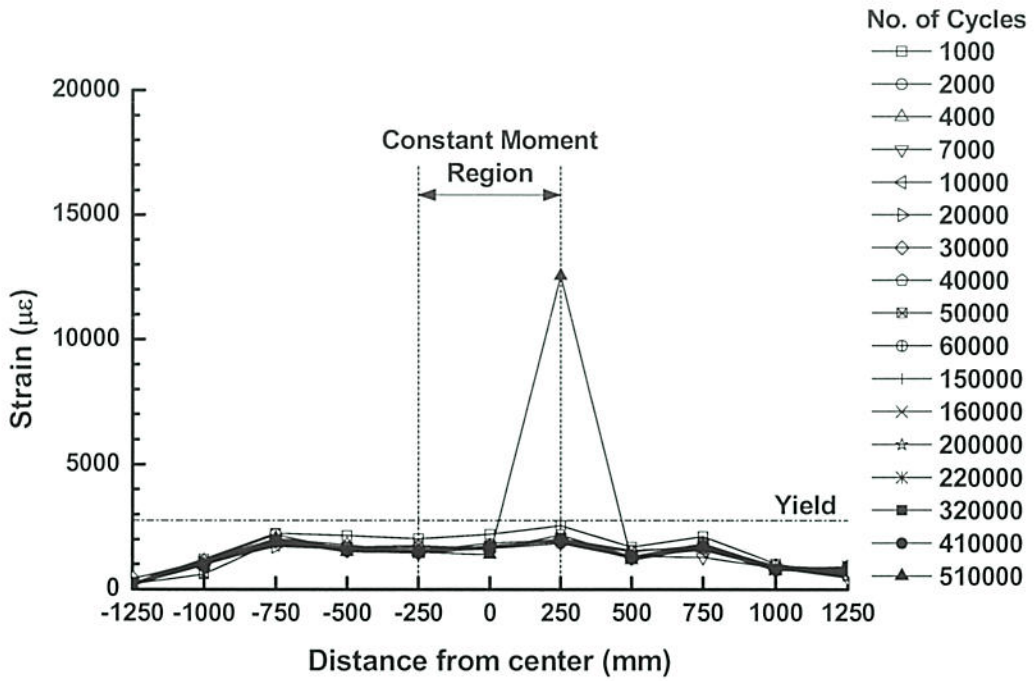

Figure 4.19 – Strain data of Demec gauges 6 to 15 along beam B1 taken at the mean cyclic load of 50 kN.

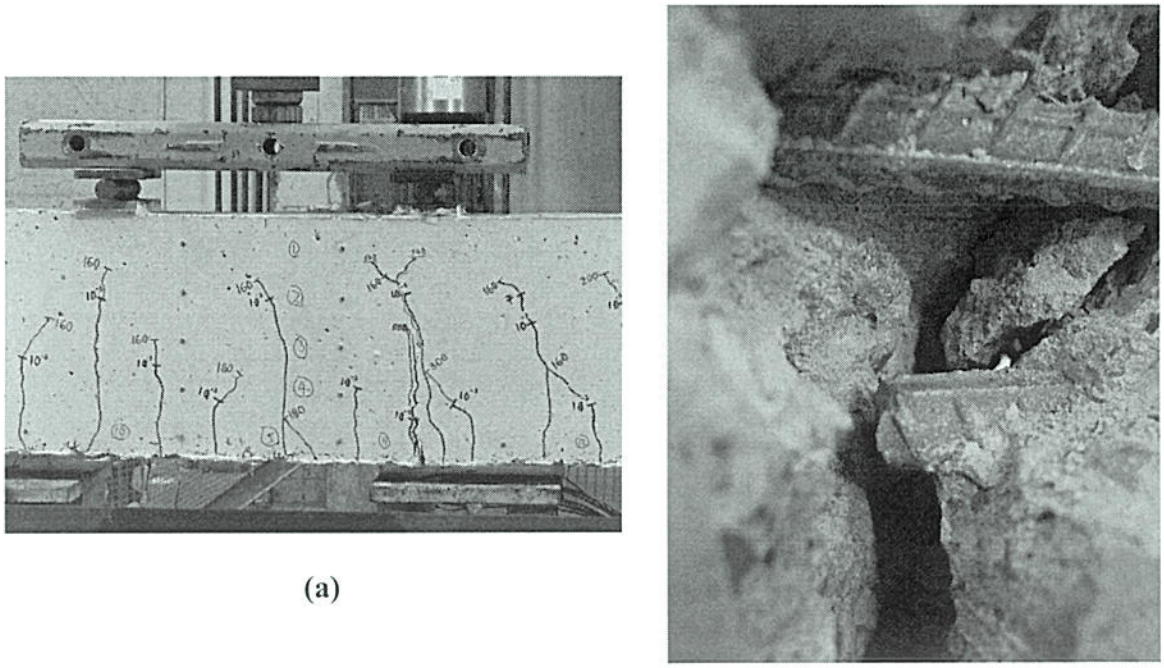

(a)

(b)

Figure 4.20 – (a) Failure of beam B1 near midspan and (b) fracture of bottom tensile bar.

4.3.5 Specimen B2

Specimen B2 was corroded and then repaired with mortar. It was to be subjected to the same cyclic loading conditions as beam B1. However, the beam failed at the first load cycle. Failure occurred under one of the load points, as shown in Figure 4.21 and no data was recorded, other than the load, as the failure was unexpected. The beam failed at 79.3 kN. Only a single crack was observed in the specimen at the point where the reinforcing steel fractured.

4.3.6 Specimen B3

Specimen B3 was corroded, repaired with mortar and then further repaired with one strip of CFRP at the soffit. At the first load cycle, 13 cracks formed at intervals of approximately 100 mm within a length of 1000 mm at the midspan. Up to 100,000 load cycles, seven new cracks developed on either side of the midspan at approximately the same interval. Also the existing cracks had lengthened. A primary crack was identified at 300,000 cycles under one of the load points. Upon close inspection, there was a bond crack at the interface between the CFRP and the concrete. This crack originated from the primary crack and propagated towards the near end of the beam. The primary crack on the beam progressed until failure occurred by fracture of the tensile reinforcement bar. This was followed immediately by debonding of the CFRP.

Figure 4.22 shows the maximum and minimum deflections of beam B3 during testing. Beam B3 deflected by 8.0 mm and 1.4 mm when subjected to the first cycle of maximum and minimum loads, respectively. The deflections increased steadily throughout the test until a rapid increase was observed from 300,000 load cycles onwards, signally imminent failure.

Figure 4.23 shows the steel strains at midspan and under the load points. Demec data taken through the section depth at midspan and along the beam at the level of tensile steel is given in Figures 4.24 and 4.25, respectively. From 200,000 cycles to 300,000 cycles, the strains changed noticeably due to the rapid increase in the size of the primary crack. Figure 4.26 shows the strains in the CFRP as the load cycles progressed. The specimen failed at 308,946 cycles and the failure is shown in Figure 4.27.

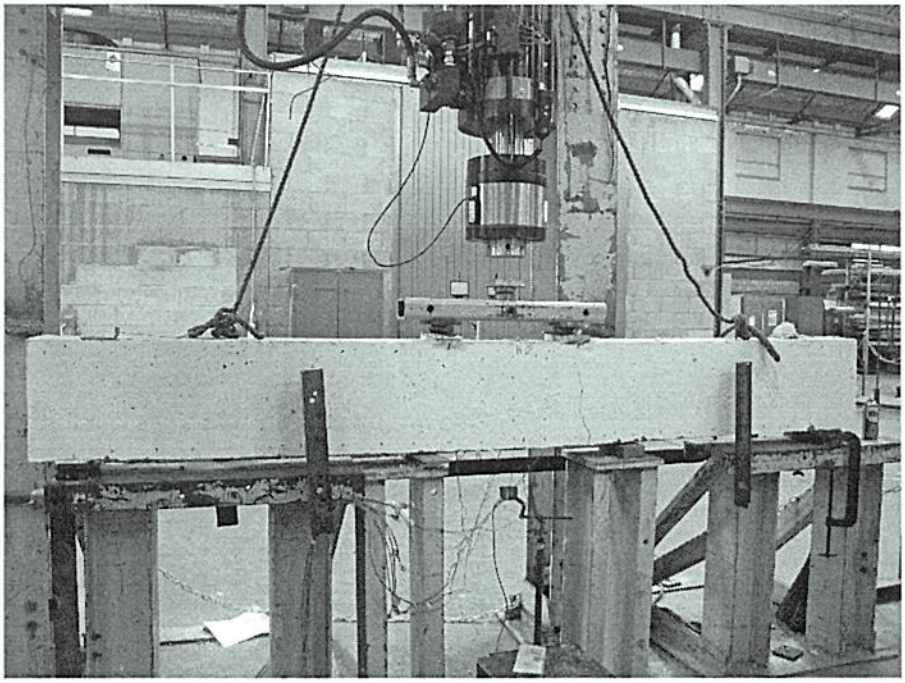

Figure 4.21 – Beam B2 at failure.

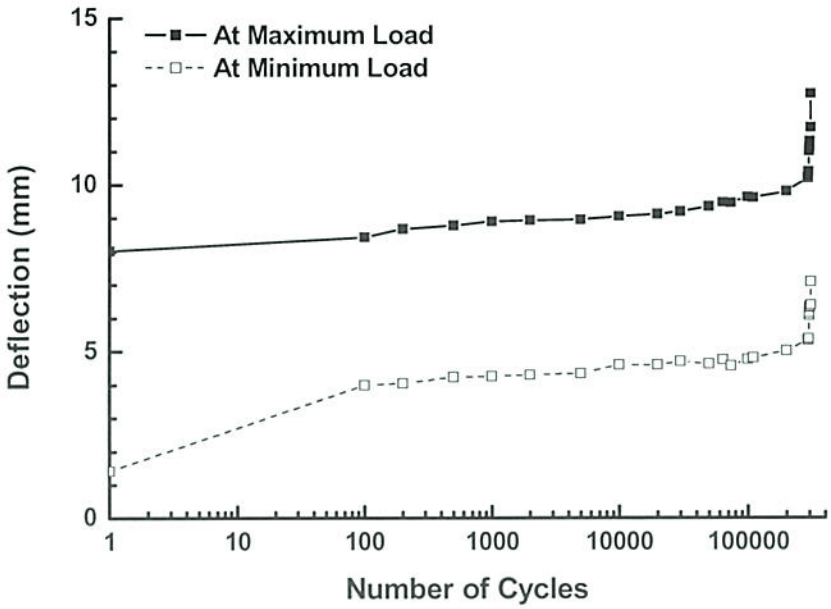

Figure 4.22 – Deflection versus number of cycles for beam B3 (at midspan).

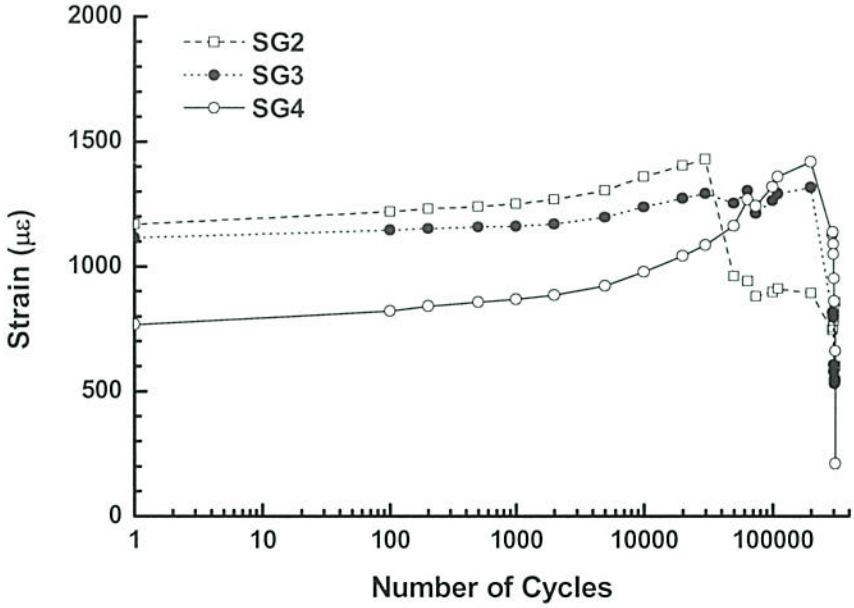

(a)

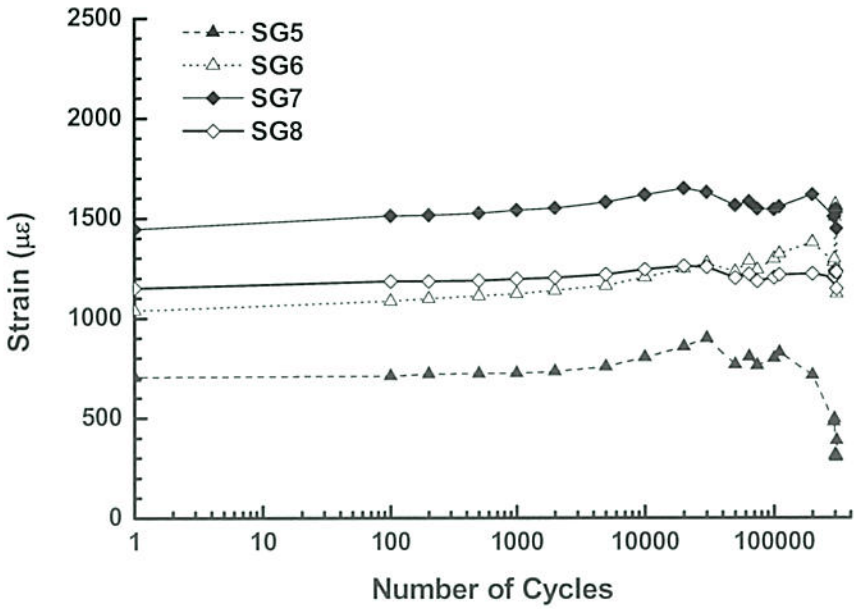

(b)

Figure 4.23 – Steel strain versus number of cycles for beam B3 taken at the maximum cyclic load of 80 kN (a) at midspan and (b) at load points.

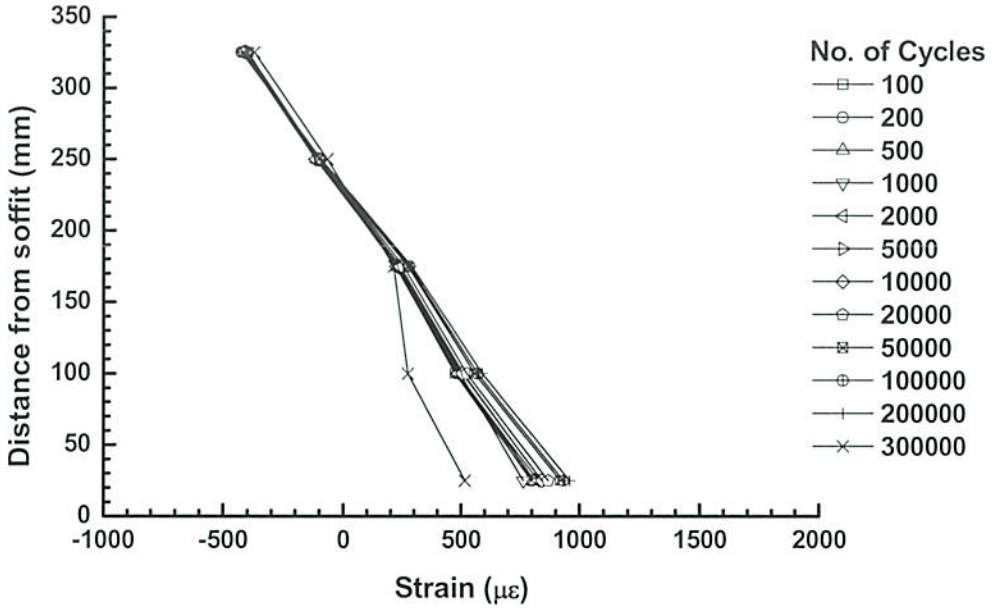

Figure 4.24 – Average strain measured using Demec gauges versus distance from beam soffit for increasing load cycles for beam B3 at the mean cyclic load of 50 kN.

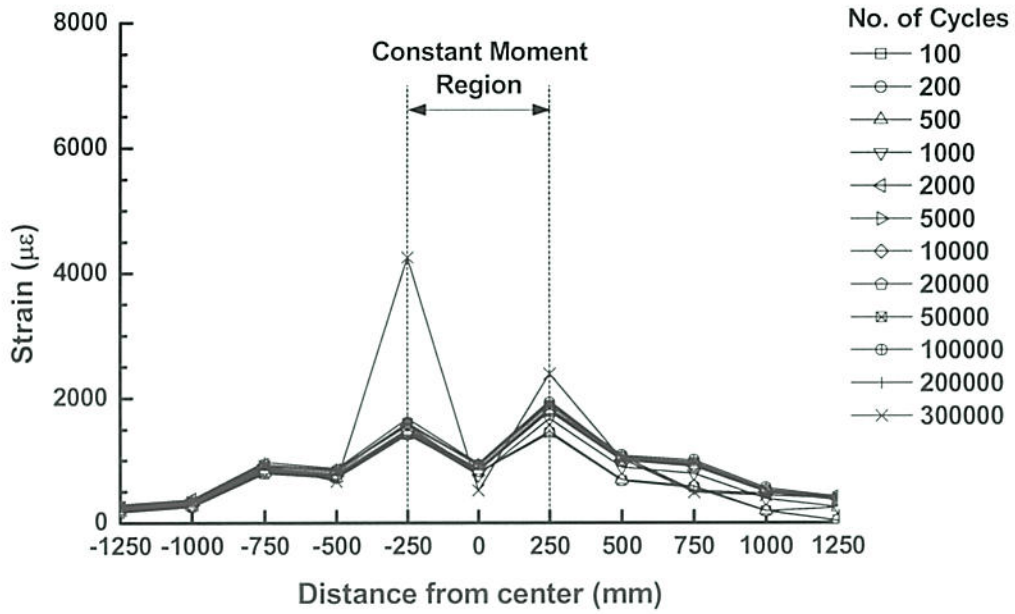

Figure 4.25 – Strain data of Demec gauges 6 to 15 along beam B3 taken at the mean cyclic load of 50 kN.

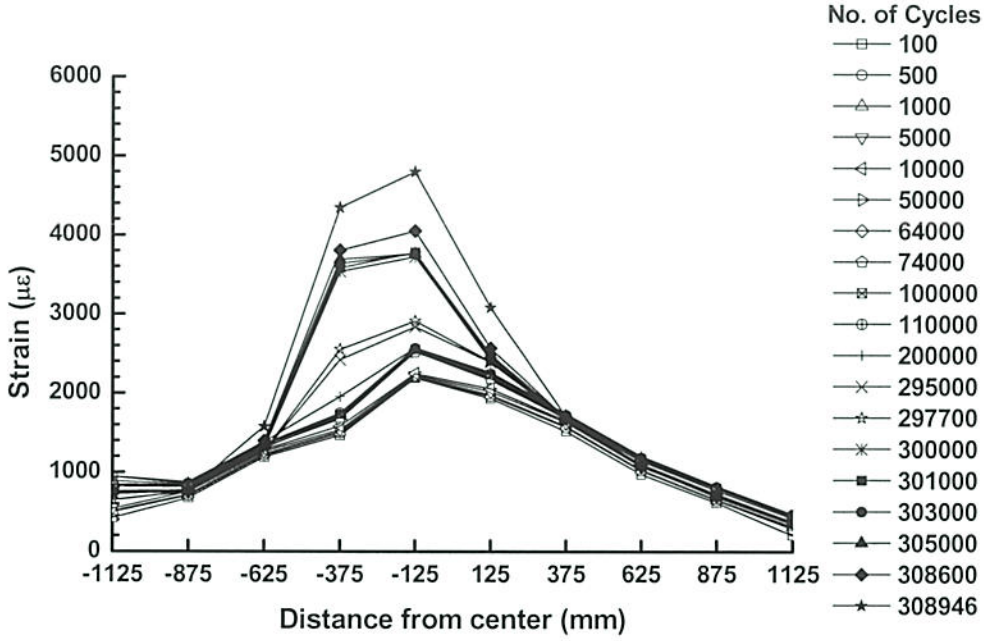

Figure 4.26 – CFRP strain along soffit of beam B3 at maximum cyclic load of 80 kN.

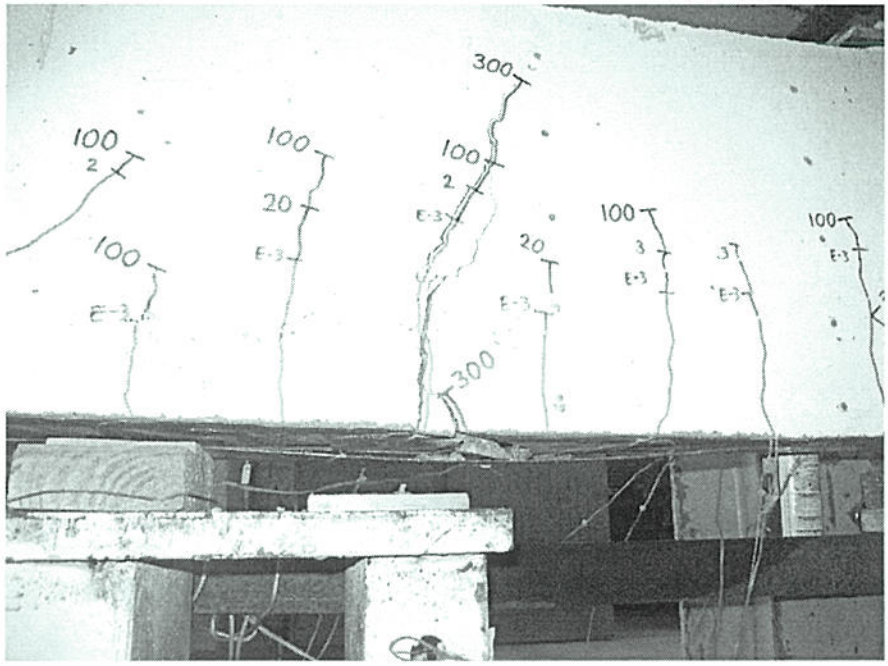

Figure 4.27 – Debonding of CFRP originating from the primary crack under one of the load points.

4.3.7 Specimen C1

Specimen C1 served as the control for the large-sized beams. The specimen was loaded between 75 kN and 245 kN at a loading rate of 1.5 Hz. Prior to the cyclic loading, the beam was loaded to the mean load of 170 kN. Twenty six flexural cracks were visible on the concrete surface. The cracks in the constant moment region had developed to approximately 70 percent of the beam depth. The beam was then loaded with one load cycle. Flexural-shear cracks formed at about 700 mm from each end support, in addition to propagation of the existing flexural cracks. These cracks developed further for the next 600,000 cycles, although most of the crack development occurred within the first few hundred thousand cycles. After 600,000 load cycles, the crack pattern stabilized until at 1.5 million cycles when crack propagation again continued. The crack pattern stabilized once again and a major crack was identified at the midspan.

Figure 4.28 shows the deflections of beam C1 during loading. The deflections were at 14.3 mm and 6.8 mm during the maximum and minimum loads, respectively, at the first load cycle. The deflections increased at a steady rate throughout the test. The last recorded deflections were at 34.8 mm and 24.5 mm at the maximum and minimum loads, respectively, after 1.7 million load cycles.

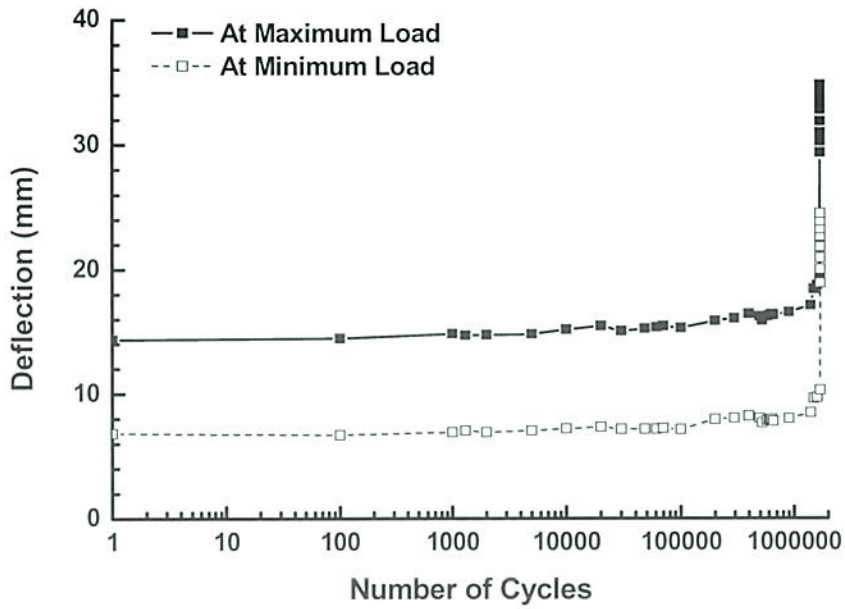

Figure 4.28 – Deflection versus number of cycles for beam C1 (at midspan).

Figure 4.29 shows the data from strain gauges attached to the tensile bars at midspan and under the load points. The Demec strains measured through the section depth at the beam midspan are shown in Figure 4.30 and the strains along beam length at the level of tensile reinforcement are shown in Figure 4.31.

Failure was by the fracture of the bottom tensile bar, adjacent to the primary crack, as shown in Figure 4.32. Beam C1 failed after 1.705 million load cycles.

4.3.8 Specimen C2

Specimen C2 was the corroded and mortar-repaired beam of the large beams. The beam was first loaded to the mean load of 170 kN and approximately 25 flexural cracks formed. The beam was then loaded with one cycle and paused at the mean load. New flexural-shear cracks had formed and the existing flexural cracks had further propagated. The cracks continued to propagate for the next 50,000 cycles. The crack pattern then remained stable until further crack propagation occurred at the midspan after 95,000 load cycles. By then, the major crack had developed in length, to about 80 percent of the beam depth.

The midspan deflections are shown in Figure 4.33. Beam C2 started with deflections at the maximum and minimum cycle loads of 16.3 mm and 7.8 mm, respectively. A steady increase in deflections was observed for the first 50,000 cycles, after which the deflections increased at a slightly higher rate until 95,000 cycles. After 95,000 load cycles, the deflections increased at a rapid rate, signalling the onset of failure. The last recorded deflections were 39.7 mm and 30.2 mm at maximum and minimum loads, respectively, after 100,590 load cycles.

Figure 4.34 show strains in the tensile bars of beam C2. The Demec strain data at midspan and along the beam length are shown in Figures 4.35 and 4.36, respectively. Beam C2 failed at the midspan, after 100,590 load cycles (Figure 4.37).

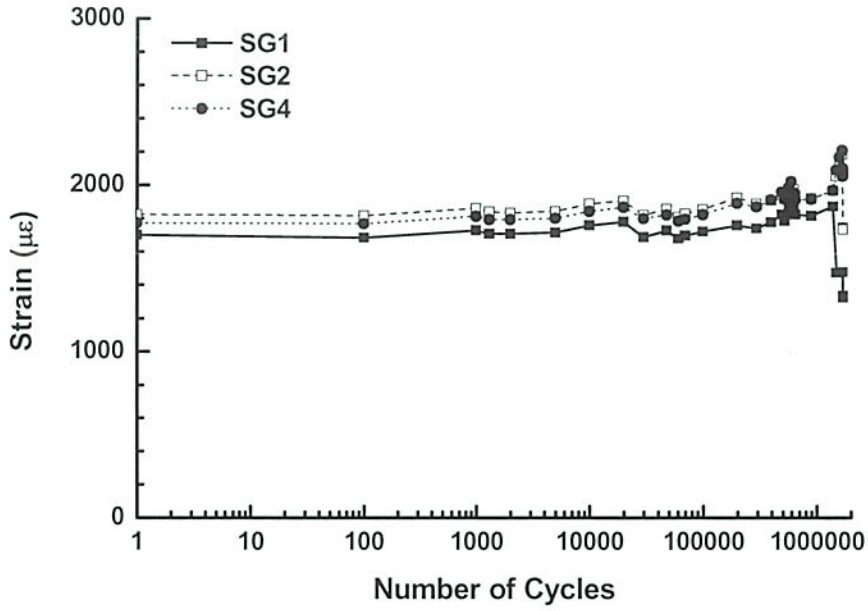

(a)

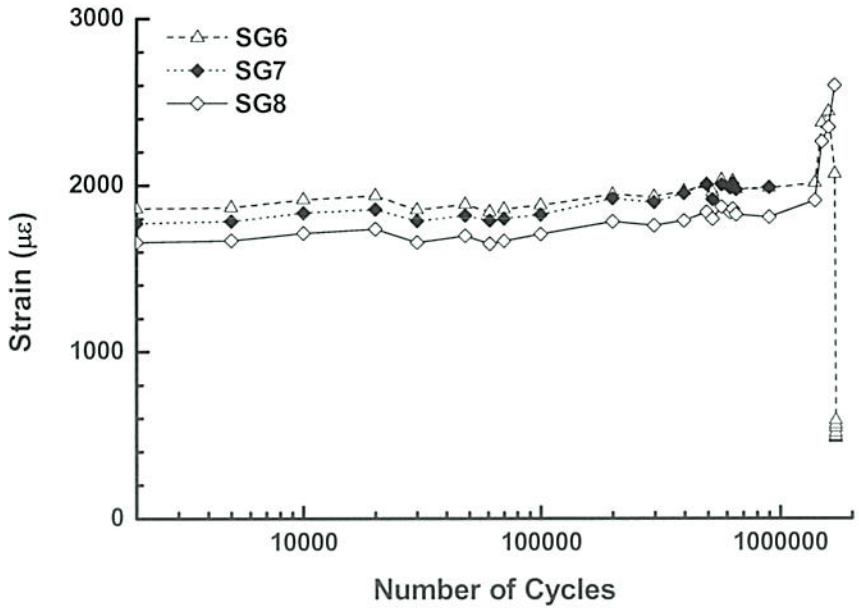

(b)

Figure 4.29 – Steel strain versus number of cycles for beam C1 taken at the maximum cyclic load of 240 kN (a) at midspan and (b) at load points.

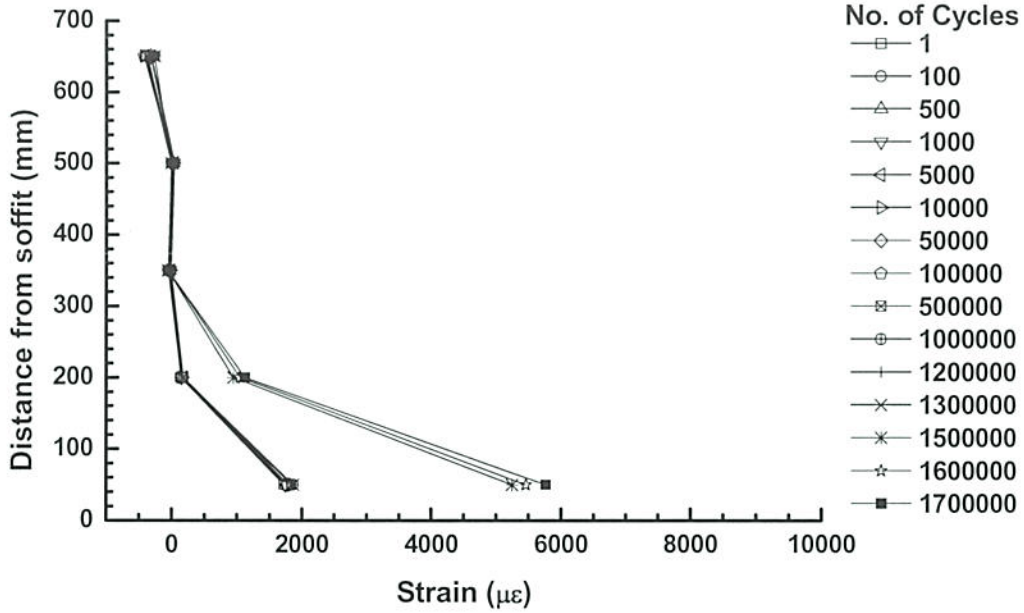

Figure 4.30 – Average strain measured using Demec gauges versus distance from beam soffit for increasing load cycles for beam C1 at the mean cyclic load of 170 kN.

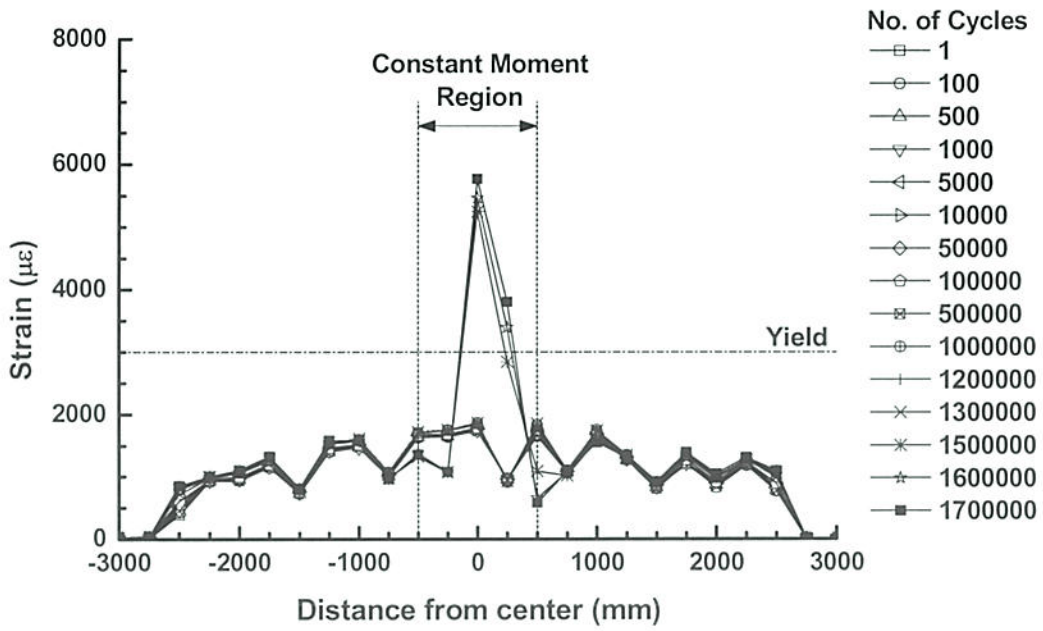

Figure 4.31 – Strain data of Demec gauges 6 to 29 along beam C1 taken at the mean cyclic load of 170 kN.

Figure 4.32 – Fracture of bottom tensile bar in beam C1 adjacent to the primary crack.

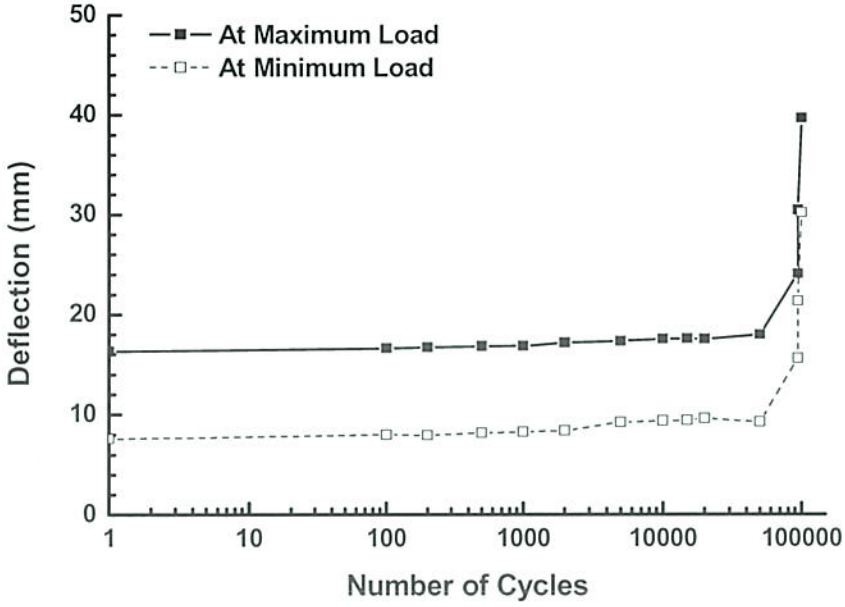

Figure 4.33 – Deflection versus number of cycles for beam C2 (at midspan).

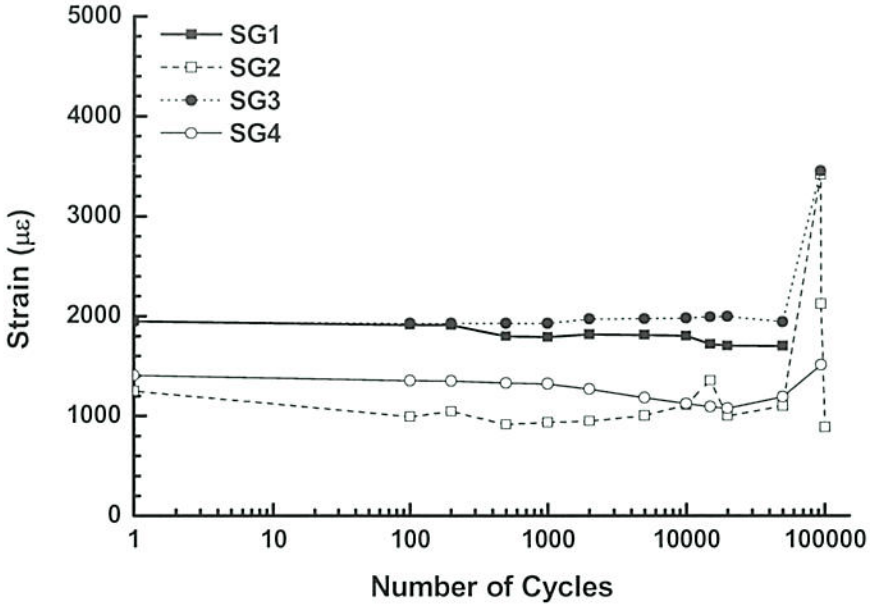

(a)

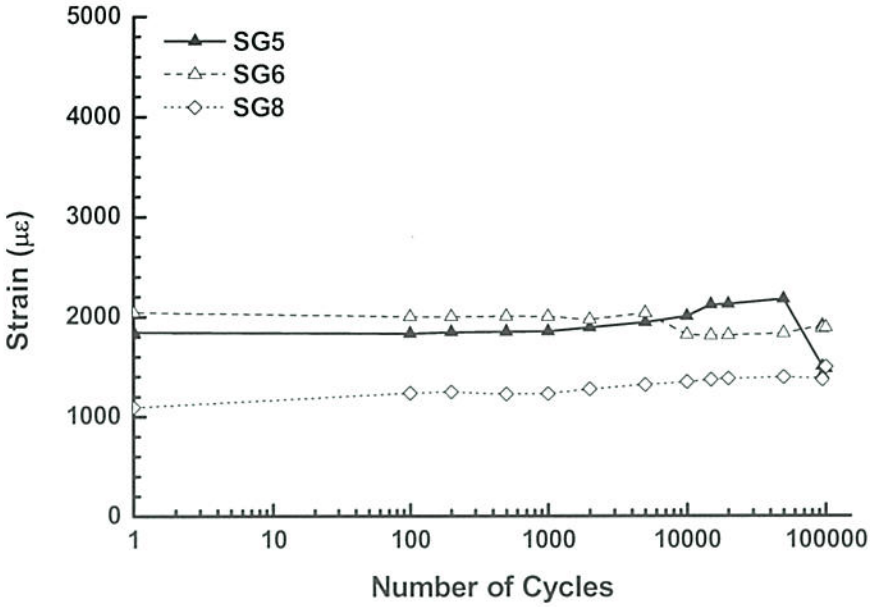

(b)

Figure 4.34 – Steel strain versus number of cycles for beam C2 taken at the maximum cyclic load of 240 kN (a) at midspan and (b) at load points.

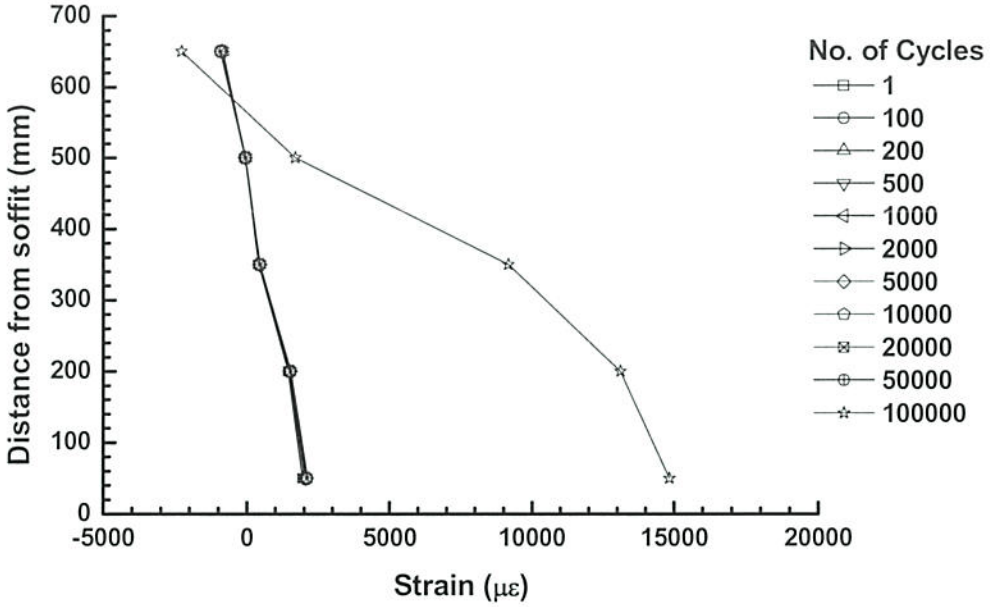

Figure 4.35 – Average strain measured using Demec gauges versus distance from beam soffit for increasing load cycles for beam C2 at the mean cyclic load of 170 kN.

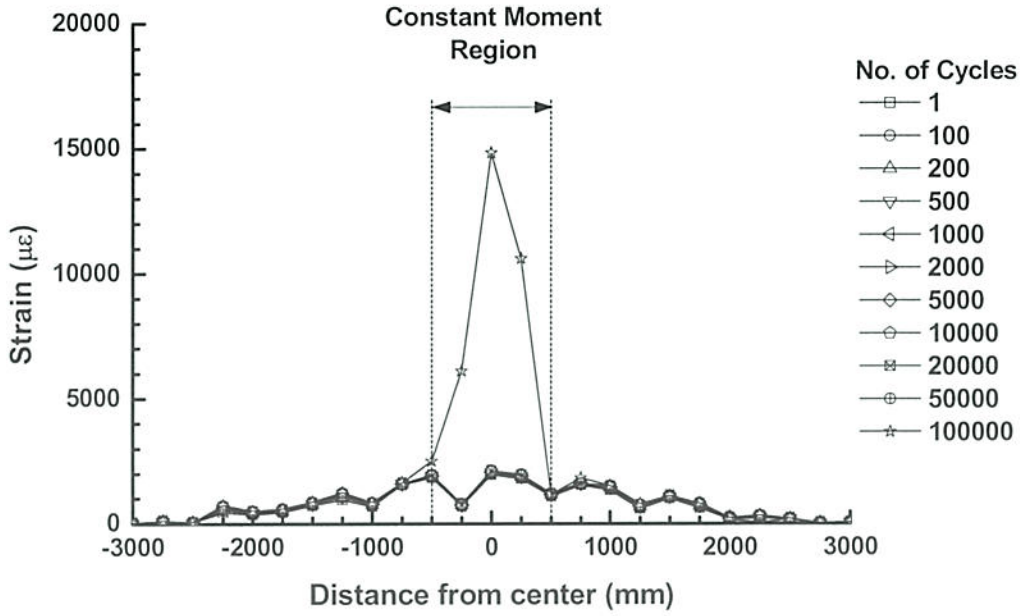

Figure 4.36 – Strain data of Demec gauges 6 to 29 along beam C2 taken at the mean cyclic load of 170 kN.

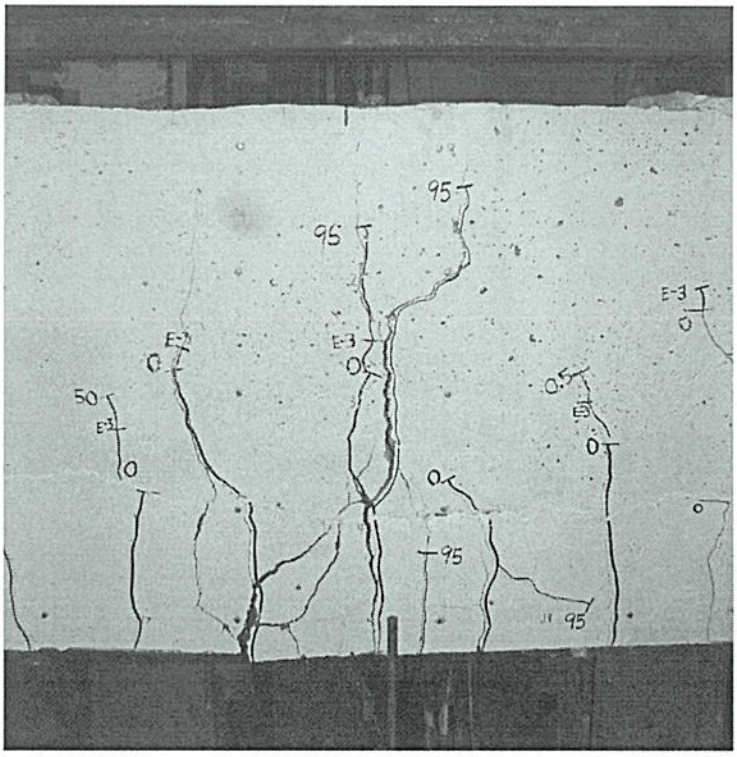

Figure 4.37 – Beam C2: Failure at midspan.

4.3.9 Specimen C3

Specimen C3 was corroded, repaired with mortar and further repaired with 2 strips of CFRP plates. The beam was subjected to the same loading conditions as beams C1 and C2.

At the first load cycle, cracks formed at approximately 125 mm intervals along the beam length, with the crack lengths only marginally shorter than those observed on beams C1 and C2. The cracks propagated and new cracks formed within the next 50,000 cycles. The crack pattern then stabilized until a sudden failure of the beam occurred. Failure was at approximately 180 mm from one of the load points, within the constant moment region of the beam.

The maximum and minimum deflections of beam C3 are shown in Figure 4.38. At the first load cycle, the deflections were 12.0 mm and 6.0 mm at maximum and minimum loads, respectively, with the deflections increasing steadily until at about 300,000 load cycles. The last recorded deflections were at 344,000 cycles, where the maximum and minimum deflections were 31.1 mm and 24.7 mm, respectively.

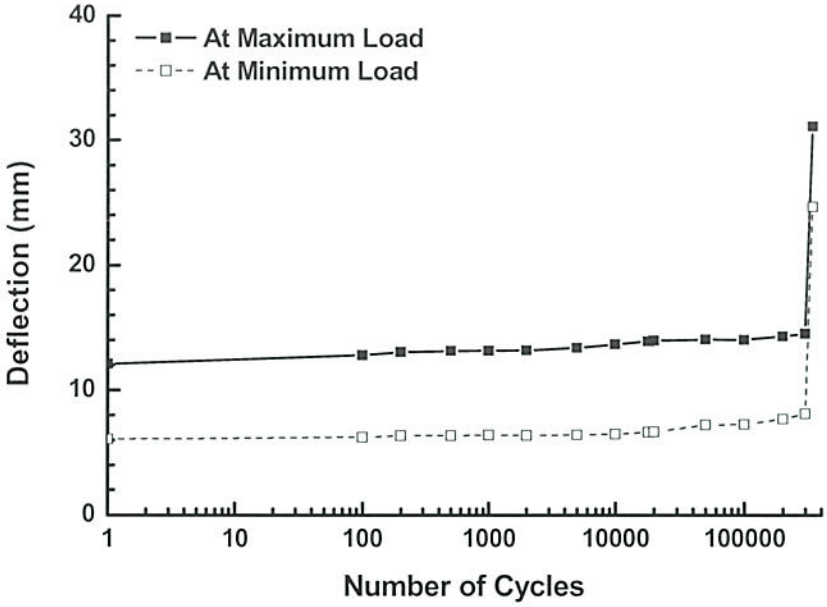

Figure 4.38 – Deflection versus number of cycles for beam C3 (at midspan).

Figure 4.39 show the steel strains during loading. The steel strains at midspan were comparably lower than those at one of the load points (gauges SG5 and SG6). This was consistent with the observation of a primary crack under that load point. The strains at midspan through the section depth are given in Figure 4.40 whereas the strain along the beam length at level of the tensile reinforcement is given in Figure 4.41.

The CFRP strains are given in Figure 4.42. The change in strains in the plate between readings at 200,000 cycles and 300,000 cycles are consistent with the other observations in that the plate is more stressed at the load point where a significant crack had occurred. Beam C3 failed after 343,695 load cycles (Figure 4.43).

4.3.10 Specimen D1

Due to the unexpected outcome of specimen A3 damaged by the loading machine, Series D was included in the testing program to replicate Series A. Similarly to specimen A1, Specimen D1 was the control beam. The beam was loaded between 6 kN and 19 kN, which was 20 and 60 percent of the theoretical failure load of specimen D1.

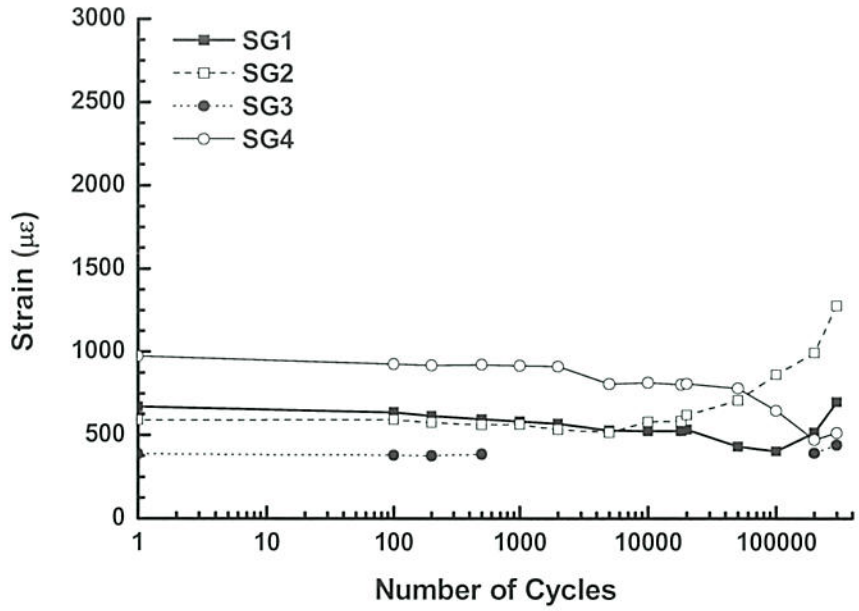

(a)

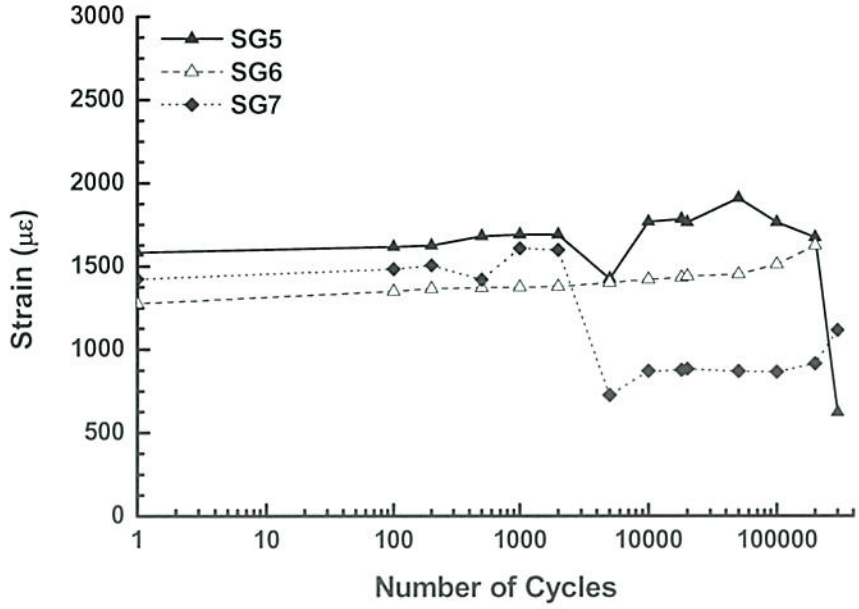

(b)

Figure 4.39 – Steel strain versus number of cycles for beam C3 taken at the maximum cyclic load of 240 kN (a) at midspan and (b) at load points.

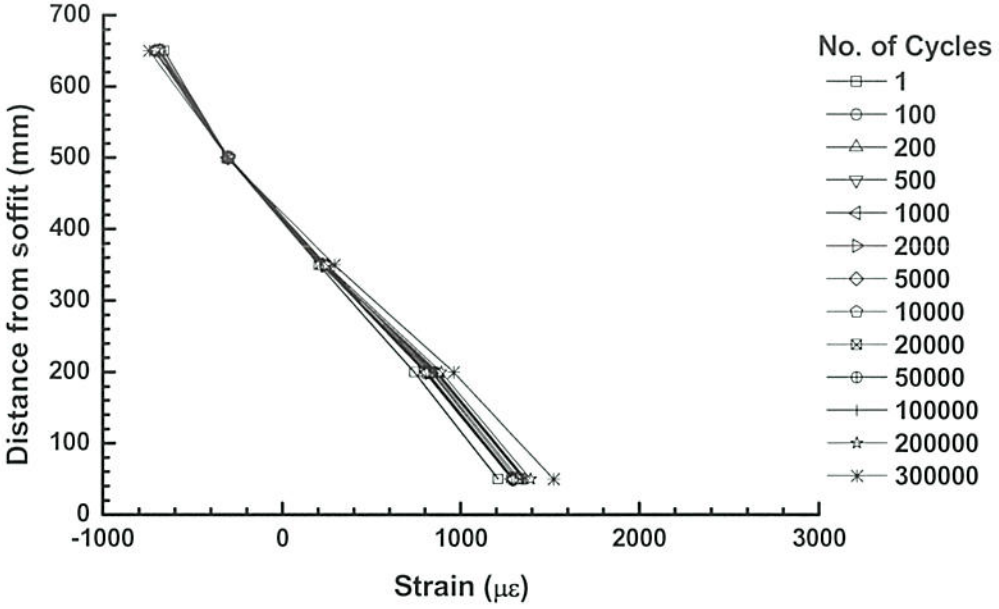

Figure 4.40 – Average strain measured using Demec gauges versus distance from beam soffit for increasing load cycles for beam C3 at the mean cyclic load of 170 kN.

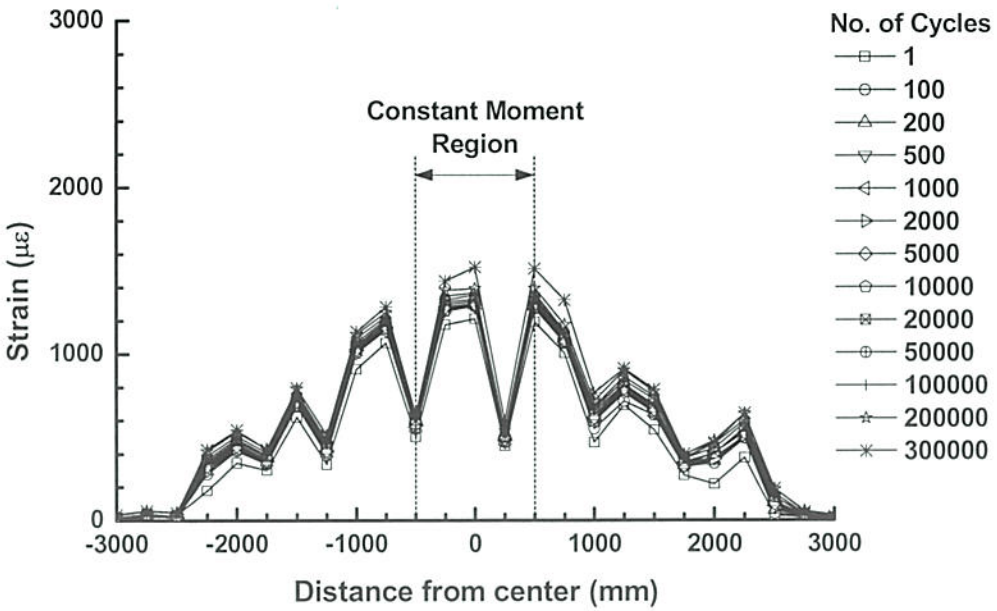

Figure 4.41 – Strain data of Demec gauges 6 to 29 along beam C3 taken at the mean cyclic load of 170 kN.

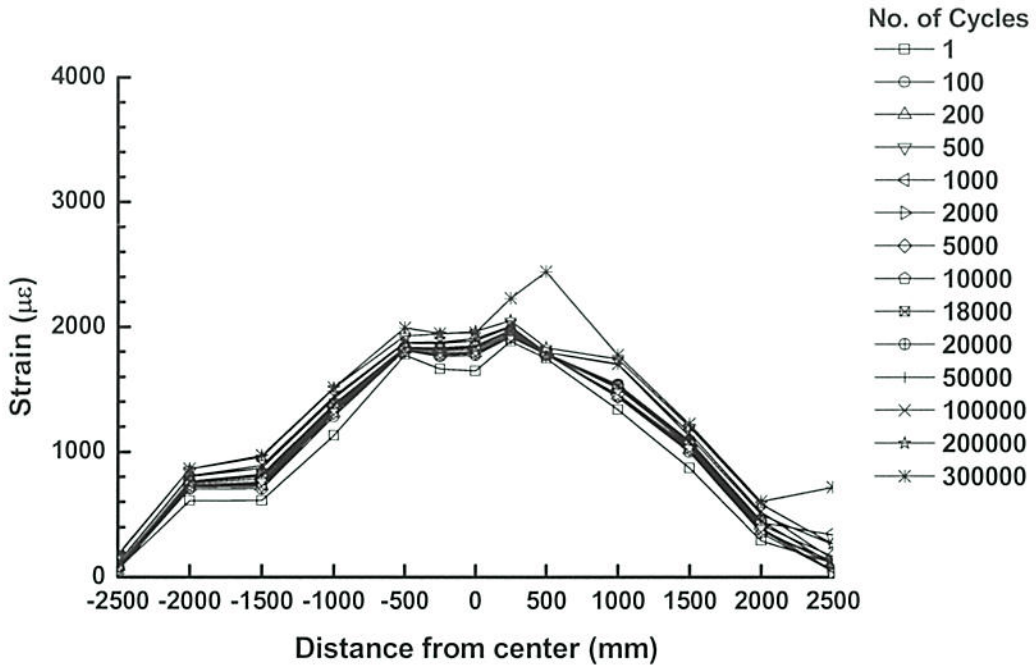

Figure 4.42 – CFRP strain along soffit of beam C3 at maximum cyclic load of 240 kN.

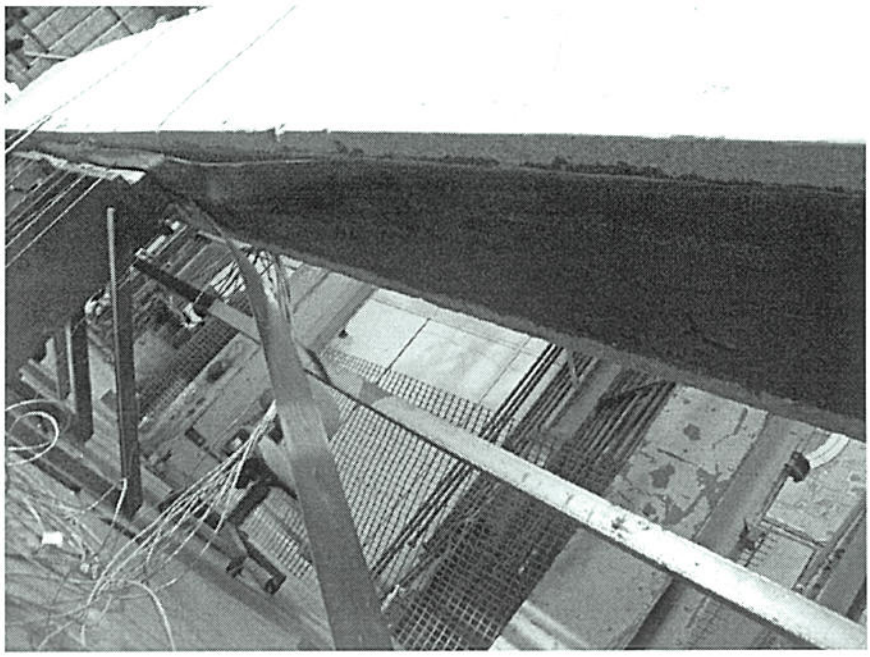

Figure 4.43 – Beam C3: Debonding of CFRP at failure.

Figure 4.44 shows the deflections of beam D1 that were recorded at the maximum and minimum loads. At the first cycle, the deflections were 3.4 mm and 2.5 mm at maximum and minimum loads, respectively. Deflections increased at the highest rate within the first 250,000 load cycles and increased steadily throughout the rest of the test. Deflections at 2 million cycles were 11.8 mm and 9.7 mm at maximum and minimum loads, respectively.

Strains in the steel bars at midspan are given in Figure 4.45. Strains in the tensile steel bars at the bottom layer steadily increased (gauges SG1 and SG2), whereas the strains of the bar at top layer remained relatively unchanged (gauge SG3). Figures 4.46 and 4.47 show the Demec strains measured at midspan through the section depth and along the beam length at the level of tensile reinforcement, respectively. There was no significant change in strains at any specific load cycle number.

Beam D1 did not fail after 2 million load cycles. It was then loaded monotonically to failure. The load-deflection behaviour is shown in Figure 4.48. The beam failed at 32.6 kN with a deflection of 19.0 mm.

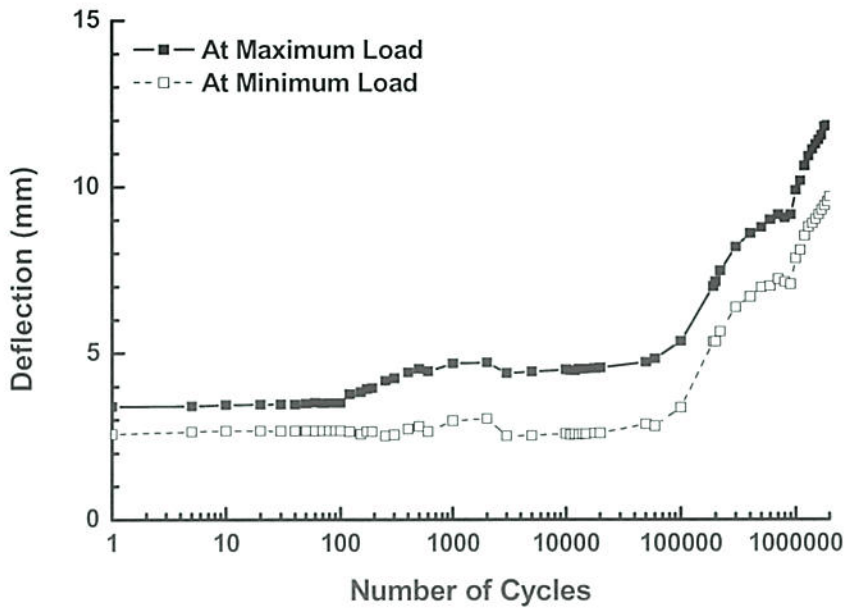

Figure 4.44 – Deflection versus number of cycles for beam D1 at midspan.

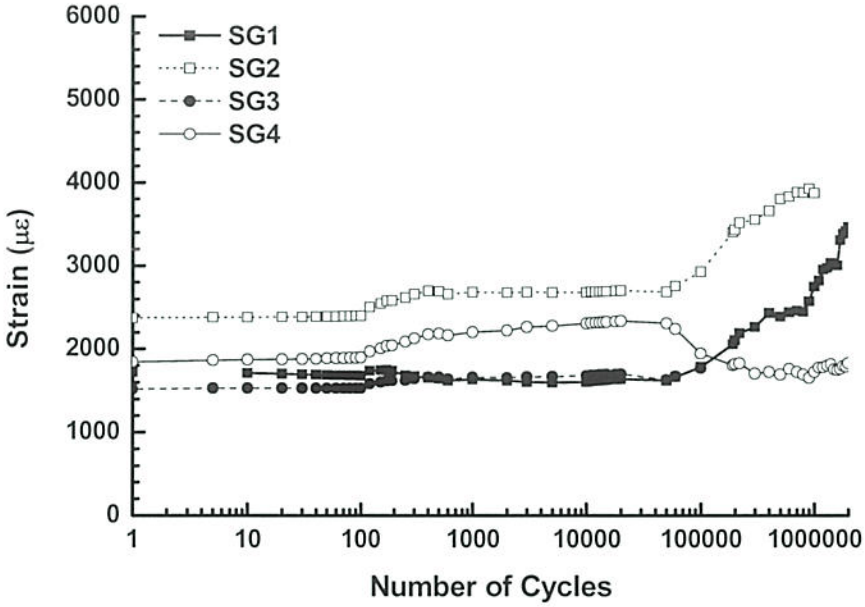

Figure 4.45 – Steel strain at midspan versus number of cycles for beam D1 at maximum load of 19 kN.

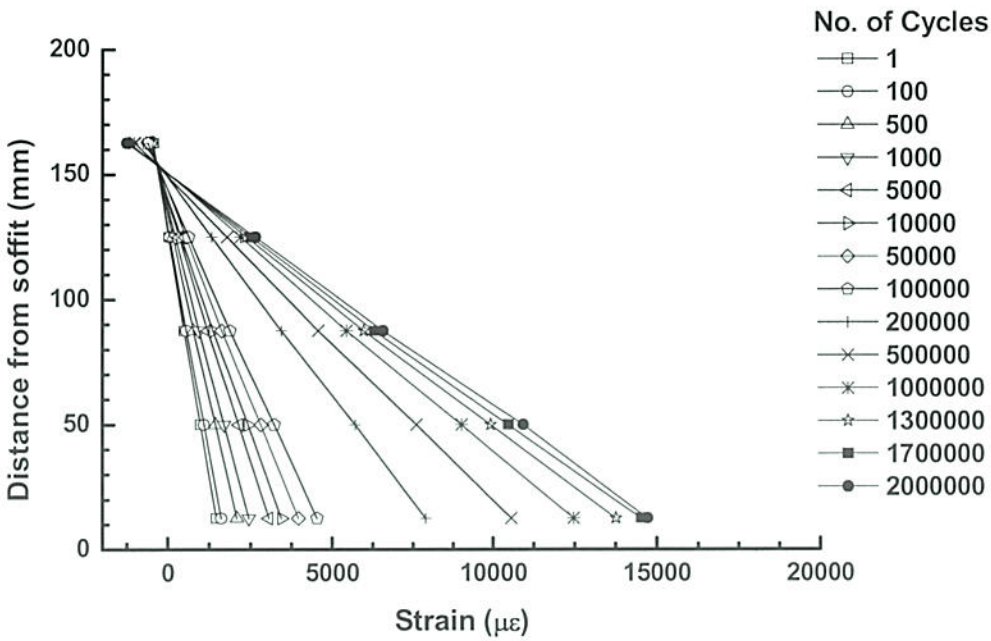

Figure 4.46 – Strain versus distance from beam soffit for increasing load cycles for beam D1 at 13 kN.

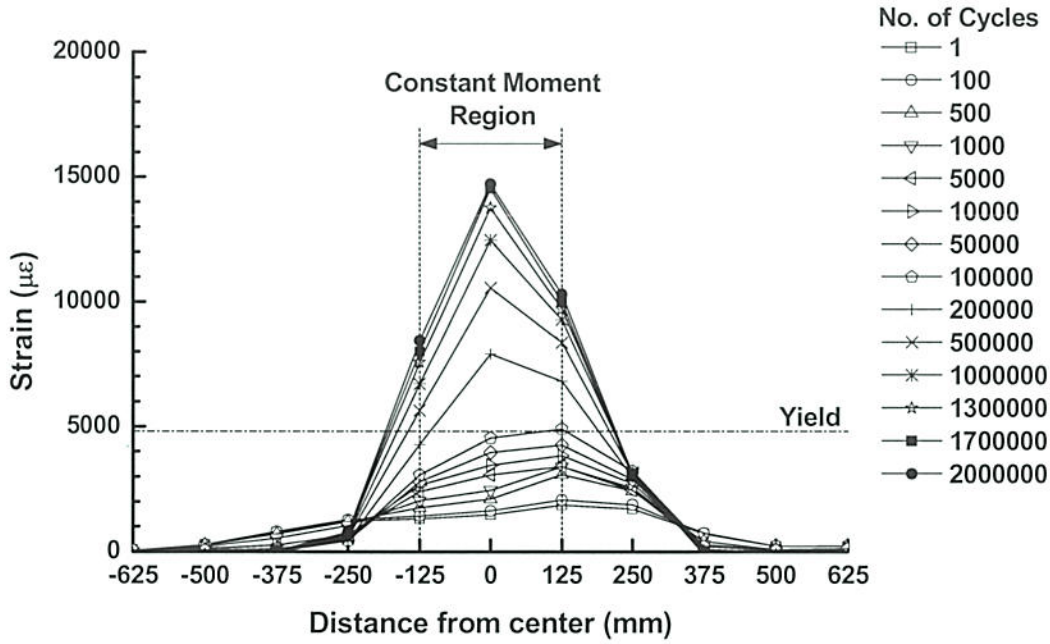

Figure 4.47 – Strain data of Demec gauges 6 to 15 along beam D1 at 13 kN.

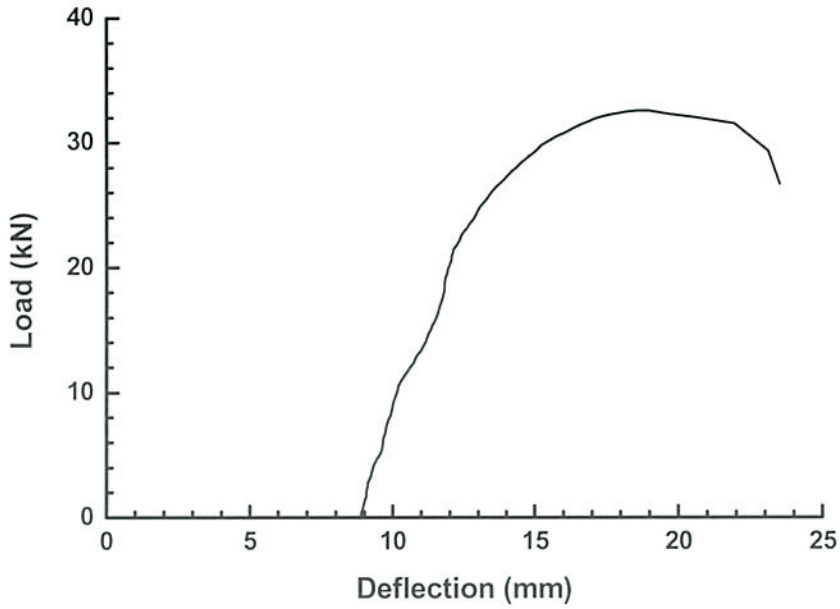

Figure 4.48 – Load versus midspan displacement for D1 tested to failure after 2 million load cycles.

4.3.11 Specimen D2

Specimen D2 was corroded and repaired with mortar. The deflections at maximum and minimum loads are given in Figure 4.49. The deflections started at 3.6 mm and 2.1 mm at 19 kN and 6 kN loads, respectively. Deflections increased at a steady rate until 2,000 load cycles. The final recordings at 3,750 load cycles were 7.4 mm and 5.4 mm at maximum and minimum loads, respectively.

Figure 4.50 shows the steel strains in beam D2. The strains were stable at approximately 2,000 με throughout the entire test. The Demec readings are given in Figures 4.51 and 4.52. Not much change in strains was noticed in the midspan. Failure occurred after 3,750 load cycles, at about 300 mm from midspan, as shown in Figure 4.53.

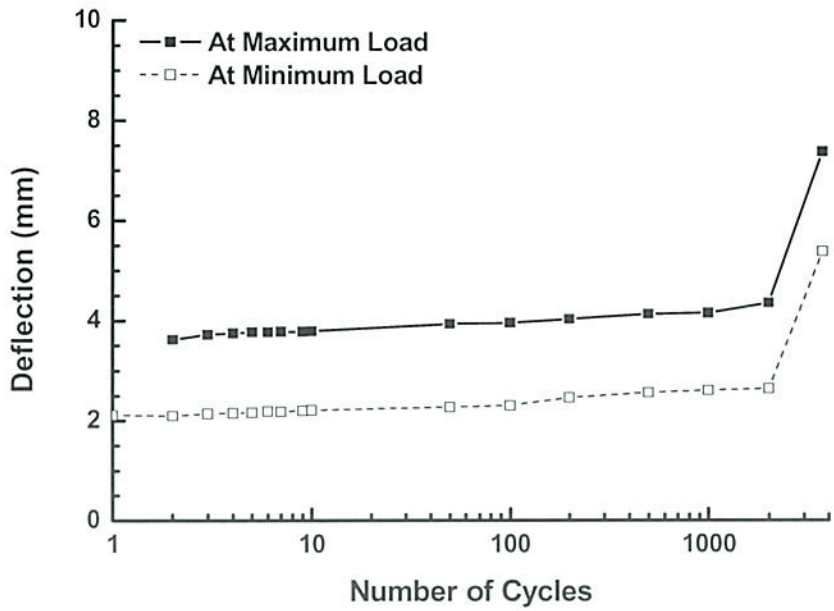

Figure 4.49 – Deflection versus number of cycles for beam D2 (at midspan).

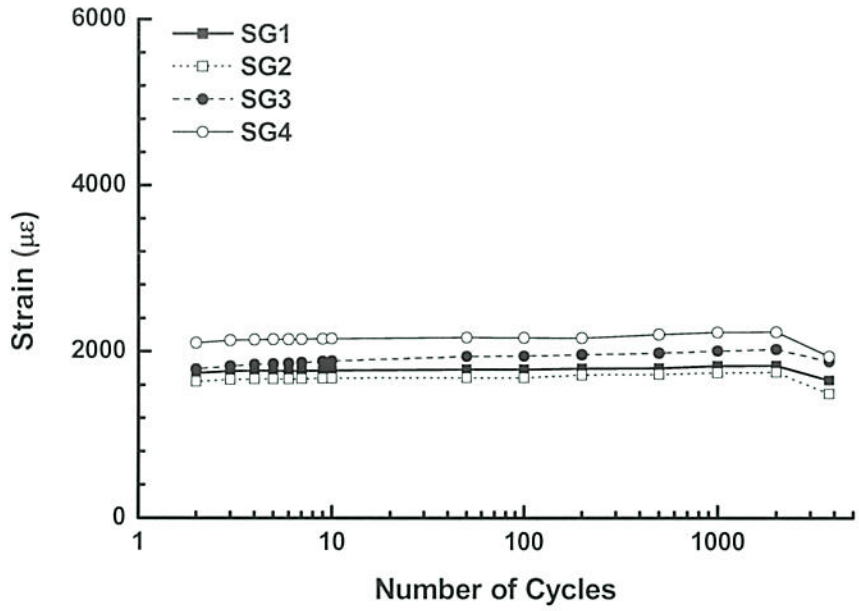

Figure 4.50 – Steel strain at midspan versus number of cycles for beam D2 taken at the maximum cyclic load of 19 kN.

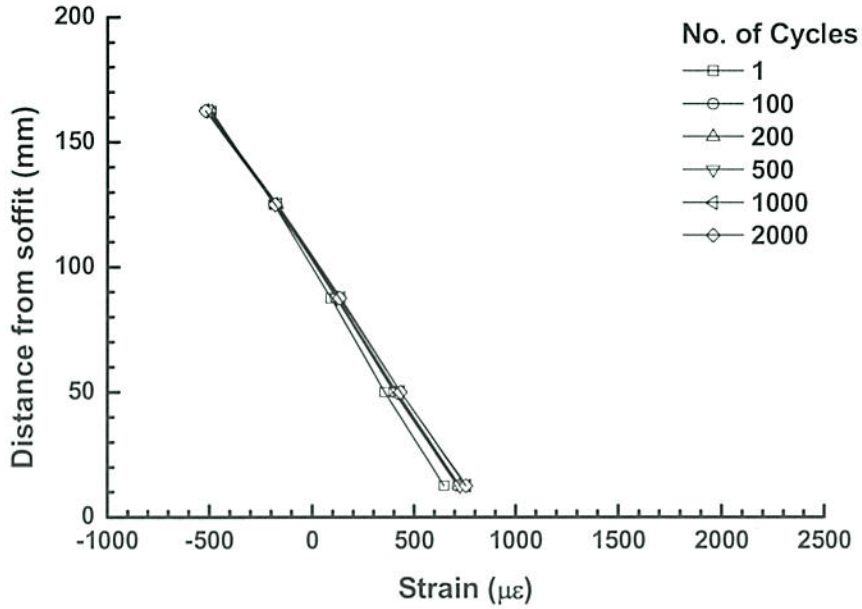

Figure 4.51 – Average strain measured using Demec gauges versus distance from beam soffit for increasing load cycles for beam D2 at the mean cyclic load of 13 kN.

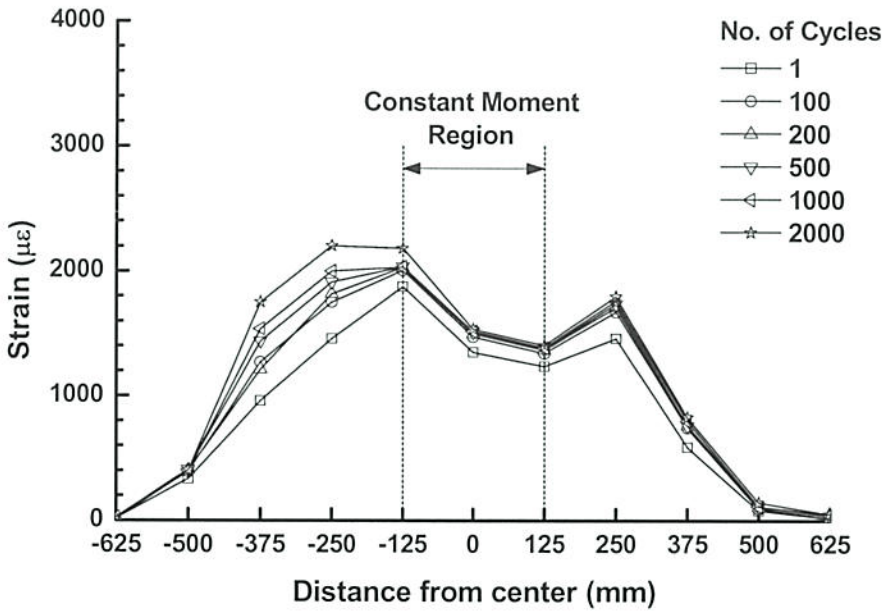

Figure 4.52 – Strain data of Demec gauges 6 to 15 along beam D2 taken at the mean cyclic load of 13 kN.

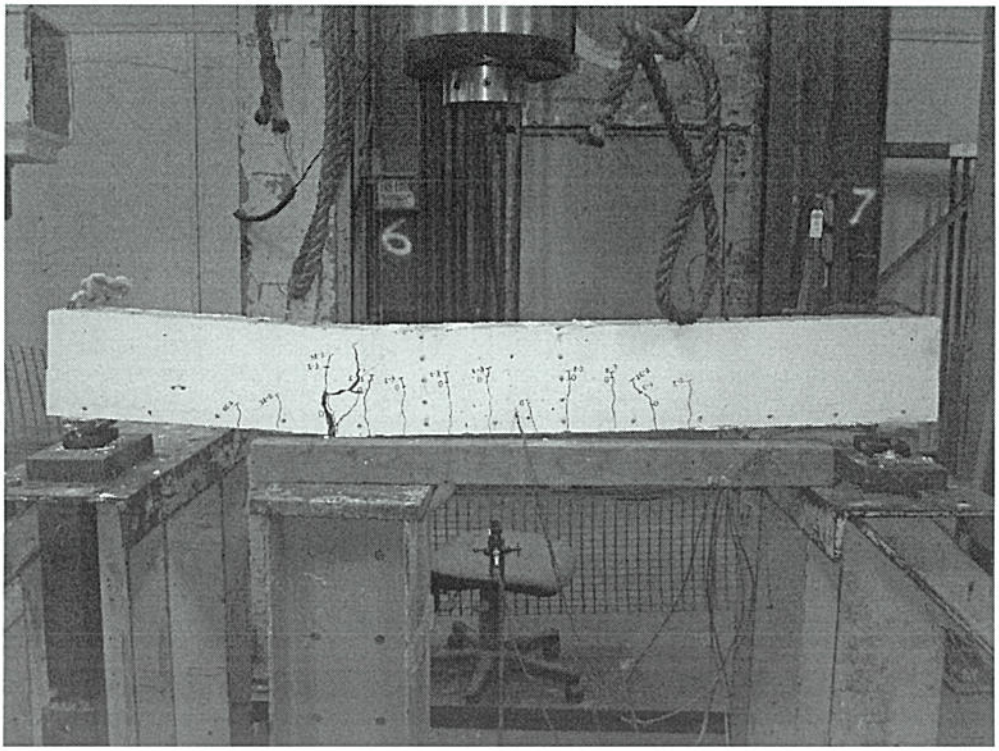

Figure 4.53 – Beam D2 at failure.

4.3.12 Specimen D3

Specimen D3 was corroded, repaired with mortar and further repaired with one strip of CFRP plate at the soffit. The beam was cyclically loaded between 6 kN and 19 kN at 1.5 Hz. The deflections at maximum and minimum loads are given in Figure 4.54. At the first cycle, beam D3 experienced deflections of 2.6 mm and 1.4 mm at 19 kN and 6 kN loads, respectively. Correspondingly, the last recorded deflections at 2 million load cycles were 3.5 mm and 2.2 mm. At the same load cycle number of 2 million cycles, beam D3 experienced a 70 percent decrease in deflection over the control beam (beam D1).

Figure 4.55 shows the tensile bar strains at midspan. The bars at the bottom layer (gauges S1 and S2) experienced increases in strains as the test progressed, whereas those at the top layer (gauges S3 and S4) experienced constant strain at about 1,000 με. Figures 4.56 and 4.57 shows the average strains measured using the Demec gauges, for increasing load cycles. Figure 4.58 shows the strains in the CFRP plate at 125 mm intervals, which were relatively constant for all loading stage.

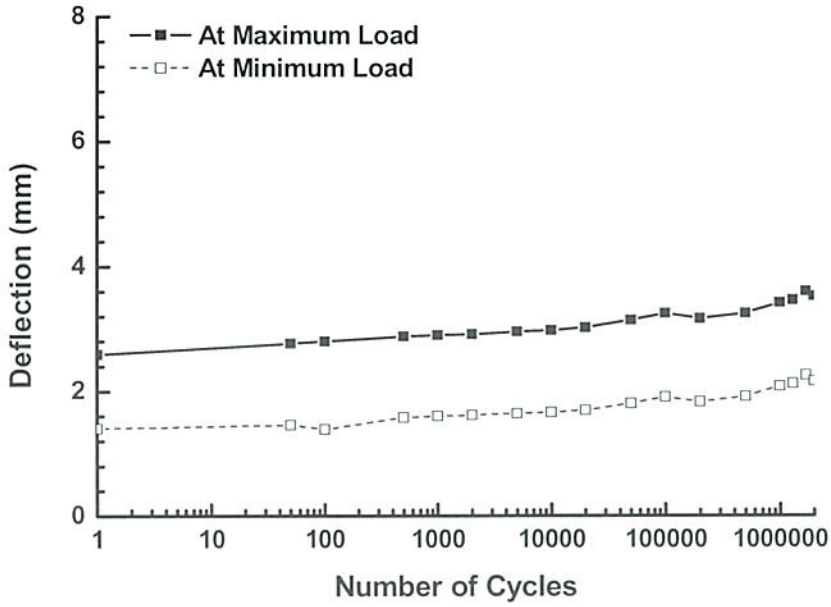

Figure 4.54 – Deflection versus number of cycles for beam D3 (at midspan).

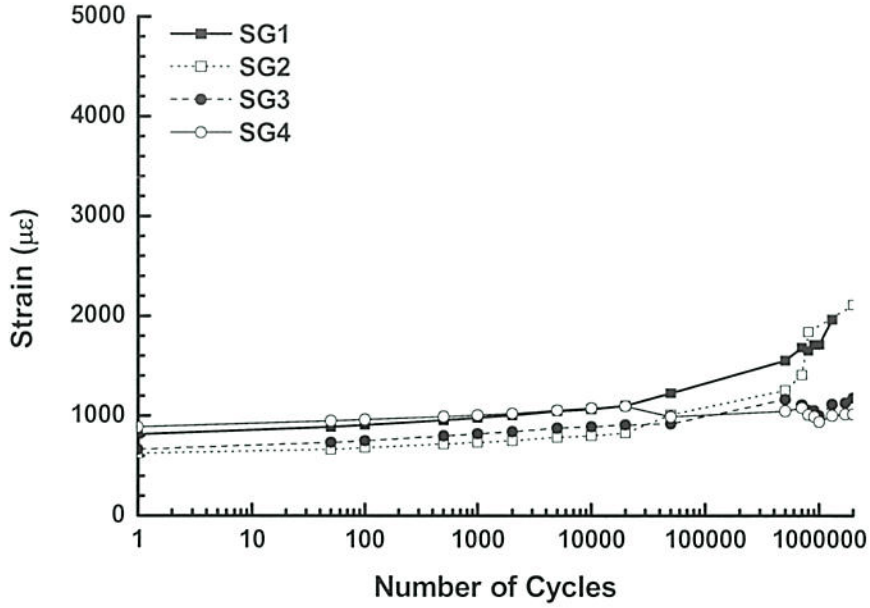

Figure 4.55 – Steel strain at midspan versus number of cycles for beam D3 taken at the maximum cyclic load of 19 kN.

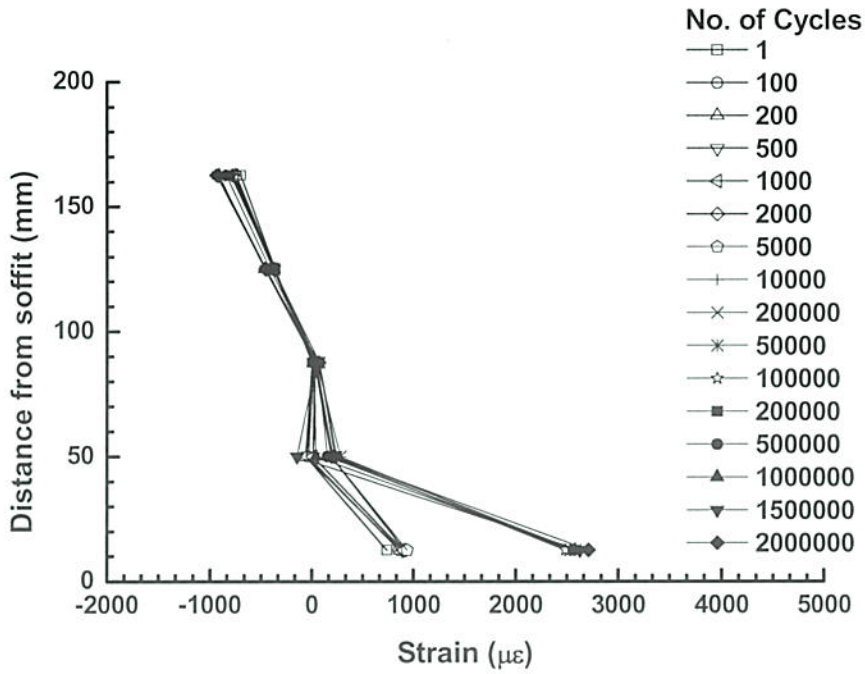

Figure 4.56 – Average strain measured using Demec gauges versus distance from beam soffit for increasing load cycles for beam D3 at the mean cyclic load of 13 kN.

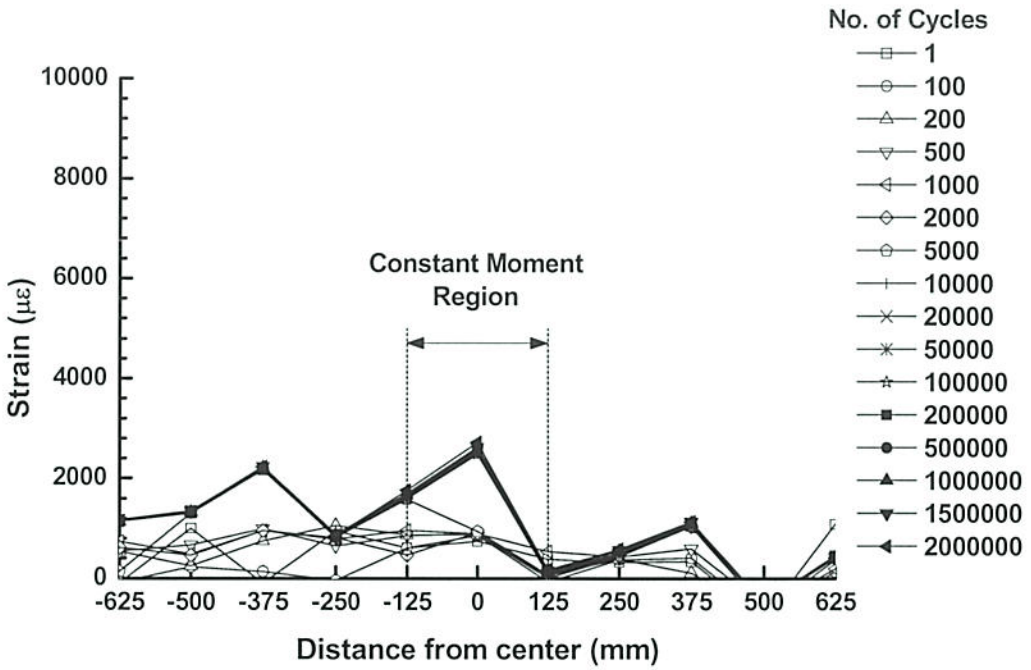

Figure 4.57 - Strain data of Demec gauges 6 to 15 along beam D3 taken at the mean cyclic load of 13 kN.

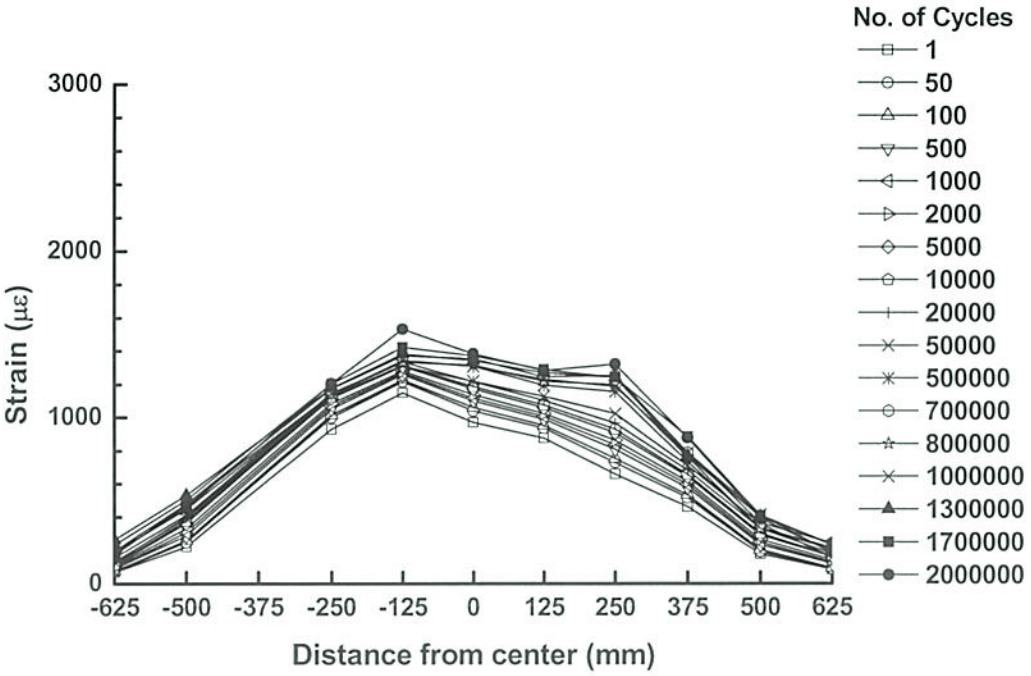

Figure 4.58 – CFRP strain along soffit of beam D3 at maximum load of 19 kN.

After 2 million load cycles, beam D3 was loaded monotonically to failure. The load versus deflection behaviour is shown in Figure 4.59. The beam failed at 55.6 kN with a corresponding deflection of 9.2 mm. Failure was by fracture of the tensile bars at a crack originating from one end of the CFRP plate, as shown in Figure 4.60. This crack only appeared during the monotonic loading stage.

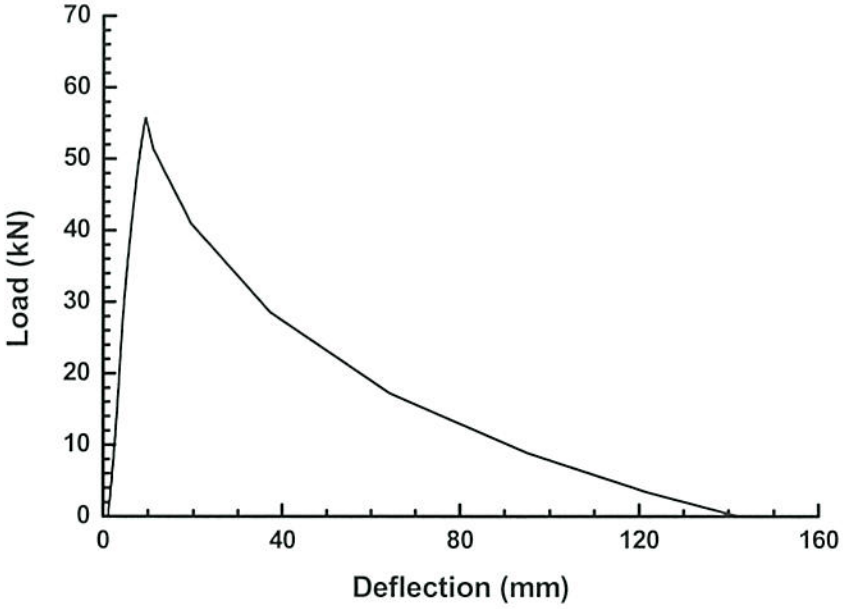

Figure 4.59 – Load versus midspan displacement for D3 after 2 million load cycles.

4.3.13 Crack Patterns

Immediately after taking readings of the Demec strains, each beam was checked for its crack pattern. This was carried out when the beam was maintained at the mean load, which was 40 percent of the theoretical failure load. The results are plotted in Figures 4.61 to 4.72. The primary cracks where failures occurred are represented as thick lines in the figures. It is evident that the CFRP significantly reduced the formation of cracks.

4.4 Mass Loss of Steel Reinforcement

After the test beams were loaded to failure, the beams with corroded steel reinforcement were broken to extract the steel bars to determine the exact mass losses due to corrosion. The extracted bars were cut to a length of approximately 300 mm. Certain bars had lengths more

or less than 300 mm because of the locations of fracture resulting from the fatigue tests. The locations of the beams from where the bars were extracted are shown in Figure 4.73a.

The mass losses were determined according to the procedure of ASTM G1-90. The loose rust was first removed from the bars using a wire brush and the initial weights of the bars were then taken. The bars were immersed in an acidic solution consisting of 500 mL of concentrated hydrocholoric acid that was diluted by distilled water to a 1000 mL solution added with 3.5 g of hexamythylene tetramine (Figure 4.73b). The bars were immersed in this solution for 15 minutes and were then washed with water and weighed. The procedure was repeated about five times until the weights of the bars were consistent. The final recorded weight is then compared with that of the original, uncorroded bar of the same length to obtain the mass loss. The results are listed in Table 4.2.

According to Table 4.2, all beams were corroded to approximately the target steel mass loss of 15 percent. The mass losses are slightly higher as the beam size increases. This can be attributed to the fact that the larger beams were subjected to accelerated corrosion for a longer period of time, which allowed the cracks to widen due to the sustained loads. Also, the distribution of corrosion is observed to be more even for the small beams compared to that of the larger beams. As expected, the corrosion is more severe in the middle of the beam than anywhere else due to the locations of the cracks. On average, the tensile bars at the bottom layer of the reinforcement experienced nearly double the corrosion compared to the bars at the top layers. This is expected because these bars were located closer to the concrete surface at the soffit and to the wider part of the cracks.

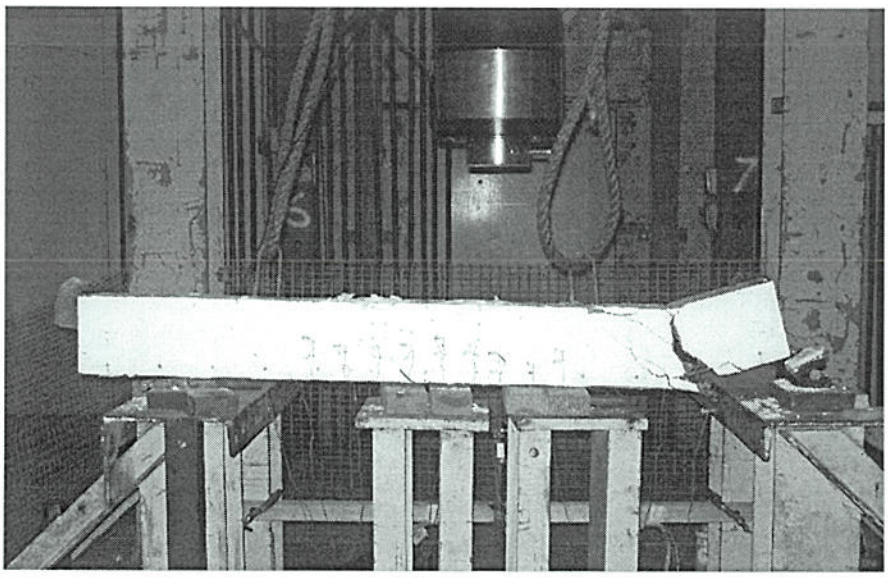

(a)

(b)

Figure 4.60 – (a) Beam B4 at failure; (b) debonding of CFRP immediately after fracture of tensile bar.

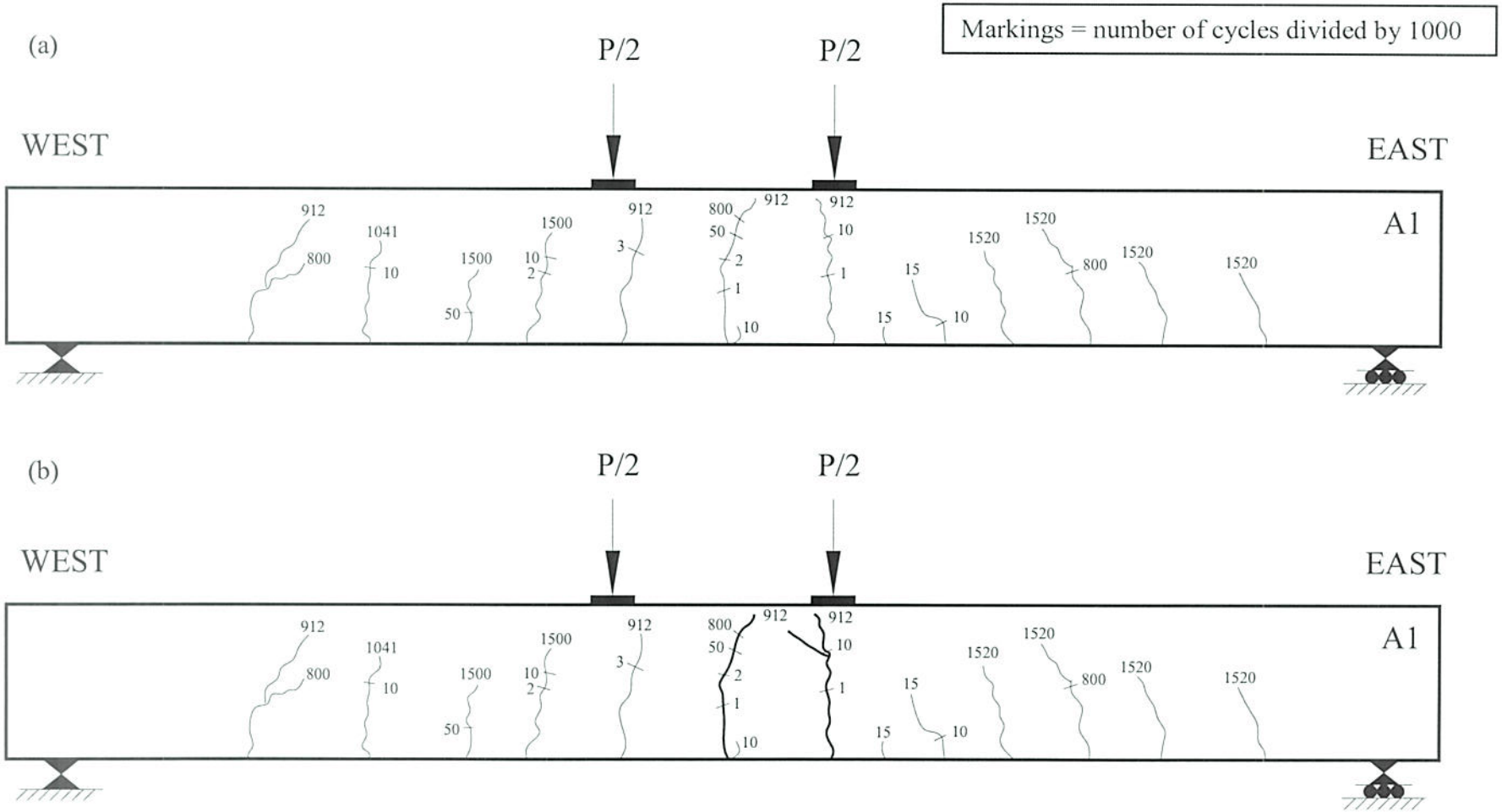

Figure 4.61 – Crack pattern for beam A1: (a) after 2 million load cycles and (b) failure by monotonic loading.

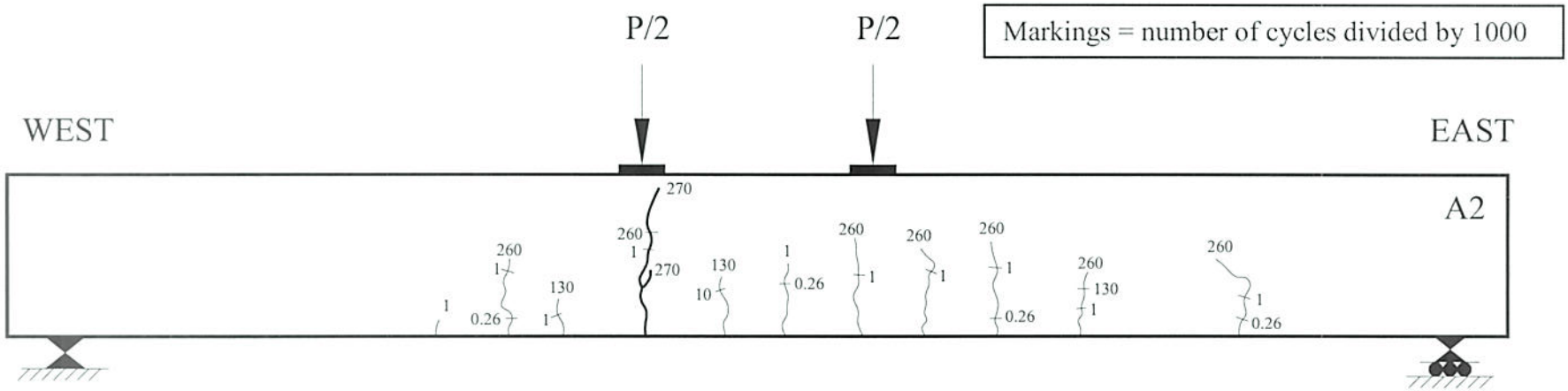

Figure 4.62 – Crack pattern at failure for beam A2.

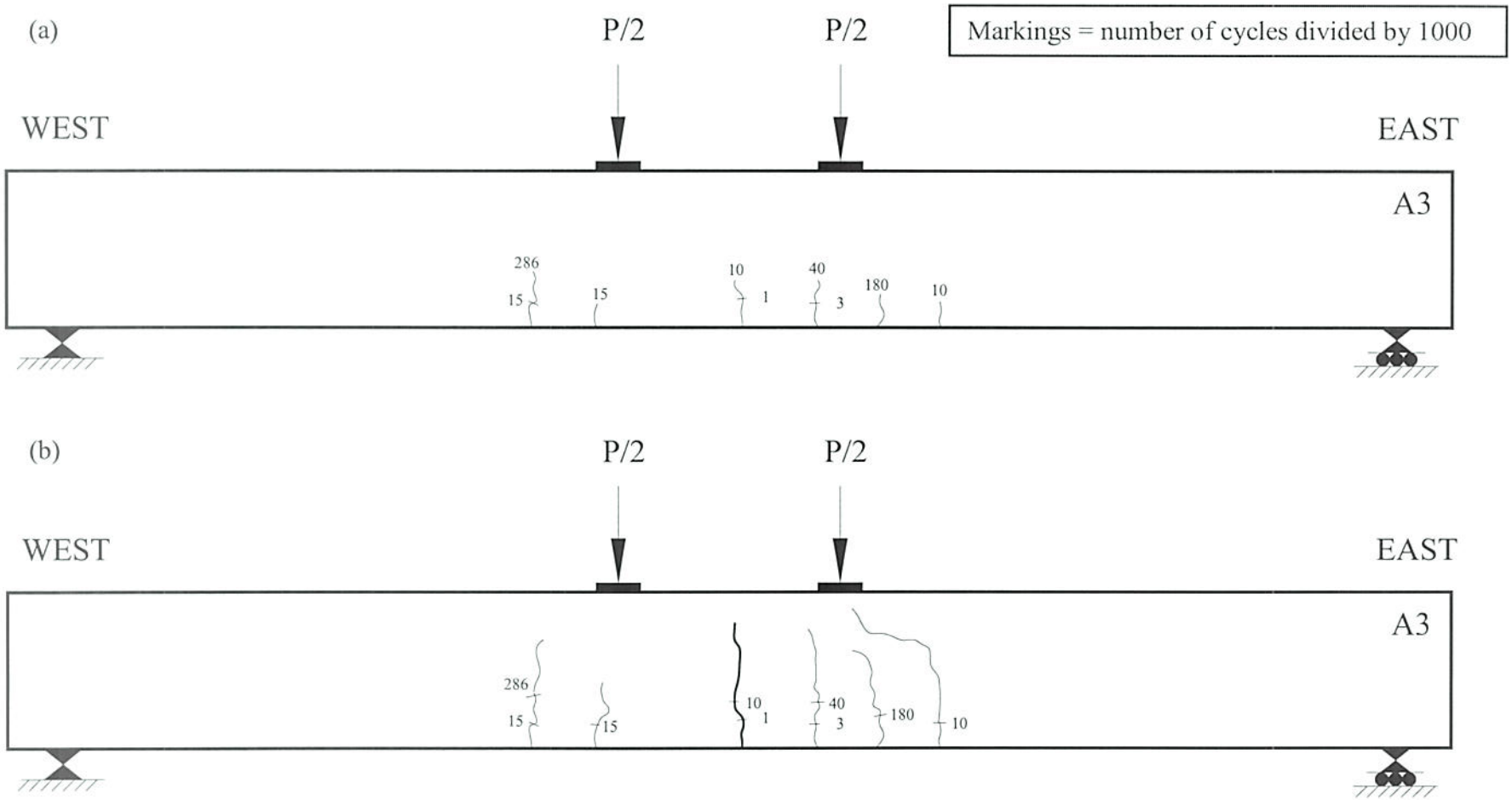

Figure 4.63 - Crack pattern for beam A3: (a) after 1.21 million load cycles and (b) pre-mature failure due to damage.

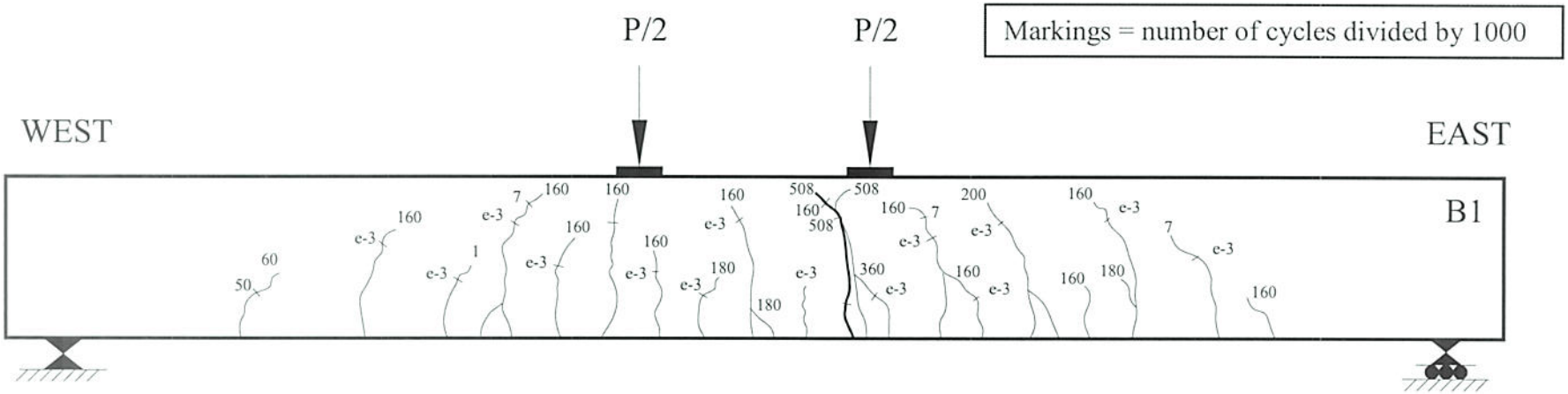

Figure 4.64 – Crack pattern at failure for beam B1.

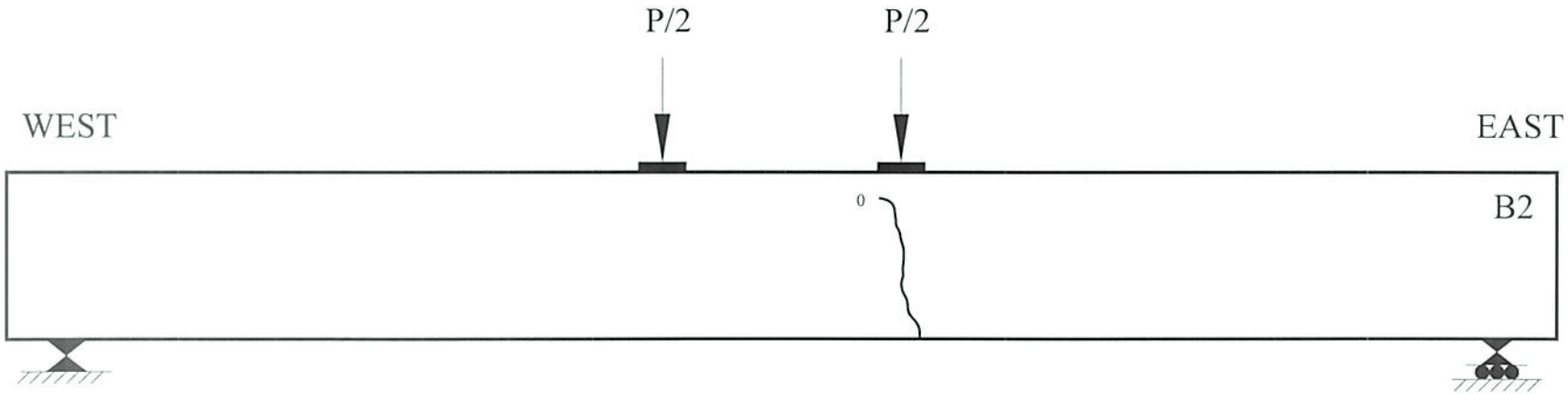

Figure 4.65 – Crack pattern at failure for beam B2.

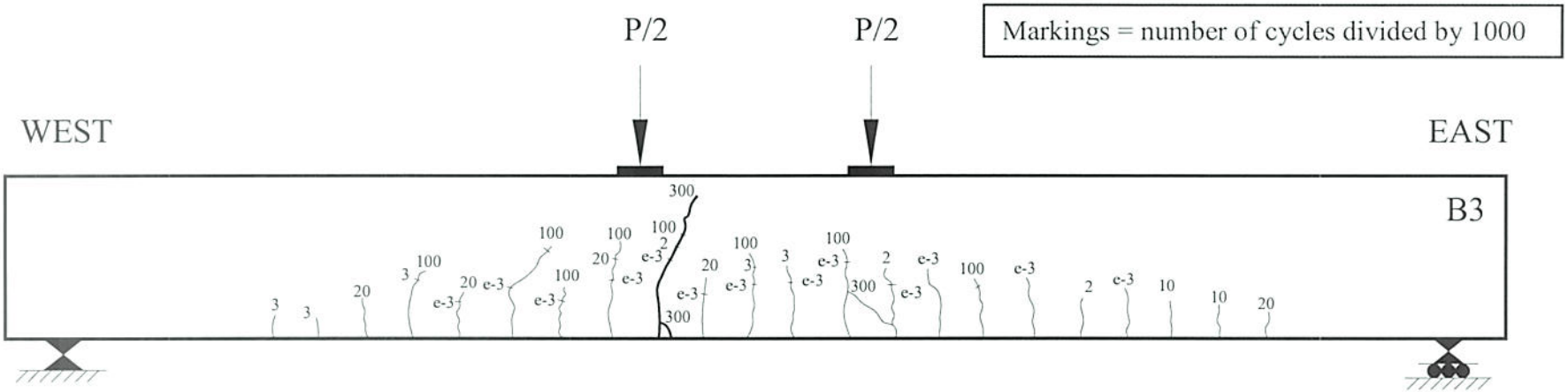

Figure 4.66 – Crack pattern at failure for beam B3.

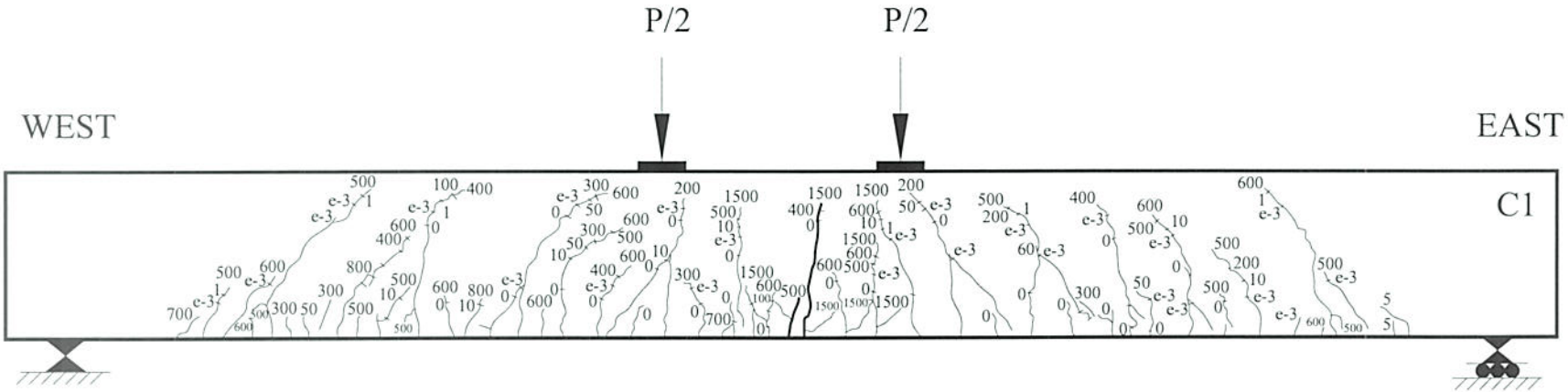

Figure 4.67 – Crack pattern at failure for beam C1.

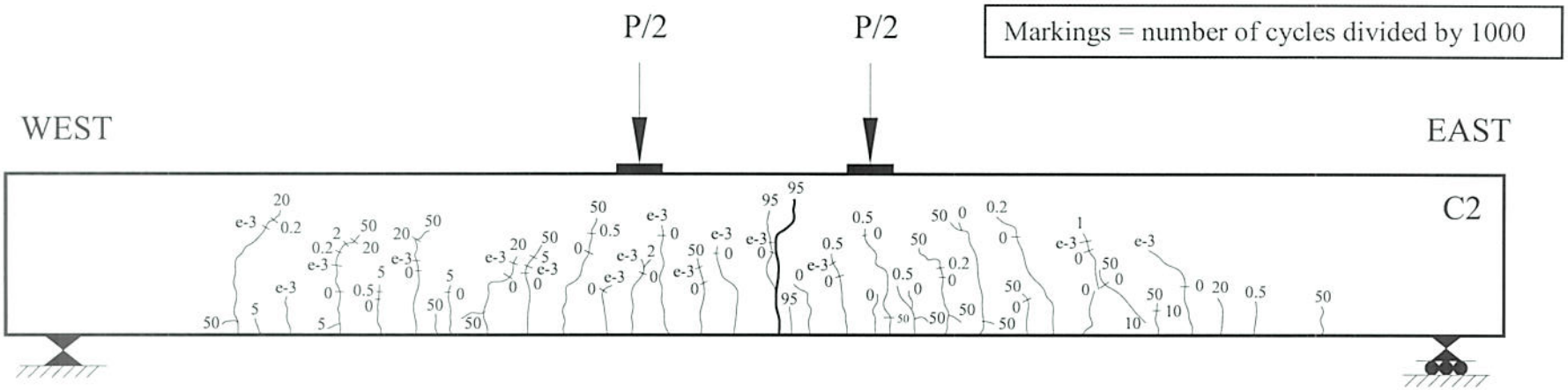

Figure 4.68 – Crack pattern at failure for beam C2.

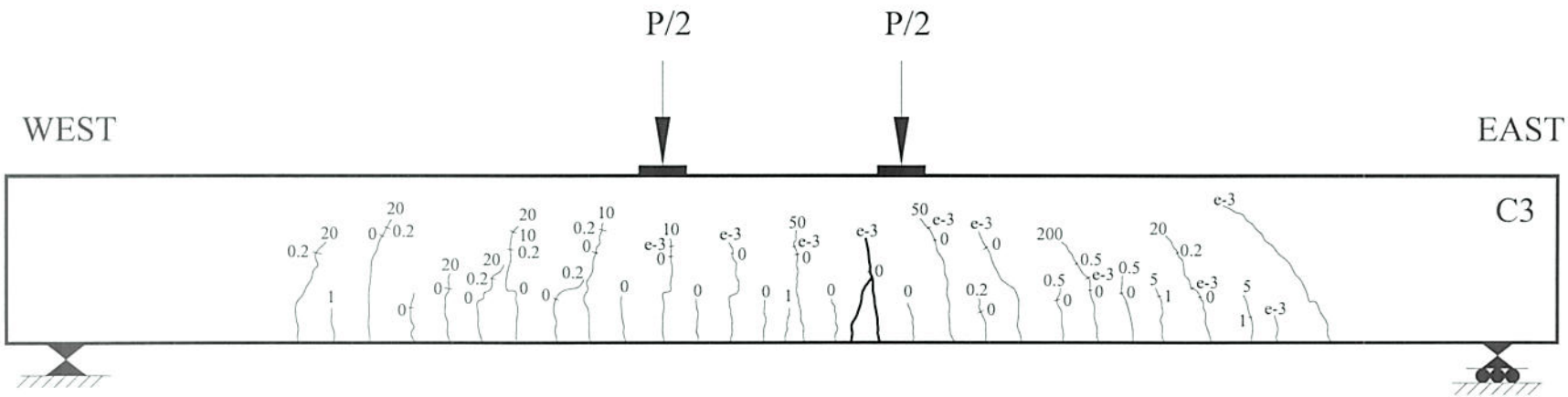

Figure 4.69 – Crack pattern at failure for beam C3.

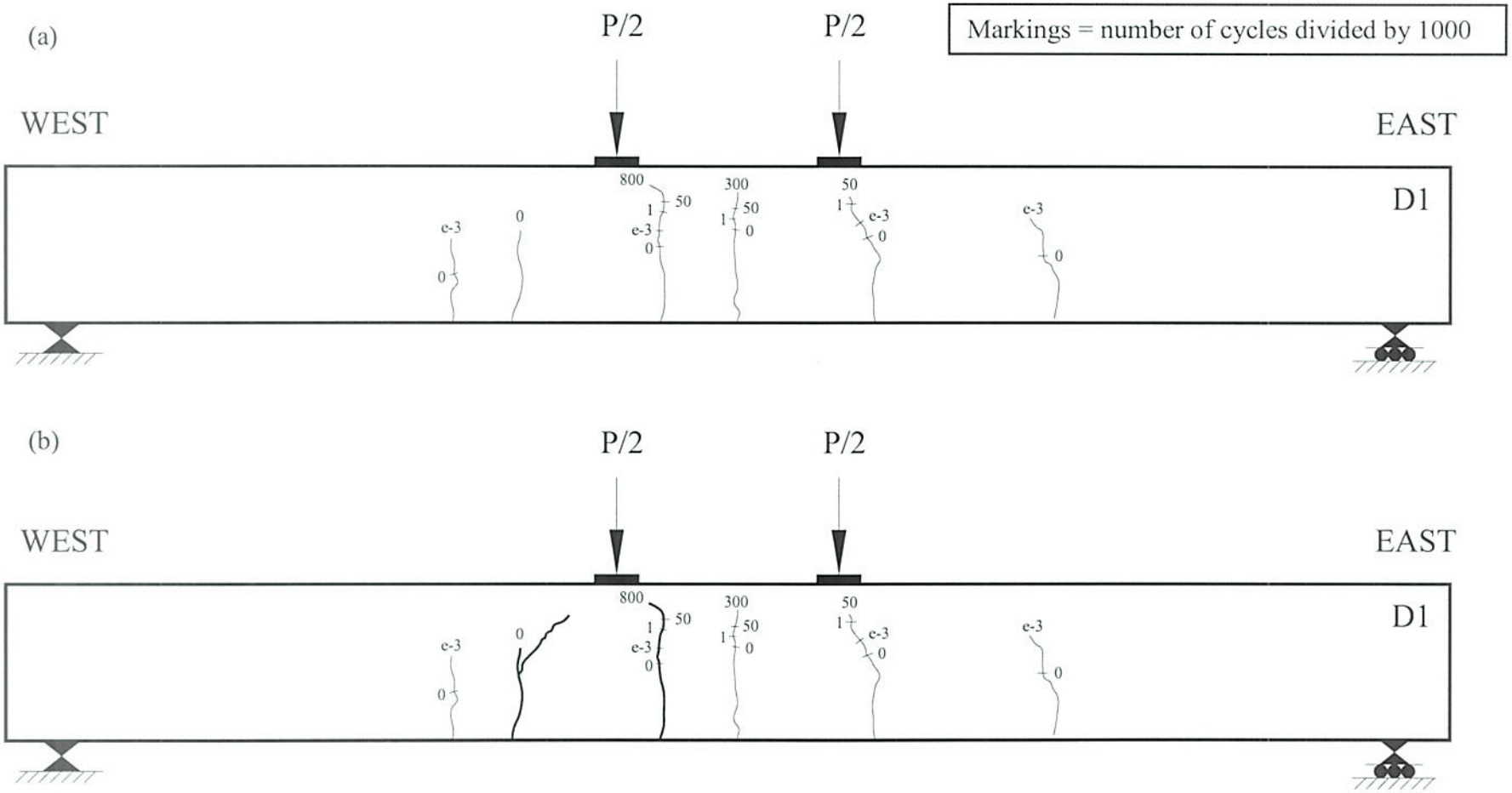

Figure 4.70 – Crack pattern for beam D1: (a) after 2 million load cycles and (b) failure by monotonic loading

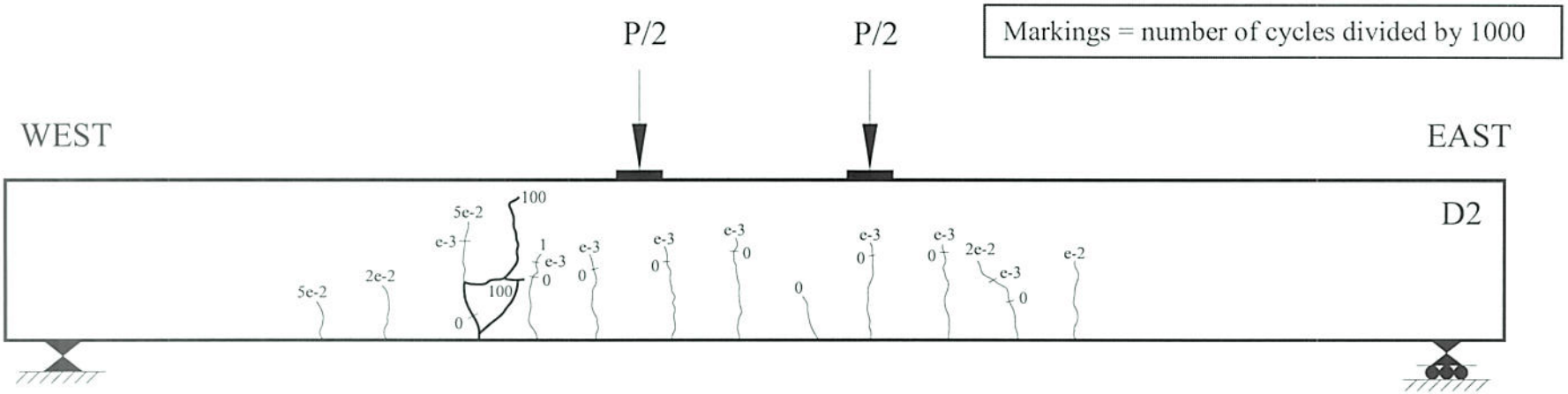

Figure 4.71 – Crack pattern at failure for beam D2.

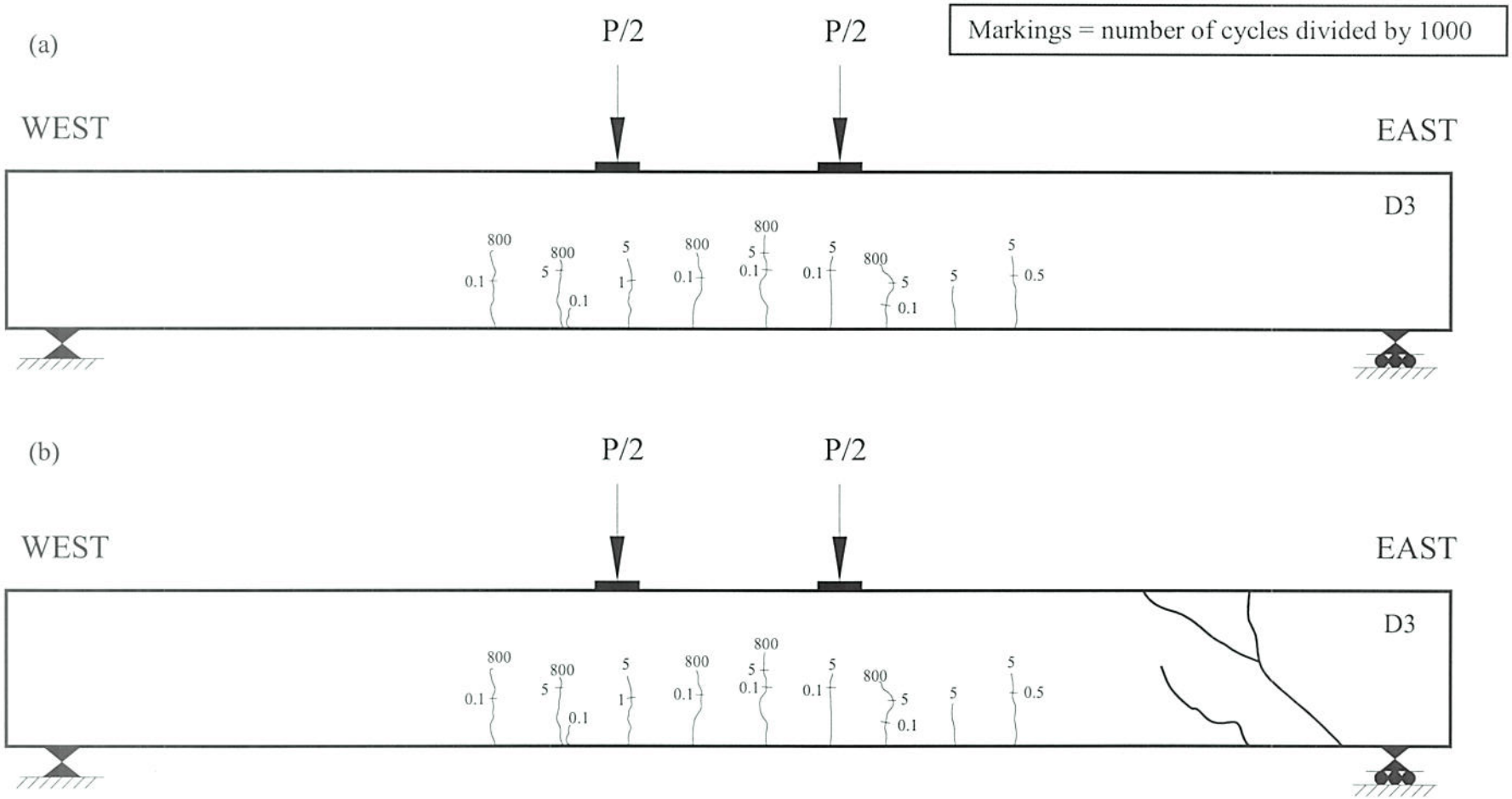

Figure 4.72 - Crack pattern for beam D3: (a) after 2 million load cycles and (b) failure by monotonic loading.

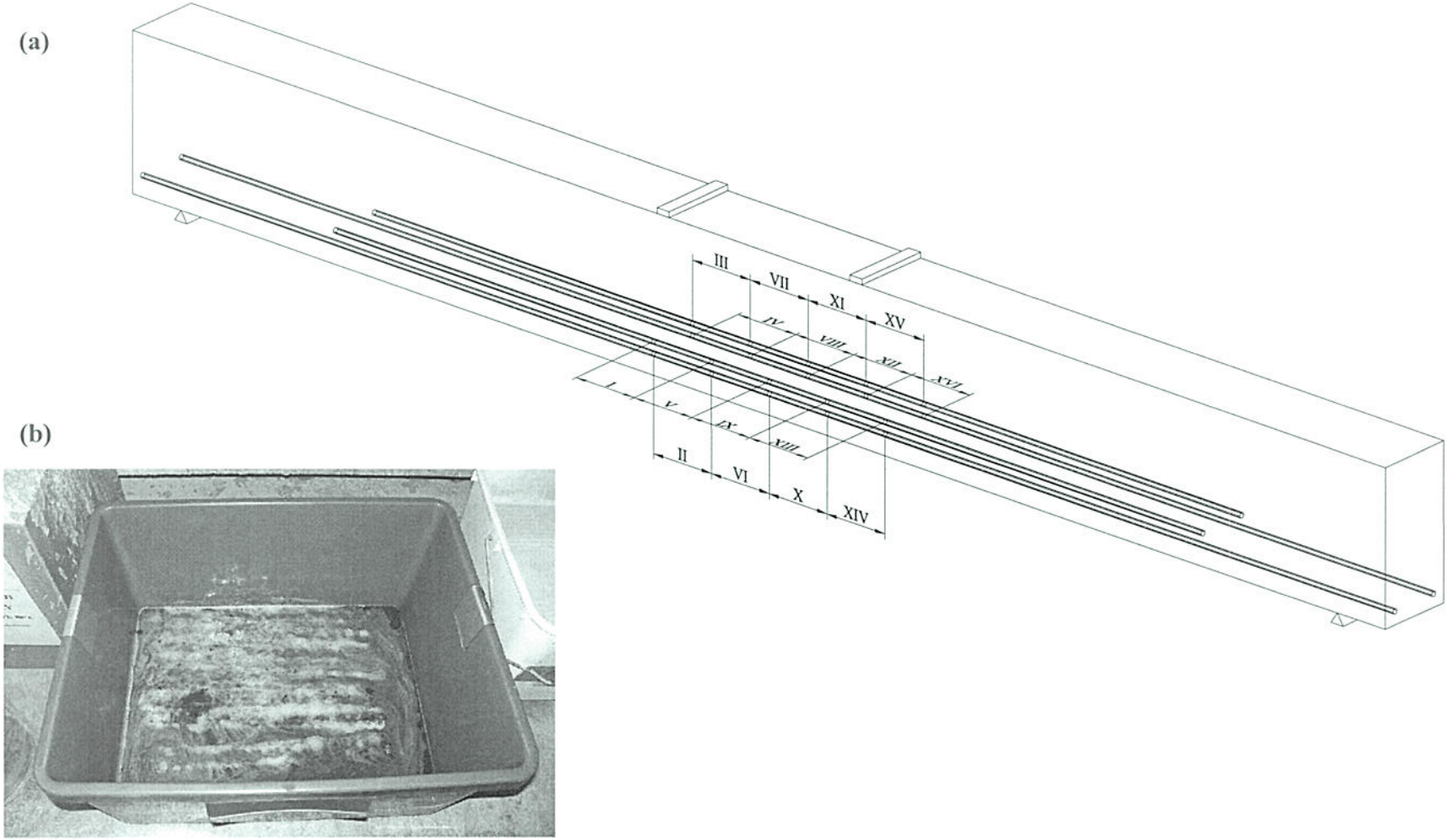

Figure 4.73 – (a) Locations of bars extracted to determine mass losses; (b) bars immersed in an acidic solution to remove corroded material

Table 4.2 – Mass loss of tensile reinforcement due to corrosion, obtained according to ASTM G1-90 procedure.

Beam	Mass Loss per Bar (%)																
	I	II	III	IV	V	VI	VII	VIII	IX	X	XI	XII	XIII	XIV	XV	XVI	Average
A2	8.0	13.6	6.9	16.0	9.4	17.2	5.1	20.4	10.3	22.5	9.6	27.7	19.9	22.4	8.3	8.9	14.1
A3	7.2	15.1	7.1	15.0	8.1	19.0	8.7	18.5	10.6	19.7	11.4	24.5	20.3	26.7	9.1	9.7	13.4
B2	7.6	19.9	10.1	11.5	6.0	23.1	9.2	23.7	8.3	24.8	10.9	24.0	9.1	26.7	10.1	35.0	16.2
B3	9.5	-	8.6	31.1	12.0	13.9	11.5	17.3	13.9	-	16.7	16.0	9.4	20.0	13.3	-	14.9
C2	12.9	-	16.1	18.8	19.0	17.4	22.2	18.6	-	21.3	17.4	12.6	-	-	-	16.1	18.8
C3	20.3	13.8	18.5	26.6	17.9	12.3	21.2	18.1	15.5	14.4	28.6	12.1	23.4	20.0	-	-	17.5
D2	7.0	12.3	6.5	17.5	9.3	15.5	7.7	19.4	8.8	23.3	10.4	24.1	9.2	23.0	9.3	10.5	13.4
D3	9.4	15.6	7.0	13.2	6.5	19.9	10.0	23.2	11.4	21.0	9.2	26.3	9.8	22.8	9.9	12.1	14.2

4.5 Discussion

Of the 12 beams tested in this study, 7 of the beams failed by fatigue fracture of one or more of the tensile reinforcing bars, which is the typical mode of fatigue failure for under-reinforced concrete beams. The addition of the CFRP laminates in beams B3 and C3 did not alter the failure mode of the beams with debonding of the CFRP occurring immediately after the fracture of the bars.

In the case of beams D1 and D3 that did not fail after 2 million cycles, then beams were loaded statically to failure. The control beam for Series D, beam D1 failed by yielding of the reinforcing steel. Failure of beam D3 was by fracture of the tensile bars at a crack originating from one end of the CFRP plate. The tests for beams A1 and A3 (tested in parallel) were curtailed prematurely after 1.2 million cycles due to an error by the technical operator in making an adjustment to the loading system and overloading the specimens. However, the evidence strongly suggests that fatigue failure was imminent for beam A1 with the steel tensile strain measured at almost 1.5 percent elongation and with a large increment in the deflection. This compares to a tensile strain of 0.05 percent for the CFRP-reinforced specimen (beam A3) taken at the same cycle number. Beam B2 failed before one full load cycle was completed.

The midspan deflections, at the maximum load in the cycle, versus number of load cycles are given in Figure 4.74. Test specimens that failed by fatigue, or were at near failure, follow a similar deflection trend. Table 4.3 shows the deflections taken at the beginning of the test, point X in Figure 4.75, at the point prior to rapid increment, point Y, and close to the end of the test, point Z. Corrosion of the tensile reinforcement is observed to have increased the deflection of a beam with the relative increment most significant in the larger series specimens. As expected, the fatigue lives of the corroded and unstrengthened beams were reduced significantly compared to the control and CFRP-strengthened beams. In test series A and B, repair using CFRP reduced the deflection of the corroded beams to that of the deflection of the control specimens. In series C and D, the deflection of the CFRP-repaired beam was lower than that of the control. The repair with CFRP improved the fatigue lives of the corroded beams but for beams B3 and C3, not to that of their respective controls.

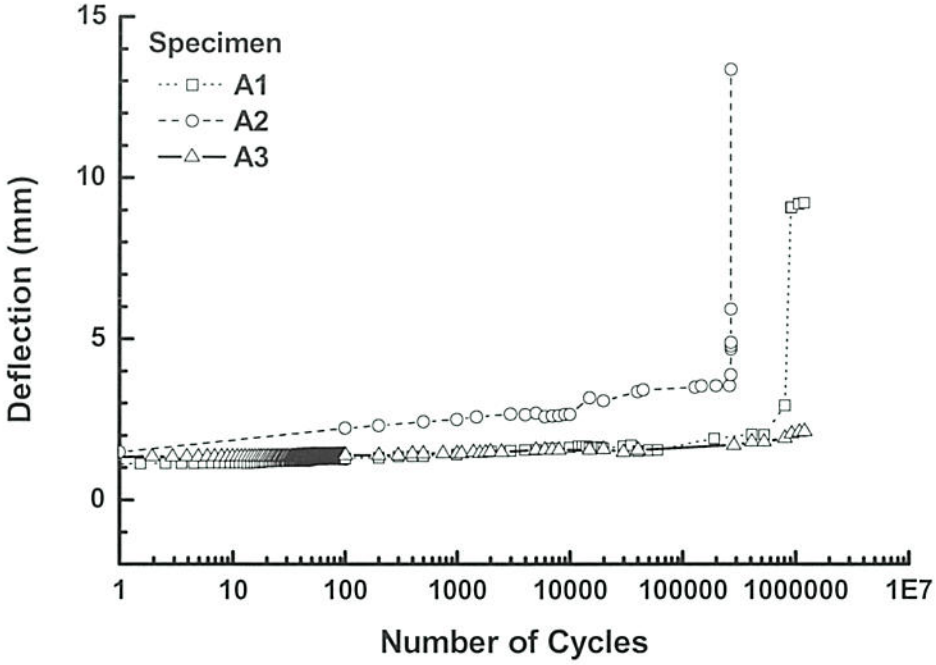

(a)

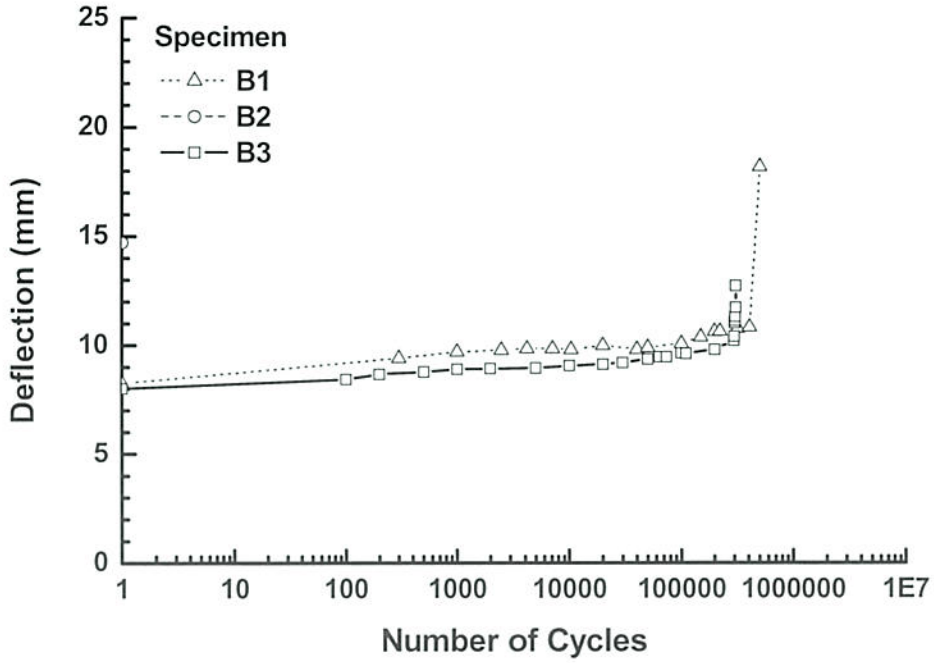

(b)

Figure 4.74 – Deflection versus number of cycles at mid span during maximum load for beams in (a) Series A (b) Series B (c) Series C and (d) Series D.

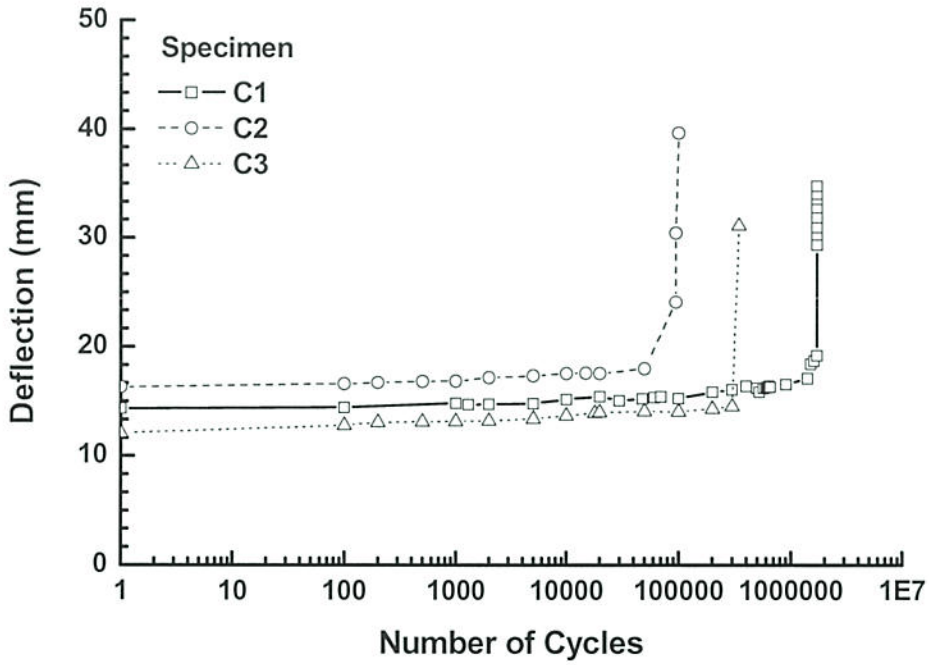

(c)

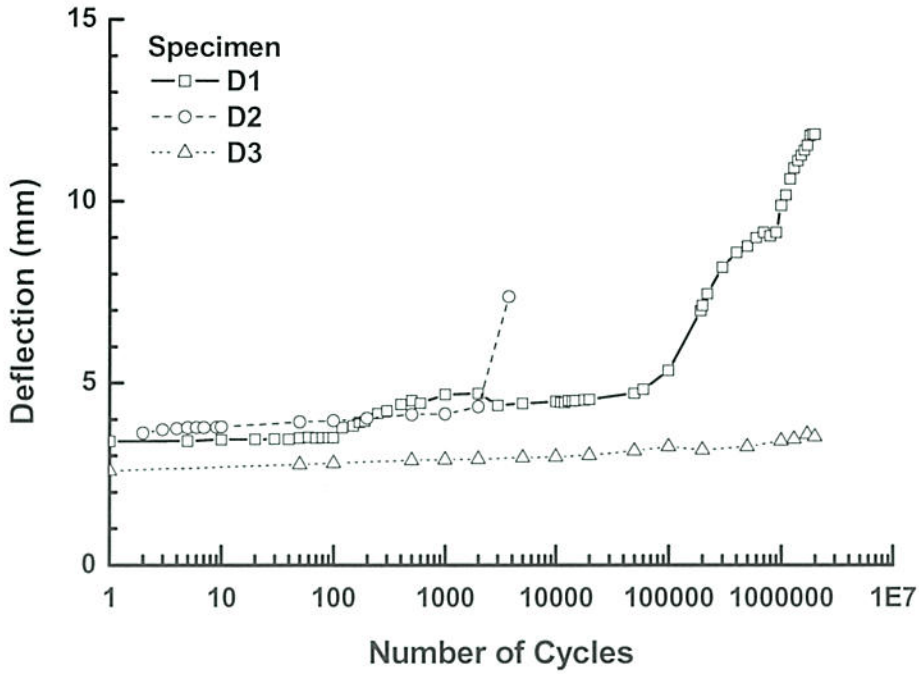

(d)

Figure 4.74 (continued).

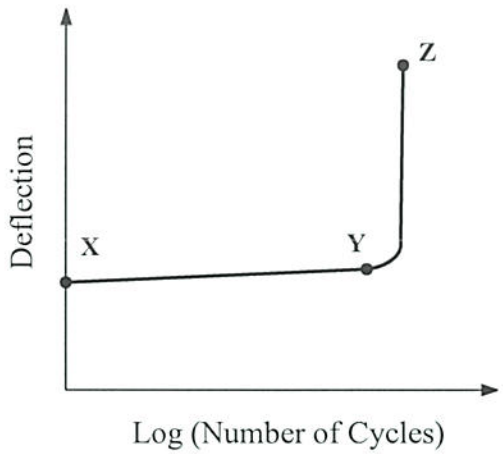

Figure 4.75 – Midspan deflection versus number of cycles for test specimens.

Table 4.4 shows the average of the maximum steel tensile strain (measured using the strain gauges) at mid-span and the strain at the concrete surface at the top and bottom of the beam at mid-span (measured using Demec gauges), taken at the beginning of the test and close to the end of the test. It is observed that the concrete compressive strain increases under fatigue loading, which signifies concrete softening due to racking effects, that, in turn, leads to the increase in tensile strain in the steel. This observation is consistent with that of Masoud, 2002. The concrete tensile strain increases under fatigue loading as well, and varies significantly among the test specimens at near the end of the test. Towards the end of each test, the damage of a specimen occurs rapidly and may not have been captured exactly prior to ultimate failure, hence the variability of the recorded strains among test specimens. Significant variability of tensile strains in the steel bars is also exhibited because of stress concentrations due to formation of cracks in the concrete relative to the location of the strain gauges. Overall, the tensile strain in the steel bars is observed to be lower in the FRP-repaired specimens than that in the control specimens due to the forces carried by the FRP laminates reducing the forces, and hence stresses in the bars. The reduction in the steel strains were calculated to be approximately 80 percent for test series A, 50 percent for test series B and 60 percent for both test series C and D.

On fracture of a steel bar in beams B3 and C3, the load transferred to the CFRP plate as observed by a marked increase in strain in the CFRP (see Figures 4.26 and 4.42). The CFRP plate was observed, in beams B3, to withstand more than 40,000 service load cycles

Table 4.3 – Summary of deflections of test specimens.

Beam	No. of cycles to failure	Deflection at maximum load (mm)		
		Initial, X	Intermediate, Y (at cycle)	End, Z
A1	> 1.2 million	1.1	2.9 (815,500)	10.3*
A2	272,400	1.4	3.9 (270,000)	13.4
A3	> 1.2 million	1.3	-	2.1*
B1	508,000	8.3	10.8 (408,000)	18.2
B2	0	-	-	-
B3	308,946	8.0	10.4 (297,700)	12.5
C1	1.705 million	14.3	19.2 (1.7 million)	34.8
C2	100,590	16.3	18.0 (50,000)	39.7
C3	343,695	12.0	14.5 (300,000)	31.1
D1	> 2 million	3.4	5.3 (100,000)	11.8# 19.0^
D2	3,750	3.6	4.4 (2,000)	7.4
D3	> 2 million	2.6		3.5# 9.2^

Notes: * Measured at 1.2 million cycles; # Measured at 2 million cycles prior to monotonic loading to failure; ^ Measured prior to failure under monotonic loading

Table 4.4 – Summary of strains in test specimens.

Beam	No. of cycles to failure	Maximum steel tensile strain* (με)		Concrete tensile strain# (με)		Concrete compressive strain# (με)	
		Initial	End	Initial	End	Initial	End
A1	> 1.2 million	737	14800^	1000	1500	-235	-706
A2	272,400	332	1680	1500	3500	-933	-1270
A3	> 1.2 million	121	464	500	681	-430	-500
B1	508,000	2150	2570	1500	2500	-188	-500
B2	0	-	-	-	-	-	-
B3	308,946	1050	1130^	850	1067	-397	-372
C1	1.705 million	1770	2020	2250	7250	-313	-563
C2	100,590	1640	2950	2220	15250	-1110	-3890
C3	343,695	655	732	1380	1700	-778	-890
D1	> 2 million	1860	2650	1625	16000	-500	-2625
D2	3,750	1820	1740	750	900	-577	-635
D3	> 2 million	747	1430	1000	3500	-808	-1077

Notes: * Measured using electronic strain gauges; # measured using Demec gauges; ^ last measurement taken before gauge breakdown (not at end of test).

after bar fracture and before debonding occurred at the mortar-adhesive layer. Based on these findings, the CFRP delays the impeding failure of a structure subjected to fatigue by reducing the stress in the reinforcing bar and supporting the service load for a short period after bar fracture. Given the mode of failure, it is hypothesised that considerable benefit would be gained with use of mechanical anchorage at the CFRP ends.

While, as expected, the CFRP strengthening improved the behaviour of the beams, compared to that of the corroded repaired but non-strengthened specimens, the capacities in beams B3 and C3 was not restored to that of their respective control specimens. Importantly, a strong size effect is observed with a decreasing fatigue capacity of the repaired specimens with increasing size. This is attributed to two effects, firstly a breakdown in local bond between the steel and surrounding concrete in the smaller specimens and the increased fatigue life of smaller diameter bars.

5 CONCLUSIONS

A series of 12 beams, 4 corroded and repaired with mortar, 4 corroded and repaired with mortar and strengthened with CFRP and 4 control specimens, were tested in fatigue. The beams were designed for a nominal 1 million cycles of fatigue loading in their pristine condition. Three beam sizes were tested to evaluate size effect.

To accelerate the corrosion process to the desired level of 15 percent mass loss, two beams of each series were placed in a water tank in an electrolytic solution and with a current passing through the reinforcement. The electrolytic solution was cycled regularly so that the beams were subjected to wet and dry periods. The beams were also held under load during the corrosion process so that the crack widths were representative of that of beams in practice.

As expected, in the corroded specimens the tensile reinforcing bars had become more susceptible to fatigue failure than for the bars in the non-corroded control beams. The CFRP strengthening delayed the fatigue life of corroded specimen by reducing the stress level of the tensile reinforcement. The dominant failure was by fracture of one or more of the tensile reinforcing bars, followed by debonding of the CFRP plate.

On fatigue failure of the reinforcing steel in beams B3 and C3, the load transferred to the CFRP plate as observed by a marked increase in strain in the CFRP. After the load transfer, however, the beams were capable of withstanding just a few thousand additional cycles before debonding. While the CFRP delayed the fatigue failure it did not restore the cyclic resistance of the beams to that of the control specimens. It is postulated that the system would be improved considerably with provision of mechanical end anchorages to the CFRP and/or prestressing of the CFRP. Further testing is required using large scale specimens to test this postulate.

Lastly, a size effect was observed with a decreasing fatigue capacity of the repaired specimens with increasing size. This was attributed to a breakdown in local bond between the steel and surrounding concrete and, in the smaller specimens, an increased fatigue life of smaller diameter bars.

6 REFERENCES

ACI Committee 215, 1981. "Fatigue of concrete structures", American Concrete Institute, Farmington Hills, USA, 401 pp.

ACI Committee 215, 1974. "Considerations for design of concrete structures subject to fatigue loading", *ACI Materials Journal*, Vol. 71, No. 3, pp: 97-121.

Aidoo, J., Harries, K.A. and Petrou, M.F., 2004. "Fatigue behaviour of carbon fiber reinforced polymer-strengthened reinforced concrete bridge girders", *Journal of Composites for Construction*, ASCE, Vol. 8, No. 6, pp: 501-509.

American Society for Testing and Materials, 1991. "Standard Test Method for Fundamental Transverse, Longitudinal, and Torsional Frequencies of Concrete Specimens", ASTM C 215-91, West Conshohocken, USA.

Apostolopoulos, C.A. and Papadopoulos, M.P., 2007. "Tensile and low cycle fatigue behavior of corroded reinforcing steel bars S400", Construction and Building Materials, Vol. 21, No 4, pp: 855-864.

Aas-Jacobson, K., 1979. "Fatigue of concrete beams and columns", Bulletin No. 70-1, Norwegian Institute of Technology, Trondheim, Norway, 148 pp.

Balaguru, P.N. and Shah, S.P., 1982. "A method of predicting crack widths and deflections for fatigue loading" in "Fatigue of concrete structures", ACI Special Publication 75, Detroit, pp: 153-175.

Barnes, R.A. and Garden, H.N., 1999. "Time-dependent behaviour and fatigue" in "Strengthening of reinforced concrete structures using externally bonded FRP composites in structural and civil engineering", edited L.C. Hollaway and M.B. Leeming, Woodhead Publishing Limitied, Cambridge, pp 83-134.

Barnes, R.A. and Mays, G.C., 1999. "Fatigue performance of concrete beams strengthened with CFRP plates", *Journal of Composites for Construction*, ASCE, Vol. 3, No. 2, pp: 63-72.

Bizindavyi, L., Neale, K.W. and Erki, M.A., 2003."Experimental investigation of bonded fiber reinforced polymer-concrete joints under cyclic loading", *Journal of Composites for Construction*, ASCE, Vol. 7, No. 2, pp: 127-134.

Booth, E.D., Leeming, M.B., Paterson, W.S. and Hodgkiess, T., 1986. "Fatigue of reinforced concrete in marine conditions", *Proceedings of the International Conference on Concrete in the Marine Environment*, London., UK, pp: 1878-198.

Brandshaug, T., 1978. "A comparative evaluation concrete reinforced with straight steel fibers and collated fibers with deformed ends", Masters Thesis, South Dakota School of Mines and Technology, USA.

Breña, S.F., Wood, S.L. and Kreger, M.E., 2002. "Fatigue tests of reinforcement concrete beams strengthened using carbon fiber reinforced polymer composites", *Proceedings of the Second International Conference on Durability of Fiber Reinforced Polymer (FRP) Composites for Construction*, Montreal, Canada, edited B. Benmokrane and El-Salakawy, pp: 575-585.

Cairns, J. and Millard, S., 1999. "Section 13.2: Reinforcement corrosion and its effect on residual strength of concrete structures", *Proceedings of the Eighth International Conference on Structure Faults and Repair*, Edinburgh, U.K, edited M. Forde.

Castel, A., Francois, R., and Arliguie, G., 2000. "Mechanical behaviour of corroded reinforced concrete beams. II: Bond and notch effects" *Materials and Structures*, RILEM, Vol. 33, pp: 545-551.

CEB-FIP, 1988. Fatigue of Concrete Structures: State of the Art Report Bulletin d'Information no. 190 , CEB-FIP Comité Euro-International du Béton, Paris, France.

CEB-FIP, 1988. Model Code 1990, CEB Bulletin d'Information No. 190, CEB-FIP Comité Euro-International du Béton, Paris, France.

Coronelli, D. and Gambarova, P., 2004. "Structural assessment of corroded reinforced concrete beams: Modeling guidelines", *Journal of Structural Engineering*, Vol. 130, No. 8, pp: 1214-1224.

Dai, J.G., Saito, Y., Ueda, T. and Sato, Y., 2005. "Static and fatigue bond characteristics of interfaces between CFRP sheets and frost damage experienced concrete", *Proceedings of the Seventh International Symposium on Fiber Reinforced Polymer Reinforcement for Reinforced Concrete Structures*, Kansas City, USA, edited by C.K. Shield, J.P. Busel, S.L. Walkup and D.D. Gremel, pp: 1515-1530.

Dong, Y., 2003. "Static and fatigue performance of reinforced concrete beams retrofitted with externally CFRP composites". PhD thesis, University of Illinois, Chicago, USA.

El-Tawil, S., Ogunc, C., Okeil, A. and Shahawy, M., 2001. "Static and fatigue analyses of RC beams strengthened with CFRP laminates", *Journal of Composites for Construction*, ASCE, Vol. 5, No. 4, pp: 258-267.

Emberson, N.K. and Mays, G.C., 1996. "Significance of property mismatch in the patch repair of structural concrete: Part 3: Reinforced concrete members in flexure", *Magazine of Concrete Research*, Vol 48, No. 174, pp: 45-57.

Ferrier, E., Bigaud, D., Hamelin, P., Bizindavyi, L. and Neale, K.W., 2005. "Fatigue of CFRPs externally bonded to concrete", *Materials and Structures*, RILEM, Vol. 38, pp: 39-46.

Gheorghiu, C., Labossière, P. and Proulx, J., 2006. "Fatigue and monotonic strength of RC beams strengthened with CFRPs", *Composites Part A: Applied Science and Manufacturing,* Vol. 37, No. 8, pp: 1111-1118.

Gheorghiu, C., Labossière, P. and Raîche, A., 2004. "Environmental fatigue and static behaviour of RC beams strengthened with carbon-fiber-reinforced polymer", *Journal of Composites for Construction*, ASCE, Vol. 8, No. 3, pp: 211-218.

Heffernan, P.J. and Erki, M., 2004. "Fatigue behaviour of reinforced concrete beams strengthened with carbon fiber reinforced plastic laminates", *Journal of Composites for Construction*, ASCE, Vol. 8, No. 2, pp: 132-140.

Helgason, T. and Hanson, J.M., 1974. "Investigation of Design Factors Affecting Fatigue Strength of Reinforcing Bars – Statistical Analysis", *Abeles Symposium on Fatigue of Concrete*, SP-41, American Concrete Institute, Farmington Hills, USA, pp: 107-138.

Hollaway, L. and Leeming, M., 1999. Strengthening of reinforced concrete structures, London, Woodhead Publishing.

Holmen, J.O., 1982. "Fatigue of concrete by constant and variable amplitude loading", *Fatigue of Concrete Structures*, American Concrete Institute, Detroit, pp: 71-110.

Hsu, T.T.C., 1981. "Fatigue of plain concrete", *Journal of the American Concrete Institute*, Vol. 78, No. 4, pp: 292-305.

Japan Society of Civil Engineers, Trans, 122, October 1965.

Kakuta, Y., Okamura, H. and Kohno, M., 1982. "New concepts for concrete fatigue design procedures in Japan", *Proceedings of the International Association for Bridge and Structural Engineering*, Lausanne, Switzerland, pp: 51-58.

Ko, H. and Sato, Y., 2007. "Bond stress-slip relationship between FRP sheet and concrete under cyclic load", *Journal of Composites for Construction*, ASCE, Vol. 11, No. 4, pp: 419-426.

Lopez, M.M., Naaman, A.E., Pinkerton, L. and Till, R.D., 2003 "Behavior of RC beams strengthened with FRP laminates and tested under cyclic loading at low temperatures". *Journal of Materials and Product Technology* Vol. 19, No. 1-2, pp: 108-117.

Maaddawy, T.E, 2004. "Performance of corrosion-damaged reinforced concrete beams repaired with CFRP laminates", PhD thesis, University of Waterloo, Ontario, Canada.

Mallett, G.P., 1991. "Fatigue of Reinforced Concrete" State of the Art Review 2, Transport and Road Research Laboratory, HMSO Publications, London, 166 pp.

Masoud, S., 2002. "Behaviour of corroded reinforced concrete beams repaired with FRP sheets under monotonic and fatigue loads", PhD thesis, University of Waterloo, Ontario, Canada.

Masoud, S., Soudki, K. and Topper, T., 2001. "CFRP-strengthened and corroded RC beams under monotonic and fatigue loads", *Journal of Composites for Construction*, ASCE, Vol. 5, No. 4, pp: 228-236.

Meier, U., 1995. "Strengthening of structures using carbon fibre/epoxy composites", *Construction and Building Materials*, Elsevier Science Ltd., Vol. 9, No. 6, pp: 341-351.

Moss, D.S., 1980. "Axial fatigue of high yield reinforcing bars in air", TRRL Report SR622, Transport and Road Research Laboratory, Department of Transport, Crowthorne, UK.

Moss, D.S., 1982. "Bending fatigue of high yield reinforcing bars in concrete", TRRL Report SR748, Transport and Road Research Laboratory, Department of Transport, Crowthorne, UK.

Muszynski, L.C. and Sierakowski, R.L., 1996. "Fatigue strength of externally reinforced concrete beams", *Proceedings of the Materials Engineering Conference*, Washington D.C., USA, pp: 648-656.

Neville, A.M., 1996. "Properties of concrete", John Wiley & Sons Inc., 844 pp.

Oyado, M., Hasegawa, M. and Sato, T. 2003. "Characteristics of fatigue and evaluation of RC beam damaged by accelerated corrosion". Quarterly Report of RTRI, Vol. 44, No. 4 pp: 72-77.

Papakonstantinou, C.G., Balaguru, P.N. and Petrou, M.F. 2002. "Analysis of reinforced concrete beams strengthened with composites subjected to fatigue loading", *Concrete: Material Science to Application* ACI Special Publication SP 206-3, Detroit, pp. 41-60.

Papakonstantinou, C.G., Petrou, M.F. and Harries, K.A., 2001. "Fatigue behaviour of RC beams strengthened with GFRP sheets", *Journal of Composites for Construction*, ASCE, Vol. 5, No. 4, pp: 246-253.

Paterson, W.S and Dill, M.J., 1987. "Fatigue strength of reinforced concrete in seawater – Results from Phase II", Concrete in the Oceans Technical Report No. 19, Offshore Technology Report OTH 87/243, HMSO, London.

Pong, S., 2001. "Experimental and analytical study of corroded RC beams repaired with externally bonded CFRP shear and flexural reinforcement", Masters Thesis, University of Toronto, Ontario, Canada.

Popovics, S., 1973. "A numerical approach to complete stress-strain curve of concrete" *Cement and Concrete Research*, Vol. 3, pp: 583-559.

Radain, T.A., 1989. "Effect of corrosion, freeze-thaw cycles, and their combined effects on the fatigue behavior of reinforced concrete". PhD thesis, University of Rhode Island, Rhode Island, USA.

Roper H. and Hetherington G. B., 1981. "Fatigue of reinforced concrete beams in air, chloride solution and sea water", *Recent Research on Fatigue of Concrete Structures*, American Concrete Institute, Detroit, USA.

Shahawy, M. and Beitelman, T., 1999. "Static and fatigue performance of RC beams strengthened with CFRP laminates", *Journal of Structural Engineering*, ASCE, Vol. 125, No. 6, pp: 613-621.

Täjlsten, B., 2002. "FRP strengthening of existing concrete structures design guideline" Luleå University of Technology, Luleå, Sweden, 2nd Edn.

Tilly, G.P., 1988. "Durability of Concrete Bridges", *Journal of the Institution of Highways and Transport*.

Waagaard, K., 1982. "Design recommendations for offshore concrete structures", *Proceedings of the International Association for Bridge and Structural Engineering*, Lausanne, Switzerland, pp: 59-67.

Wang, S. and Zhang, R., 1993. "The study of fiber composite plates for strengthening reinforced bridges", *Proceedings of the Ninth International Conference on Composite Materials*, Madrid, Spain, edited A. Miravete, pp: 224-231.

Wu, Z.Y., Clement, J.L., Tailhan, J.L., Boulay, C. and Fakhri, P., 2003. "Fatigue test on damaged reinforced concrete specimens strengthened by carbon cloth", *Proceedings of the Sixth International Symposium on Fiber Reinforced Polymer Reinforcement for Reinforced Concrete Structures*, Singapore, edited by K.H. Tan, pp: 913-922.

Yun, Y., Wu, Y. and Tang, W.C., 2008. "Performance of FRP bonding systems under fatigue loading", *Engineering Structures*, Vol. 30, pp: 3129-3140.

Zhang J., Li, V.C. and Stang, H., 2001. "Size effect on fatigue in bending of concrete", *Journal of Materials in Civil Engineering*, Vol. 13, No. 6, pp: 446-453.